Individual Differences in Manual Control Cybernetics

Predicting Individual Cybernetic Parameters Using the Human Controller Cost Function

Aytek Korkmaz

TU Delft

Individual Differences in Manual Control Cybernetics

Predicting Individual Cybernetic Parameters Using the Human Controller Cost Function

Thesis report

by

Aytek Korkmaz

to obtain the degree of Master of Science
at the Delft University of Technology
to be defended publicly on August 31, 2023 at 09:30

Thesis committee:

Chair:	Prof.dr.ir. M. Mulder
Supervisor:	Dr.ir. D.M. Pool
External examiner:	Prof.dr.ir. J.C.F. de Winter
Additional member:	Ir. O. Stroosma
Place:	Faculty of Aerospace Engineering, Delft
Project Duration:	November 30, 2022 - August 31, 2023
Student number:	4850459

An electronic version of this thesis is available at `http://repository.tudelft.nl/`.

Faculty of Aerospace Engineering · Delft University of Technology

Preface

This report concludes my nine-month thesis project, marking the culmination my five years of study in Delft. The thesis journey has been quite challenging for me, as I encountered several obstacles along the way, including natural *(and man-made)* disasters in my home country. Nevertheless, I've learned a great deal during this process - not just about manual control cybernetics, but also a lot about myself. I am thankful to have had the opportunity to study in Delft, where I have learned and grown significantly while enjoying a truly enriching experience.

Firstly, I would like to thank my daily supervisor, Daan, for his perpetual assistance and expertise during this project. I am genuinely impressed by how every progress meeting rejuvenated my passion and interest for my thesis. I deeply appreciate your role in this, and thank you for your understanding and encouragement in helping me to achieve my best.

I am fortunate to have shared my time in Delft with incredible friends. A special thank you goes to Alp, Artun, Irmak, Praj, Manos, Manos, Gopal, and Alex for being a part of my five-year journey. Together, we've grown substantially (and even navigated through a pandemic). Thank you all for all the moments we've had. I'd also like to extend my gratitude to my friends who joined me in sports and music, for supporting these vital aspects of my life.

Finally, I would like to thank my parents, for their endless and unconditional support. Thank you for guiding me in every step I take and for all the sacrifices you've made for me. You remain my greatest sources of inspiration and motivation, and I owe everything to your *love* and *leadership*.

Aytek Korkmaz
Delft, August 2023

Contents

List of Figures

List of Tables

Part I

Scientific Article

Predicting Individual Cybernetic Parameters Using the Human Controller Cost Function

Aytek Korkmaz
Faculty of Aerospace Engineering, TU Delft, Delft, South Holland, 2629 HS, Netherlands

Understanding individual differences in manual control cybernetics plays a principal role in personalizing human-machine systems. While much of the work in cybernetics utilizes models for the average controller, individualized models have also been explored, albeit constrained by data availability and the effectiveness of identification techniques. It has previously been theorized that human controller behavior may be defined by a cost function that the controller minimizes for a given control task. This cost function comprises weighted performance and effort terms, and the weightings have been connected to cybernetic models before, but not on an individualized basis. A proposed connection is through the equalization component of the cybernetic model, which has also been outlined as an indicator of individual differences. This claim was reinforced by the analysis of previously collected experiment data in this paper: Across three independent experiments, the equalization parameters, on average, showed 33.84% higher variation than the others and a greater impact on the cost function. Thus, this paper presents a human-controller-cost-function-centered approach to predict and generate individualized sets of cybernetic parameters. Individual cost function weightings were determined using the identified equalization parameters from earlier human-in-the-loop experiments. This process exhibited clear groupings in participants, as clusters of participants with similar equalization were not identified adequately. Individual cost function weightings were then employed to predict full sets of cybernetic parameters. The results indicated that the utilized cost function is incapable of reflecting the physical limitations of the human controller, as these parameters (time delay, neuromuscular natural frequency, and neuromuscular damping coefficient) showed 56.06%, -94.43%, and -170.34% deviation compared to the experimental values. Hence, a hybrid cybernetic data augmentation method was devised, yielding signal values within 15% of experimental data.

I. Nomenclature

CF	=	Crossover Frequency
HC	=	Human controller
HCCF	=	Human controller cost function
HQR	=	Handling qualities ratings
LTI	=	Linear Time-invariant
OCM	=	Optimal Control Model
PM	=	Phase Margin
RMS	=	Root mean square
RNG	=	Random number generator
H_p	=	Human controller dynamics
H_c	=	Controller element dynamics
f_t	=	Target forcing function
f_d	=	Disturbance forcing function
e	=	Tracking error signal
x	=	System output
u	=	Control input signal
$\dot{u}$	=	Control input rate
σ_e	=	Root mean square of the tracking error signal
σ_u	=	Root mean square of the control input signal
$\sigma_{\dot{u}}$	=	Root mean square of the control input rate
$K1$	=	Coefficient of the control input signal
$K2$	=	Coefficient of the control input rate
θ	=	Set of cybernetic parameters *(listed below)*
K_v	=	Visual gain constant
T_L	=	Lead-time constant
T_I	=	Lag-time constant
τ	=	Time delay
ω_{nm}	=	Neuromuscular natural frequency
ζ_{nm}	=	Neuromuscular damping coefficient

II. Introduction

While the question of how humans control aircraft has been a part of scientific research since the inception of airplanes[1], the cybernetic theory and the mathematical pilot models developed by McRuer and Jex [2] is considered a groundbreaking piece of work in the field. Cybernetics is the study of the human controller (HC) using an approach rooted in mathematical systems theory[3]. The crossover model developed by McRuer in the 1960's [4, 5], describing human control dynamics, forms the basis of the "cybernetic approach". Mathematically modeling the HC using a set of parameters is useful for understanding the nature of human control. The cybernetic theory, originating in aerospace, has been commonly applied in other fields such as robotics [6], medicine [7, 8], automotive [9, 10], and other vehicles [11].

There has been extensive research on the "goal" of the human when performing a control task, and how differences in task performance could be explained using the cybernetic theory. A cost function defining the human controllers' attitude (the human controller cost function, HCCF) towards performing a control task was proposed by Kleinman et al. [12, 13]. This cost function is defined as a weighted sum of error signal and control input terms, to represent the balance between "performance" and "error" respectively, and has been adopted in many technical fields [14–24]. Due to being closely associated concepts, there have been several attempts to link the weightings in the cost function to the parameter settings of cybernetic models [12, 13, 17, 20, 21]. While the connection between the HCCF and the cybernetic parameters was initially devised to be established using the neuromuscular component of the cybernetic model [12, 13, 17], attention was turned towards equalization later on [20, 21]. Despite these efforts, there has been no set guidelines on how the cost function should be formulated, how the weightings could be determined, or how the cost function could be connected to the cybernetic HC model. Nevertheless, the HCCF remains a useful concept to address matters in cybernetics, as novel cost functions for more specific purposes (e.g., predicting HQR) are being propounded [25–27].

Even though cybernetics has been considerably effective in explaining human control behavior, it is still incapable of capturing the full extent, despite several efforts to update and advance the theory [3]. A limitation in current manual control cybernetics that calls for progress is the lack of "personalized support" [3, 10, 28], just like other fields related to automation and human-machine interaction [29–32]. In cybernetics, much of the work done has been for an "average" HC [11, 33], although the individual differences between humans also need attention [34, 35]: Acknowledging individual differences provide several benefits, such as "making systems more acceptable and useful"[31], designing safer systems[32], and providing a basis for training [36]. Studies regarding individual differences in cybernetics have focused mostly on topics directly related to classifying HC (e.g., pilot gain and handling qualities ratings [16, 25–27, 37]). A key finding has been to label pilot gain as a "misnomer" [16, 38, 39], instead proposing pilot "bandwidth", hence pointing towards HC equalization of the control task as an indicator of individual differences. Nonetheless, individualized HC parameters could currently be acquired using identification techniques only, which are complicated and prone to biases [40]. An even larger problem for this process is that it relies heavily on the availability of data: i.e., it is constrained by the number of participants in the experiment, and that the experiment has actually been conducted. To tackle this dependence on experimentally collected data, cybernetic data augmentation has been attempted, proving limited success so far [41]. Thus, a need for a method to predict and generate *individual* cybernetic data for given experimental conditions is clear.

Therefore, this paper proposes a HCCF centered approach to personalization in cybernetics. Therefore, this paper approaches personalization in manual control cybernetics based on the human controller performance-effort cost function (simply referred to as human controller cost function, HCCF). As mentioned earlier, it has been attempted to link the cost function weightings defining the HC balancing of performance and effort to the cybernetic parameters [12, 13, 17, 20, 21], although without paying much attention to individual differences. The approach followed in this research thus introduces *individualized* cost function weightings, to be linked to *individual* sets of cybernetic parameters. Following the methods presented in [20, 21], the individual cost function weightings will be identified using the equalization component of the cybernetic HC model. This is in line with the "bandwidth" of a controller being proposed as a measure of individual differences [16, 38, 39].

This research involves simulating data from three prior experiments [21, 42, 43], each with a different controlled element, to avoid specific conclusions. The analysis has four steps: first, examining participant variability in cybernetic parameters and its effect on HCCF signals; second, determining personalized cost function weights using HC equalization; third, testing the extent to which cybernetic model parameters can be predicted using these weights; and finally, using this method as cybernetic data augmentation. It is thus aimed to contribute a novel method to predict individual differences and to accurately account for them when setting up offline HC model simulations (e.g., analyses using Monte Carlo methods). Overall, the feasibility of an approach based on the HCCF is tested, and the analyses provide insights into between-participant variability in cybernetics by observing for which parameters this approach is successful.

First, an overview on the theory that lies behind the procedure followed in this report is given to contextualize the work. This section briefly explains the cybernetic HC model, the HCCF, and highlights the equalization component of the model as a key concept in the approach. Next, in section IV, the methodology is explained in detail, starting with the data used and moving on into the four main steps of analysis. Following this, section V the results from these analyses performed in this research. The paper is wrapped up with a discussion and conclusions.

III. Background

Before explaining the work carried out for the current study, the relevant context that surrounds it must be presented. Thus, this section provides a comprehensive overview of the topics and concepts that lay the foundation for this research. In this paper investigating individual differences in human-machine systems, the focus is on compensatory tracking tasks, where HC exerts control based on the error between the target command input and the actual command output. An overview of the compensatory tracking task is visualized as a control loop in Figure 1.

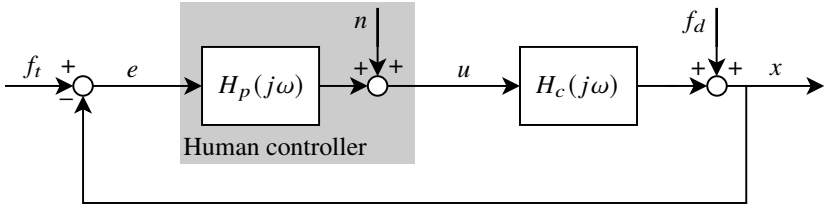

Fig. 1 Block diagram of a compensatory control task

This feedback loop representation is essential for this research, as the representation of the HC ($H_p(j\omega)$) will be the basis for observing individual differences. Moreover, other components represented here such as the controlled element ($H_c(j\omega)$) also carry importance, due to its heavy influence on the HC. This paper conducts analyses for three distinct controlled elements to mitigate such biases. Finally, Figure 1 clearly depicts the relationship of the HC with the tracking error signal, e, and the control input signal u. The former is the input of the HC while the latter is the output, and hence this representation visualizes the rationale for using them as a means to measure the changes in the HC.

A. Cybernetic Human Controller Model

The cybernetic HC model, and how the parameters that make it up behave among people, is the primary means for quantifying individual differences. The *precision model* developed by McRuer and Jex[2] is the most commonly accepted way for modeling the HC. It consists of a LTI component that could be modeled mathematically as a transfer function, and a "remnant" component that represents the nonlinear, noisy element of human control. This remnant component is neglected in this research as the focus has been purely on the behavior of the parameters that make up the LTI HC model between individuals.

The LTI component itself is comprised of three main parts: delay, neuromuscular dynamics, and equalization. The delay and the neuromuscular dynamics components together are referred to as *physical limitations*, as they reflect certain intrinsic hindrances of the human body. The equalization, however, models the deliberate adaptation and amplification of the HC input to the specific control dynamics, and could take up various forms and show more diversity. What each component means and represents is useful to understand individual differences in the parameters.

A comprehensive HC model is given in Eq. (1) [44]. Note that this HC model itself is not used in this paper, as the equalization is different for the experiments considered here. The precise HC models used in this paper could be found in Table 1 (in subsection IV.A). The cybernetic parameters that make up this model are: the visual gain, K_v, the lead-time constant, T_L, the lag-time constant, T_I, the time delay, τ, the neuromuscular natural frequency, ω_{nm}, and the neuromuscular damping coefficient, ζ_{nm}.

$$H_p(j\omega) = \overbrace{K_v \frac{T_L j\omega + 1}{T_I j\omega + 1}}^{\text{equalization}} \underbrace{\overbrace{e^{-j\omega\tau}}^{\text{delay}} \overbrace{\frac{\omega_{nm}^2}{(j\omega)^2 + 2\zeta_{nm} j\omega + \omega_{nm}^2}}^{\text{neuromuscular dynamics}}}_{\text{physical limitations}} \tag{1}$$

B. Human Controller Performance-Effort Cost Function

A key element to the approach to individual differences in this paper is the HCCF. This is defined as the cost function that the human controller internally minimizes while performing a control task and its history could be traced back to the Optimal Control Model (OCM) devised by Kleinman et al. [12]. The foundation for the cost function lies in the assumption that the human controller "chooses" a control input to provide as a response when performing a tracking task, and that this choice is made based on the solution that strikes the right balance between performance and effort.

For a control task, controllers are instructed to minimize the error. However, it is intrinsically impossible to simply ignore the work involved, and try to get to the best performance level. Therefore, the cost function must also include a term for the "effort" that the controller makes. The "ideal" approach would be to minimize the performance error only, and thus the weighting for the "effort" term is nominally zero. It could also be inferred from this that the "deviation" from the nominal weighting value indicates individual differences. This is the rationale behind the use of an HCCF in this paper.

The HCCF has been expressed and adapted in different forms. However, the common ground has been the use of the e and the u signals seen in Figure 1. In this case, the tracking error signal, e, represents performance and the control input signal, u, represents effort. The control work done by the HC, as well as how different HCs value this differently, could thus be investigated using the input and output of the HC system. The initial cost function developed by Kleinman et al. [12] comprised a weighted sum of the variances of the error signal, σ_e^2, control input signal, σ_u^2, and the derivative of the control input signal, $\sigma_{\dot{u}}^2$. The rationale for including the control rate is to account for the rapid control movements, which are avoided by trained controllers [12].

While it has been proposed to include further derivatives too [14], some research have utilized a simplified cost function with *only* a control rate term to represent the "effort" (no control input term) [12, 15–18]. A cost function with only a control input term has also been used [15, 19–21], but the cost function formulation that include both terms to account for "effort" remains commonplace [13, 22–24]. In addition to these versions of the original HCCF, several novel cost functions have been developed for more tailored purposes such as predicting pilot workload and handling qualities ratings [25–27]. These make use of more complicated terms (e.g., peak open-loop neuromuscular amplitude, phase margin linearization term, or the difference in the open loop phase). Even though these terms directly link to the cybernetic HC model, these cost functions are not preferred in this research due to their complex and specific nature.

For this research, a cost function utilizing the error signal, e, control input signal, u, and the control rate signal, $\dot{u}$, has been found to be the best fit, as it has a larger breadth compared to the simpler options without adding much complexity. Preliminary analyses fortified the conclusion that the a cost function employing the standard deviations of e, u, and its derivative, $\dot{u}$, (σ_e, σ_u, $\sigma_{\dot{u}}$) is the most effective overall. This is later confirmed in subsection V.B. Furthermore, the preliminary analyses suggested that it is sufficient and simpler to use the *standard deviations* of these signals rather than their *variances*, as the decrease in magnitude does not blunt the individual differences. The HCCF that is utilized in this paper is thus given in Eq. (2). As could be seen in this equation, the σ_e, σ_u, and $\sigma_{\dot{u}}$ values depend on the cybernetic parameter set, θ. $K1$ and $K2$ in this equation are the *individualized* cost function weightings that mathematically represent the HC balancing of performance and effort.

$$J(\theta) = \sigma_e(\theta) + K1 \cdot \sigma_u(\theta) + K2 \cdot \sigma_{\dot{u}}(\theta) \ , \quad \theta = [K_v, T_L, (T_I), \tau, \omega_{nm}, \zeta_{nm}] \tag{2}$$

IV. Methodology

The method followed in this research is into four steps (see Figure 2). First, a sensitivity analysis is conducted to investigate how much the cybernetic parameters vary between participants. How much these variations impact the e, u, and $\dot{u}$ signals that make up the HCCF is also examined in this step. Next, the individualized cost function weightings are identified for each participant. In the third step, the identified individual weightings are used to predict individual sets of cybernetic parameters. Finally, how generating a set of cybernetic parameters using this method fares against other conventionally used methods is assessed. It must be mentioned that the aforementioned steps are conducted for three sets of experimental data with varying controlled elements.

A. Experimental Data

In this study of individual differences in cybernetics, data sets from experiments conducted by Butijn et al. [21], van der El et al. [42], and Pool et al. [43] will be used. These data sets and experiment conditions are henceforth referred to as (I), (II), and (III) in the paper. The rationale for using data from multiple experiments with different controlled element dynamics is to mitigate any bias in the results caused by the controlled element. Moreover, increasing the

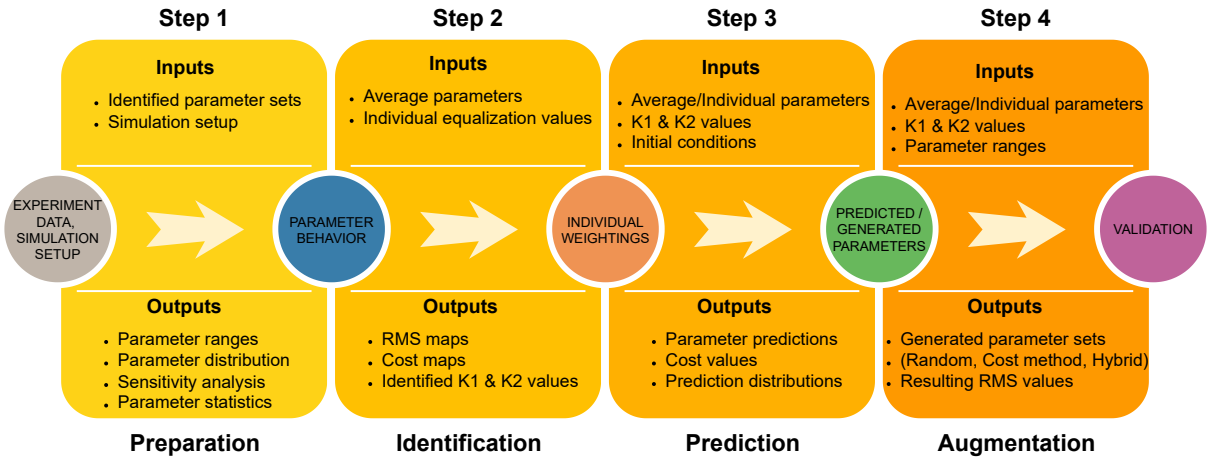

Fig. 2 Methodology overview

sample size and diversity are crucial to avoid reaching conclusions that do not generalize. All three experiments involve participants performing a compensatory tracking task in a human-subject experiment and utilize sum-of-sines forcing functions that dictate the control task. Moreover, experiment (II) does not employ a disturbance signal while the other two do, thus preventing any additional biases that might be introduced by it.

These experiments were picked based on availability and diversity: controlled element dynamics that have different characteristics lead to different values of the cybernetic parameters. HC model parameters (especially equalization) are highly related to the controlled element dynamics and therefore validating results with different experiments is necessary in order to reach comprehensive conclusions and not to make any case-specific claims. (I) made use of a low-order equivalent system, (II) made use of a double integrator, and (III) made use of the elevator-to-pitch dynamics of a Cessna Citation I. An assessment on how controlled element dynamics compare was conducted by Zolner et al. [44], and results from this research suggest that the double integrator is a more "difficult" task, as error and control input scores are both higher on average. This gives an early indication that (II) could produce more distinct results.

The HC models used in these experiments also show slight variation in the equalization part. (I) and (II) utilized a single-lead equalization, while (III) had a double lead and a single lag in order to account for the more complicated controlled element. In order to understand why the equalization components are formulated as such, the precision model introduced by McRuer and Jex [2] must be looked into. The precision model states that the HC shows single-integrator-like behavior near the crossover region. This means that for a second-order controlled element (as seen in (I) and (II)), a single order lead is needed to equalize, and achieve single-integrator dynamics overall. The controlled element in (III) has an additional pole and an additional zero, thus requiring additional lead and lag terms. As the equalization is the HC compensation for the controlled element poles, lower lead-time values are expected for controlled elements with higher break frequencies [44]. An overview of the controlled elements and HC models used in the three experiments are given in Table 1.

Table 1 HC models and controlled element dynamics from the experimental data sets used

Experiment	# of Participants	HC Model, $H_p(j\omega)$	Controlled Element, $H_c(j\omega)$
(I)	9	$K_v(T_L j\omega+1)e^{-j\omega\tau}\frac{\omega_{nm}^2}{(j\omega)^2+2\zeta_{nm}j\omega+\omega_{nm}^2}$	$\frac{-4.5}{j\omega(j\omega+3)}$
(II)	9	$K_v(T_L j\omega+1)e^{-j\omega\tau}\frac{\omega_{nm}^2}{(j\omega)^2+2\zeta_{nm}j\omega+\omega_{nm}^2}$	$\frac{5}{(j\omega)^2}$
(III)	12	$K_v\frac{(T_L j\omega+1)^2}{T_I j\omega+1}e^{-j\omega\tau}\frac{\omega_{nm}^2}{(j\omega)^2+2\zeta_{nm}j\omega+\omega_{nm}^2}$	$10.6189\frac{j\omega+0.9906}{j\omega((j\omega)^2+2.576j\omega+7.612)}$

B. Step 1: Sensitivity Analysis

The first part of the sensitivity analysis considers the identified sets of cybernetic parameters for all participants. Between-subject variation in each cybernetic parameter, as well as a breakdown of how the parameters of every participant compare to the others will be observed to gain insights. Distributions on how much each parameter deviates from the average will be key findings from this analysis, to set the parameters ranges for the sensitivity analysis later on.

As will be explained in detail in subsection IV.C, the link between cybernetic parameters and the tracking error and control input signals form the centerpiece of this research. Thus, how "sensitive" σ_e, σ_u, and $\sigma_{\dot{u}}$ signals are to variations in cybernetic parameters will be analyzed in the second part of Step 1. The baseline for the sensitivity analysis will be the averaged set of cybernetic parameters, and the resulting σ_e, σ_u, and $\sigma_{\dot{u}}$ values. The sensitivity analysis will then be conducted by individually varying each parameter by ±30%, and calculating the percentage difference in σ_e, σ_u, and $\sigma_{\dot{u}}$ compared to the baseline. It is worth noting that no remnant is considered in this analysis, as the focus is purely on the LTI component of the HC model. To see the level of influence of each parameter on these values is useful to formalize how the connection between the cybernetic parameters and the cost function weightings will be established. Findings from this step show which parameters are more forceful in the cost function and in which ways the variations in parameters influence the different components of the cost function. These are useful to explain why certain parameters take certain values as the HC minimizes the cost function.

C. Step 2: Estimating Individual Cost Function Weightings

The fundamental assumption is that the HC "picks and adjusts" a control attitude based on the HCCF that takes into account the performance and the effort, and operates at the point at which this cost function is minimal. This is taken to be the case for every individual, implying that each HC has their own "optimal" cost function weightings, represented with $K1$ and $K2$ in Eq. (2).

As mentioned previously (and verified later in subsection V.A), equalization parameters (namely K_v and T_L) carry a higher level of influence on the σ_e, σ_u, and $\sigma_{\dot{u}}$. This, combined with the fact that Butijn et al. [21] have established a connection among those two parameters and the cost function weighting, make it attractive/feasible to investigate whether these parameters could also be used to identify personalized weightings. The cost function could thus be restated as a function of individual K_v and T_L (θ_{ind}) and constant T_I, τ, ω_{nm}, and ζ_{nm} (θ_{con}); shown in Eq. (3), a modified version of Eq. (2). This formulation is to clearly state that σ_e, σ_u, and $\sigma_{\dot{u}}$ in the cost function depend on K_v and T_L, while the remaining parameters are assumed constant at the average.

$$\begin{gathered} J(\theta_{ind}, \theta_{con}) = \sigma_e(\theta_{ind}, \theta_{con}) + K1 \cdot \sigma_u(\theta_{ind}, \theta_{con}) + K2 \cdot \sigma_{\dot{u}}(\theta_{ind}, \theta_{con}) \\ \theta_{ind} = [K_v, T_L],\ \theta_{con} = [(T_I), \tau, \omega_{nm}, \zeta_{nm}] \end{gathered} \tag{3}$$

Therefore, simulations of the control loop depicted in Figure 1 are run with a wide range of K_v and T_L combinations, and the σ_e, σ_u, and $\sigma_{\dot{u}}$ values are computed for each system that is stable. Then, the cost values (a weighted sum of the three aforementioned values were calculated for varying $K1$ and $K2$ weightings, at a resolution of 0.001. By using this data, the set of equalization parameters that minimize the HCCF for each weighting are found. Consequently, these equalization values would be the operating point of a HC whose control attitude is defined by such cost function weightings.

With this method, the K_v and T_L values of each participant from the experimental data sets were then used to identify the $K1$ and $K2$ weightings of that participant. For each combination of $K1$ and $K2$, the equalization that minimizes the cost function (the optimum equalization) will be different. Hence, identification will be done by finding the combination of $K1$ and $K2$ that result in the optimum equalization that is the closest to the measured equalization of the participant. This identification will be presented via "cost maps"; contour plots that mark the separate σ_e, σ_u, and $\sigma_{\dot{u}}$ values and the final cost function value for varying equalization values. The cost map is essentially a two-dimensional grid, with the two equalization parameters on the axes and the color signifying the cost value. The outcomes of this step are the individual $K1$ and $K2$ values for each participant, as a means of personalizing the performance-effort trade-off. Therefore, the individual control attitude of a HC could be represented with two coefficients. Finally, the simplification that the θ_{con} could be assumed at the average value is validated by repeating the process outlined here with individual θ_{con} values (referred to as the individual case). Here, the θ_{con} consists of the *personal* parameters rather than the average (still kept constant), and θ_{ind} parameters are varied to identify the individual $K1$ and $K2$.

D. Step 3: Predicting Cybernetic Parameters

In essence, this next step will invert the relationship established in the previous step as now the cybernetic parameters will be estimated, using $K1$ and $K2$. The previous step had identified the cost function weightings that match the best for given equalization values, and this step will instead predict the set of parameters that match the best for given weightings. Therefore, the output of Step 2, the identified $K1$ and $K2$ values ($K1_{ID}$ & $K2_{ID}$), are used as inputs for prediction. This step focuses on working with this connection between the cost function and the cybernetic model, to see how effective the cost function weightings are in predicting individual cybernetic parameters: K_v, T_L, T_I (when applicable), τ, ω_{nm}, ζ_{nm}. For this purpose, the predictions begin with just the equalization parameters (K_v and T_L first, T_I later), and then expanded step by step to involve the HC limitation parameters ($\tau, \omega_{nm}, \zeta_{nm}$). This process is represented in the cost function (see Eq. (4)) as here the full parameter set θ is split into the predicted ("optimized") individual parameters, θ_{opt}, and the parameters assumed constant at the average value, θ_{con}. Through the optimization cases, predicted parameter set expands by taking one parameter at a time from the θ_{con} set, ultimately reaching $\theta_{ind} = \theta = [K_v, T_L, T_I, \tau, \omega_{nm}, \zeta_{nm}]$. The optimization cases are shown in Table 2.

$$J(\theta_{opt}, \theta_{con}) = \sigma_e(\theta_{opt}, \theta_{con}) + K1_{ID} \cdot \sigma_u(\theta_{opt}, \theta_{con}) + K2_{ID} \cdot \sigma_{\dot{u}}(\theta_{opt}, \theta_{con}) \tag{4}$$

Table 2 Optimization Cases

Optimization Case	θ_{opt}	θ_{con}
A	$[K_v, T_L]$	$[(T_I), \tau, \omega_{nm}, \zeta_{nm}]$
A1: (III) only	$[K_v, T_L, (T_I)]$	$[\tau, \omega_{nm}, \zeta_{nm}]$
B	$[K_v, T_L, (T_I), \tau]$	$[\omega_{nm}, \zeta_{nm}]$
C	$[K_v, T_L, (T_I), \tau, \omega_{nm}]$	$[\zeta_{nm}]$
D	$[K_v, T_L, (T_I), \tau, \omega_{nm}, \zeta_{nm}]$	$[-]$

Prediction will essentially be formulated as an optimization problem; the set of cybernetic parameters that minimizes the cost function for a particular pair of weightings will be means of prediction. First, the identified individual cost function weightings from Step 2 will be used to define the cost function of a participant. Then, for each optimization case, the θ_{opt} values that minimize the *defined* cost function are computed. This optimization process will be carried out using MATLAB's *fmincon* function, as the ranges of values that the cybernetic parameters will be constrained. To ensure that all possible HCs will be encompassed, the upper bounds are set at double the maximum values in the experimentally measured data set for each parameter and the lower bounds are set at half the minimum measured values.

There are two approaches for these optimization cases; the parameters that are not predicted are either assumed at the average measured value for the specific experiment considered, or at the individual parameter value corresponding to the participant whose $K1$ and $K2$ values are used. Both approaches are followed to investigate the sensitivity to a priori assumed parameters.

Moreover, in order to avoid local minima, ten randomized initial conditions for the optimized θ are tested. These are generated by sampling from a uniform distribution based on the maximum and the minimum parameter values observed in each data set. This randomization process assumes the extremities of the data set as the extremities that could be observed in a population, and uniform distribution is used to consider a wide range of options and to avoid biases. For each participant-optimization case combination, the set of cybernetic parameters that correspond to the lowest cost among the ten initial conditions is taken as the result. Finally, the "predicted" sets of parameters are directly compared with the measured parameters to depict how the distributions fare against each other visually. This will make it possible to have an objective assessment on how realistic and reliable these predictions are. Step 4 will conclude which parameters could be accurately predicted using the cost function approach. The process is repeated with individualized values for θ_{con} (just like the individual case in subsection IV.C), to assess the validity of assuming them at the average values.

E. Step 4: Cybernetic Data Augmentation

The last step of analysis that is performed in this paper is to test the effectiveness of the individual cost function weightings as a data augmentation tool. In the previous step, the set of cybernetic parameters are predicted using the

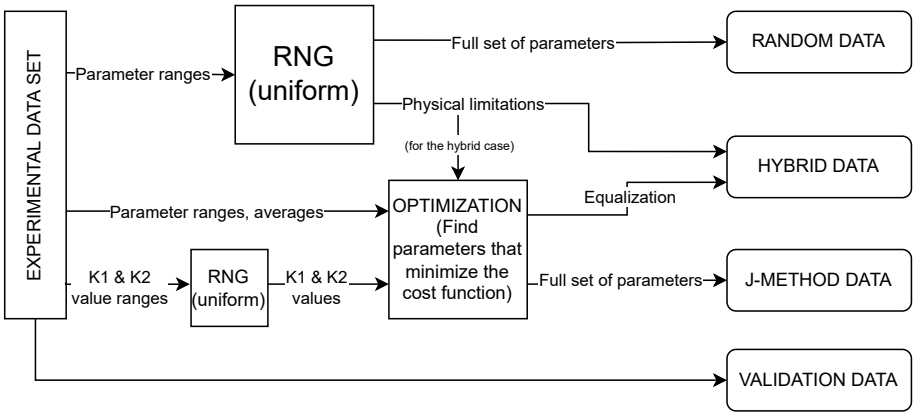

Fig. 3 Step 4 data generation cases

identified cost function weightings and in this step, a similar approach is followed to generate cybernetic parameter data for "simulated participants". The aim of this step is to generate "simulated participants" such that they resemble real-life data as closely as possible, and in turn could be used to augment data.

Data is generated using three data augmentation methods in this step (see Figure 3): fully random method, cost function method, and the hybrid method. The generated data contains 100 "simulated participants" for each case. The fully random method randomly generates parameter values by the uniform sampling method, where parameters are randomly sampled from a uniform distribution between the maximum and minimum parameter values in each data set, similar to how the initial conditions have been generated in the previous step. Since the exact distributions of cybernetic parameters among a population can't be replicated effectively, and the data available for each condition is limited, uniform distribution is preferred in this step. Thus, a fair and random set of "simulated participants" could be obtained with a simple method.

The cost function (J) method makes use of the cost function weightings and the optimization procedure outline in the previous step to generate sets of cybernetic parameters. The cost function weightings are selected randomly by using the maximum and the minimum value for each weighting and sampling in between that range. The $K1$ and $K2$ weightings are assumed to be uniformly distributed, as the randomness introduced by the uniform distribution could help avoid any bias towards any part of the range. Moreover, the lack of knowledge on the behavior of these weightings between participants support the assumption of a simple distribution over these variables. These cost function weightings are then used to define the exact cost functions to be minimized for each "simulated participant". The optimal sets of cybernetic parameters obtained as the outputs of this minimization are going to be the data generated using this method.

Finally, the hybrid approach follows a mix of the two: it generates equalization (including T_I for (III)) data using the cost function optimization and the remaining (physical limitations) parameters randomly. This method incorporates the assumption that the equalization is "selected" by the HC based on the control attitude and that the other parameters are intrinsically limited, by "optimizing" only the equalization based on the cost function and randomizing the rest. Furthermore, the procedure for the cost function method is heavily centered upon the equalization parameters, and thus the hybrid method would keep it methodologically consistent, as the weightings have also been identified from the equalization only.

These generated data are used to calculate the predicted sets of cybernetic parameters, and the corresponding σ_e, σ_u, and $\sigma_{\dot{u}}$ values for each case. These are plotted in histograms to compare the distributions. The experimental data that is relatively limited in quantity is also shown to provide a reference on the "realistic" range of values. The there data augmentation methods are then compared based on the sets of parameters and these distributions, to determine the strengths and weaknesses of each data augmentation approach. Overall, comparing these three methods and the real data could also provide an assessment on how "optimized", "random", and "real" human behavior compare, and which aspect each method lacks. This step thus shows how to best select parameters to augment data for simulations.

V. Results

A. Step 1: Sensitivity Analysis

1. Between-subject parameter variation

The variation in each cybernetic parameter between the participants is shown in an independent figure for each experiment. These variations are depicted based on how much individual parameters deviate from the average values, as box plots. Furthermore, individual participant parameter data are superimposed on the box plots with color coding in each figure. Figure 4 shows the variation in the identified cybernetic parameters of the participants for (I), Figure 5 for (II), and Figure 6 for (III). Plus, Table 3 shows the mean parameter values (to provide an overview on the orders of magnitude) and the interquartile range data for the three experiments.

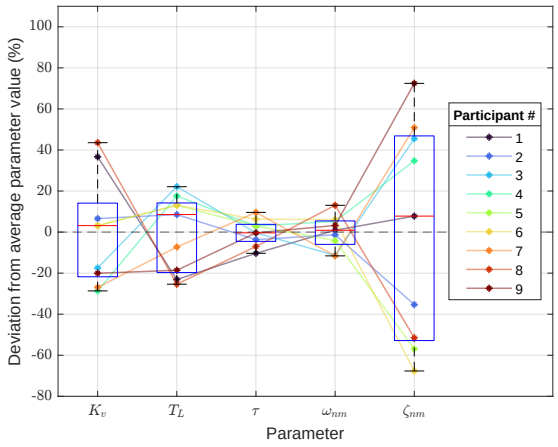

Fig. 4 Parameter deviation - (I)

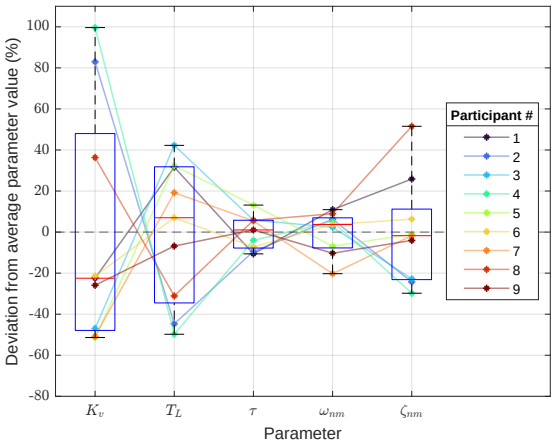

Fig. 5 Parameter deviation - (II)

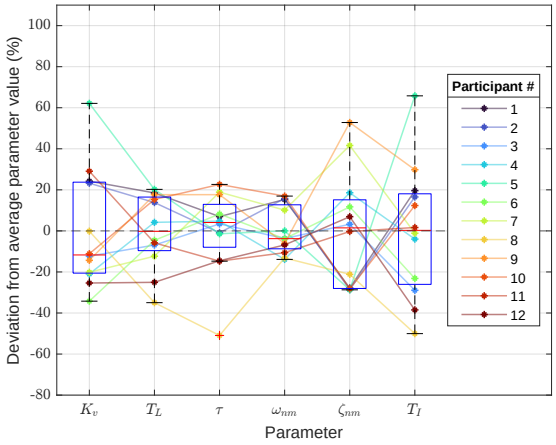

Fig. 6 Parameter deviation - (III)

These figures show that the three experiments show similar results when it comes to which parameters vary more and which ones vary less. τ and ω_{nm} (two of the three parameters labeled as "physical limitations") are the two parameters that show the least between-participant variation. All their data remain within ±20% range of the average value except for two τ data points from experiment (III): one being slightly above (22.64%), and another being a significant outlier (-50.94%). The latter could possibly be an identification error, since in HC a delay value of 0.10 is unusually low (see Tables 5 to 7). The similarity in trends imply that the variation in parameters are consistent throughout different controlled elements, even though the value ranges change. Even though the parameter magnitudes and distribution vary across the data sets, the same parameters become prominent in terms of between-participant deviation.

Table 3 Parameter averages and interquartile ranges from all three data sets

Parameter	Experiment (I)			Experiment (II)			Experiment (III)		
	Mean	Q1 (%)	Q3 (%)	Mean	Q1 (%)	Q3 (%)	Mean	Q1 (%)	Q3 (%)
K_v (-)	1.16	-21.78	14.11	0.17	-47.90	47.99	3.07	-20.58	23.74
T_L (s)	0.44	-19.72	14.20	2.83	-34.51	31.81	0.44	-9.62	16.48
τ (s)	0.30	-4.52	3.78	0.30	-7.78	5.77	0.21	-7.97	12.93
ω_{nm} (rad/s)	9.46	-5.98	5.44	7.39	-7.72	6.95	10.05	-8.73	12.72
ζ_{nm} (-)	0.19	-52.84	46.86	0.18	-23.16	11.20	0.26	-28.04	15.14
T_I (s)	-	-	-	-	-	-	1.39	-26.04	18.07

ζ_{nm} showed an unexpected amount of variation: as the remaining "physical limitation" parameter, the variation for this parameter was anticipated to be similar to those of other "physical limitation" parameters. The greatest variation was observed in experiment (I), with the interquartile range being 99.7%, for which ζ_{nm} is the parameter with the most between-participant variation. In the other two data sets, it showed less variation than the equalization parameters: interquartile ranges were 34.36% for (II) and 41.19% for (III). Such unforeseen behavior in ζ_{nm} highlights that "physical limitations" may also display significant between-participant variation.

The equalization parameters (i.e., K_v, T_L and T_I) indeed showed significant differences between participants. With the sole exception of ζ_{nm} in (I), K_v and T_L (and T_I) are in general the most person-dependent parameters, as expected. The difference between the maximum and the minimum value reaches 151% (K_v) and 92.02% (T_L) in (II). Lowest difference in such values is observed in (I): 72.2% (K_v) and 47.49% (T_L). On average, the difference in deviation between the equalization and physical limitation parameters is 33.84%: -1.72% in (I) *(this is heavily skewed by the extreme variation in ζ_{nm} in this data set; it would be 37.56% if ζ_{nm} is neglected)*, 76.08% in (II), and 27.15% in (III). A further observation from these parameters' box plots is that in some cases clear groupings of participants are seen: in (I), three K_v deviation values are clustered around 20%, three around 5%, and three around -20%. Similarly in (II), three participants have markedly high K_v (around 40, 80, and 100% deviation), while the rest are below -20%, reaching -50%. Moreover, the difference between the mean and the median is also significant for K_v, with the median value having a -20% deviation from the mean for (II) and -15% for (III). These results support the claim that equalization parameters are most strongly person-dependent, meaning that there is more dissimilitude between participants.

A final aspect to consider from these box plots is that the clusters in equalization parameters correlate to a considerable extent: K_v and T_L show correlations of -54.23% in (I), 92.81% in (II), and 43.52% in (III), with K_v and T_I showing 65.91% and T_L and T_I showing 87.96% in (III). The aforementioned 20% K_v deviation cluster in (I) is also present as the three participants with the most negative deviation from the mean in T_L. Similar trends are also seen in (II), again with the three participants that have a high K_v having a lower T_L compared to the rest. In (III), this relationship gets more complicated due to the introduction of another equalization parameter (T_I), but correlations remain: the same five participants with the highest T_L also have the five highest T_I values. Theoretically, this could be explained by certain participants compensating for lower frequencies, as a lower gain and higher lead simply means that the differentiator dynamics start at an earlier frequency. A conclusion that could be drawn from these results is that clear "controller types" are observable in the cybernetic parameter data as an indicator of individual differences.

2. Effect of cybernetic parameter variation on error and control signals

The next step of analysis focused on how much these deviations from the averages impact the the e and u signals that are, respectively, the input and output of the LTI HC model (see Figure 1). Based on the observations from Figures 4 to 6, each parameter was varied within a ±30% range (a factor of 0.7-1.3) of the average value for the sensitivity analysis. This value was picked semi-arbitrarily, considering that in only 3/16 cases (K_v and T_L in (II) data and ζ_{nm} in (I) data) the interquartile range exceeded these limits. The sensitivity analysis plots showing the percentage difference in σ_e, σ_u, and $\sigma_{\dot{u}}$ for the separate variations of each parameter are given in Figure 7.

This figure shows that the variations in parameters mostly have similar effects on σ_e, σ_u, and $\sigma_{\dot{u}}$ for the different experiments. The double integrator controlled element in experiment (II) could be focused on in particular, as the effects are most extreme. For example, σ_e sensitivity for K_v already causes more than 30% change within ±20% K_v deviation

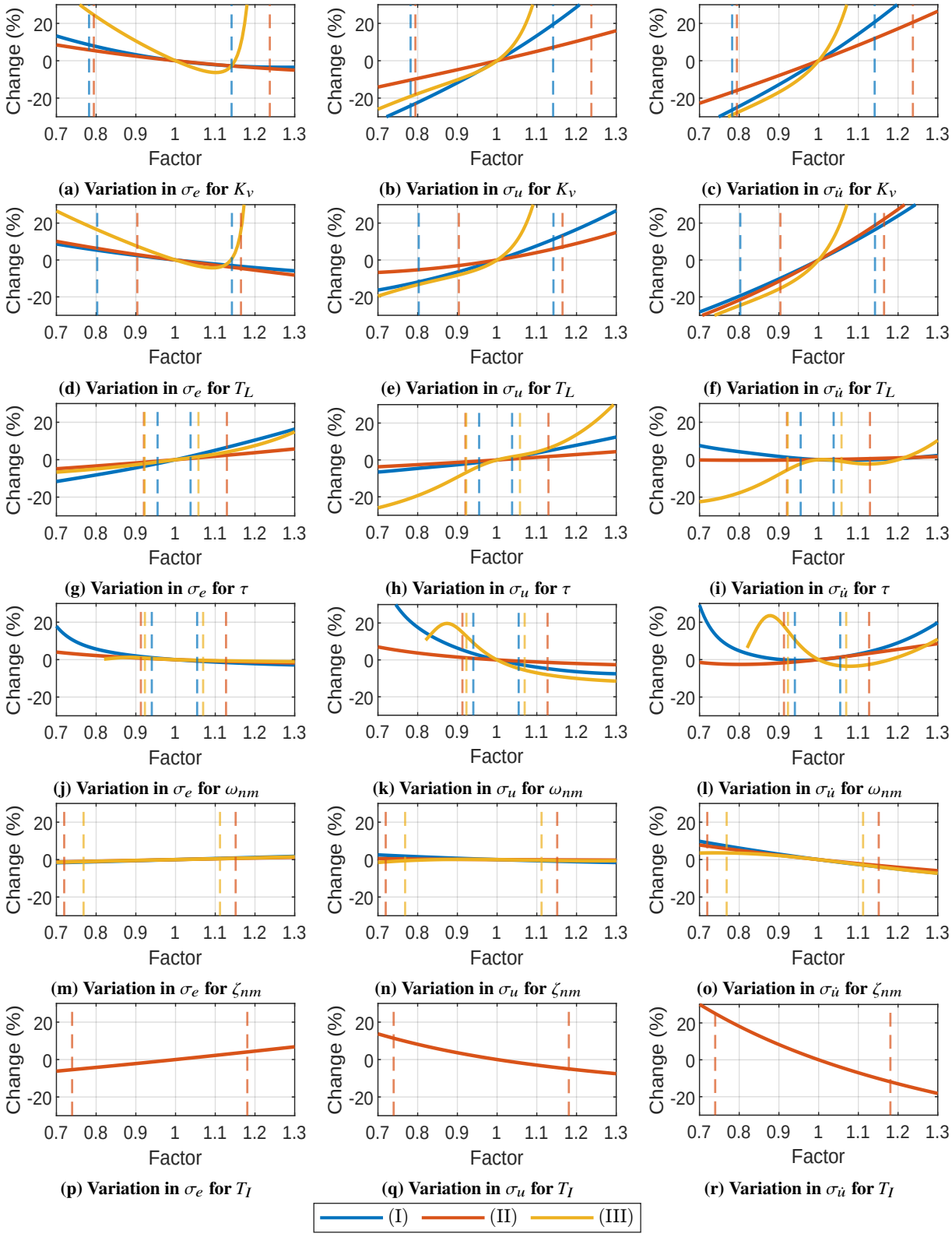

(a) Variation in σ_e for K_v (b) Variation in σ_u for K_v (c) Variation in $\sigma_{\dot{u}}$ for K_v

(d) Variation in σ_e for T_L (e) Variation in σ_u for T_L (f) Variation in $\sigma_{\dot{u}}$ for T_L

(g) Variation in σ_e for τ (h) Variation in σ_u for τ (i) Variation in $\sigma_{\dot{u}}$ for τ

(j) Variation in σ_e for ω_{nm} (k) Variation in σ_u for ω_{nm} (l) Variation in $\sigma_{\dot{u}}$ for ω_{nm}

(m) Variation in σ_e for ζ_{nm} (n) Variation in σ_u for ζ_{nm} (o) Variation in $\sigma_{\dot{u}}$ for ζ_{nm}

(p) Variation in σ_e for T_I (q) Variation in σ_u for T_I (r) Variation in $\sigma_{\dot{u}}$ for T_I

Fig. 7 Sensitivity analysis for $\sigma_{\mathbf{e}}$, $\sigma_{\mathbf{u}}$, and $\sigma_{\dot{\mathbf{u}}}$ for the three experiments

(Figure 7a), while in both other experiments an increase in K_v causes a decrease in σ_e, which is around 5%. This is also seen in the σ_u and $\sigma_{\dot{u}}$ sensitivity to ω_{nm} plots (Figures 7k and 7l), with notable fluctuations occurring around -15% deviation from the mean. These reach up to 13% and 15.49% changes for σ_u and $\sigma_{\dot{u}}$. It must also be mentioned that for (II), the ω_{nm} value could not be varied to less than -18% of the mean, as the system becomes unstable. However, as could also be seen in Figure 5, one participant actually has an ω_{nm} value beyond this limit and stability in this case is compensated via other parameters. This indicates that individualizing the parameters for the double integrator task in (II) is particularly crucial, as parameter deviations have more adverse effects.

These plots could conclude that the equalization parameters K_v and T_L (and T_I) have the most significant impact, especially when the interquartile ranges are considered. In (II), the change percentages go beyond the limits set at 30% for all three signals even before the parameter is increased to 20% more than the mean value (and when K_v is decreased beyond 80% of the mean for σ_e, Figure 7a). Similarly, σ_u and $\sigma_{\dot{u}}$ plots also reach beyond -20% change before the interquartile range is reached. Combined with the previous findings that the equalization parameters are the most person-dependent, the fact that they also cause the greatest impact on e and u verifies the assumption that the equalization is considerably more influential, though not exclusively, for linking the cybernetic parameters and the HCCF than the "physical limitations".

Except for these parameters, τ shows significant changes beyond the interquartile ranges, with the most extreme values observed within this range being -6.84% (Figure 7h, (II)) and -5.41% (Figure 7i, (II)). For the rest, the sensitivity for τ at the interquartile ranges have been below 2.5% in all occasions. ζ_{nm} has little effect on all except $\sigma_{\dot{u}}$, especially for σ_e and σ_u, never causing more than 2.5% (Figure 7n, (I)) change in any of the data sets at the interquartile ranges, despite having a large range. The impact is more for $\sigma_{\dot{u}}$, but remains below 10% change (reaching 9.78% at most, Figure 7o, (I)). Another observation that must be pointed out is that the equalization parameters' impact on e and u is balanced: an increase in K_v or T_L causes a decrease in σ_e but increases in σ_u and $\sigma_{\dot{u}}$. This is not the case for the "physical limitations" as the sensitivity of e and u to changes is consistent (e.g., a decrease in τ decreases both σ_e and σ_u). These results reflect that, across a realistic range of parameter variations, the "physical limitations" have a limited, yet consistent influence on e and u. Therefore, it could be deduced that changes in the physical limitation parameters are scarcely observable from the HCCF.

B. Step 2: Estimating Individual Cost Function Weightings

Examples of cost maps explained in subsection IV.C are presented next. Figure 8 shows two example cost maps using (I) data, Figure 9 using (II) data, and Figure 10 using (III) data (Complete sets of cost maps could be found in report Appendix C). These examples are picked to depict the most and least successful identification cases for each data set. In Figures 8 to 10, the red circle indicates the minimum cost function point for when both cost function weightings are zero (minimum tracking error). The solid green marker shows the measured equalization point while the solid red marker is the estimate. The dashed lines indicate the limit-case operating points for when either the σ_u or $\sigma_{\dot{u}}$ weightings ($K1$ and $K2$, respectively) are set to zero, and the other weighting is increased incrementally. In all three cases, the line on the right-hand side represents a cost function with the σ_u term only ($K2 = 0$), and the line on the left-hand side represents a cost function with the $\sigma_{\dot{u}}$ term only ($K1 = 0$).

Here, the identification "success" is based on how close the identified equalization point (red dot) is to the actual equalization point (green dot). Table 4 displays the $K1$ and $K2$ values for all participants in the three experiments for the average θ_{con}. The italicized values correspond to the actual equalization point falling outside the area between the dashed lines, and a close estimate being taken for the weightings (e.g, Figures 8b, 9b and 10b). This means that the control strategy of these participants could not be fully identified with the cost function weightings, as none of the tested $K1$ and $K2$ values lead to a cost function for which those participants' equalization values are optimal. This implies that the HCCF does not reflect that control strategy of these participants effectively.

The results of the individual cost function weighting identification procedure indicate mixed outcomes for the method: overall, the majority (18/30: 6/9 in (I), 3/9 in (II), 9/12 in (III)) of the participants' equalization points could directly be identified with the cost function weightings. Plus, the identified $K1$ and $K2$ values also show distinct properties in different experiments: In (I), this is characterized by very low $K1$ values (0, 0.01, or 0.007 1/rad), and vice versa in (II); $K2$ value being 0 (or 0.03 s/rad in for participant 9) and $K1$ value being near 2. The examples in Figure 8b and Figure 9b give an accurate depiction of why this is the case: in (I), the 3 participants with equalization points outside the dashed lines all have it to the top left of the $K2$ line ($K1 = 0$) and the 6 participants with the same situation in (II) have it to the bottom right of the $K1$ line ($K2 = 0$) with the "elbow" point (where the red dot is in Figure 9b) being identified as the best estimate for them (see Figure 8b). This indicates a clear limitation of the cost

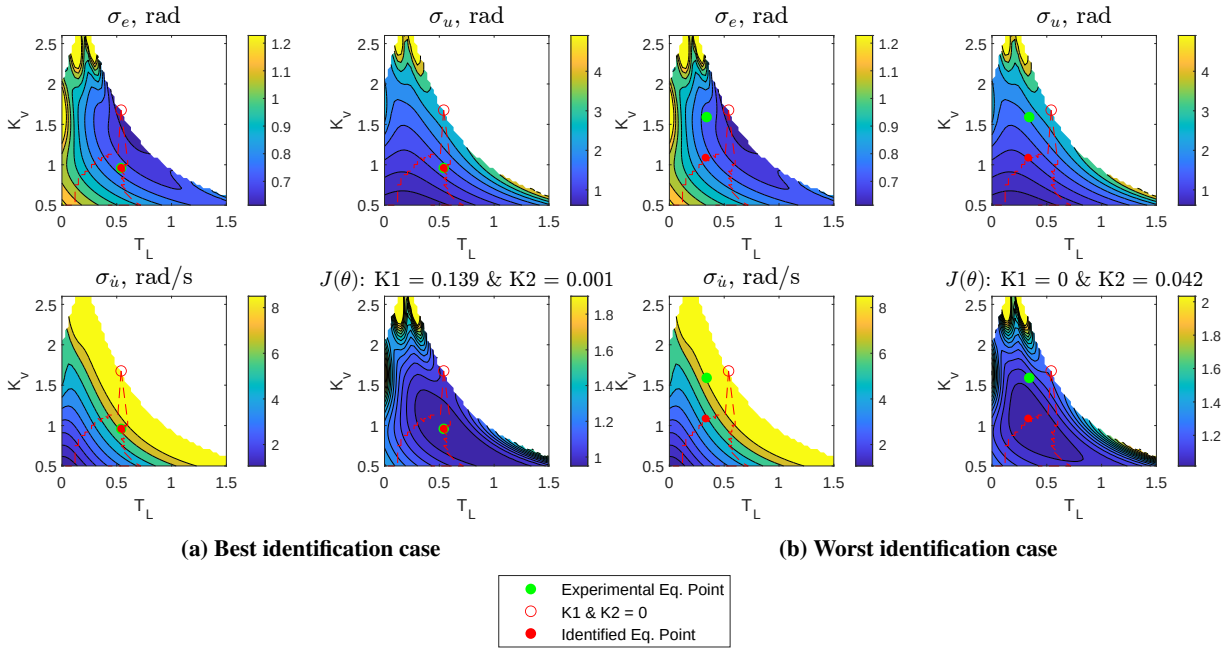

(a) Best identification case **(b) Worst identification case**

Fig. 8 Examples of cost maps - Exp. (I)

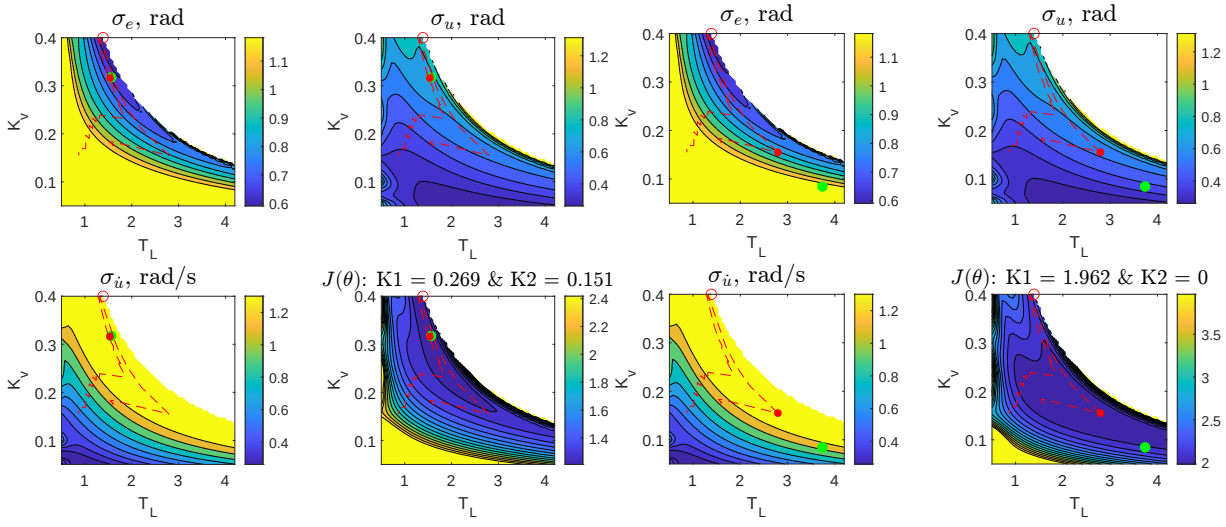

(a) Best identification case **(b) Worst identification case**

Fig. 9 Examples of cost maps - Exp. (II)

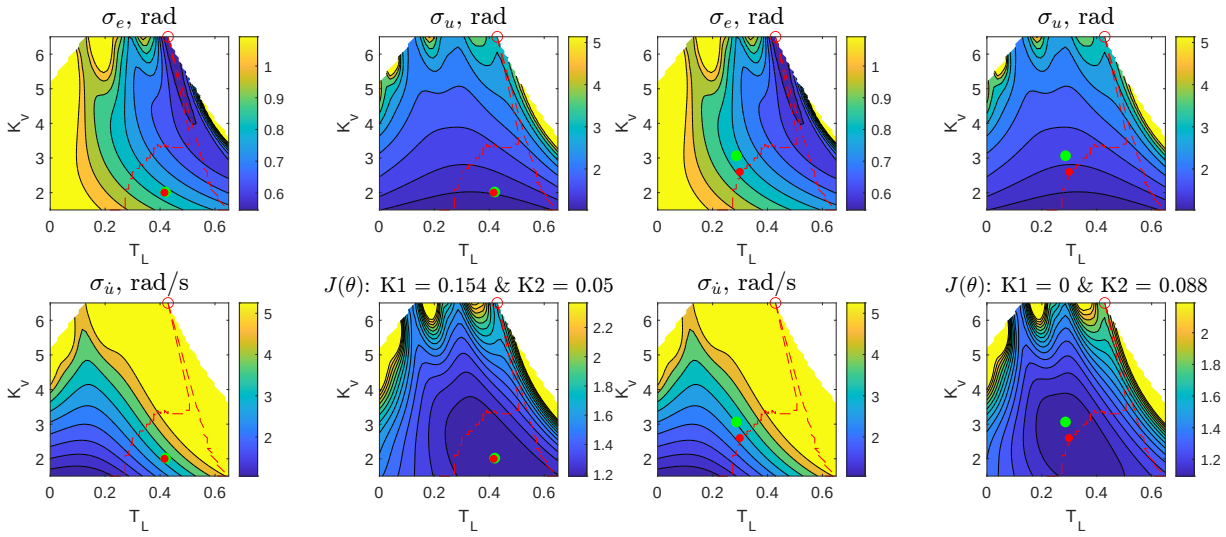

(a) Best identification case **(b) Worst identification case**

Fig. 10 Examples of cost maps - Exp. (III)

Table 4 Identified individual cost function weightings for all three data sets, italics indicate estimates

Participant #	Experiment (I)		Experiment (II)		Experiment (III)	
	K1 (1/rad)	K2 (s/rad)	K1(1/rad)	K2 (s/rad)	K1 (1/rad)	K2 (s/rad)
1	*0.000*	*0.042*	*1.962*	*0.000*	0.008	0.011
2	*0.007*	*0.017*	0.269	0.151	0.008	0.011
3	0.139	0.001	*1.962*	*0.000*	0.094	0.034
4	0.230	0.003	0.077	0.198	0.146	0.027
5	0.010	0.014	*1.962*	*0.000*	*0.049*	*0.003*
6	0.010	0.014	*1.962*	*0.000*	0.154	0.050
7	0.211	0.020	*1.962*	*0.000*	0.100	0.047
8	*0.000*	*0.042*	0.984	0.029	*0.000*	*0.088*
9	0.125	0.033	*1.830*	*0.032*	0.145	0.009
10	-	-	-	-	0.118	0.012
11	-	-	-	-	*0.000*	*0.027*
12	-	-	-	-	0.055	0.082

function identification method. Even when the individualized parameters are used (see report Appendix C), only 3/12 failed cases improve while two of the successful cases fail. A logical outcome is that this limitation in identification lies within the cost function-equalization link itself, and not in the assumption to reduce it down to the average values.

While these results could seem like the diversity in control attitude among the participants have diminished in this step, it is worth noting that the equalization values of these participants have also been similar. For example, participants 5 and 6 in (I) have the same equalization values (see Table 5 in the Appendix) and being identified with the same cost function weightings verifies method consistency. The same can be said for participants 1 and 8 in the same data set and for participants 1 and 2 in (III) (see Table 7 in the Appendix). Certain participants with similar equalization values being identified with the same weightings highlights that albeit consistent, the utilized method is not effective in capturing such subtle differences in cybernetic parameters. It is also worth noting that while the latter pair also exhibit very similar values for the physical limitation parameters, the other two pairs have considerably different sets of values (Par. 1: τ = 0.27 s, ω_{nm} = 9.54 rad/s, ζ_{nm} = 0.20 - Par. 8: τ = 0.28 s, ω_{nm} = 10.69 rad/s, ζ_{nm} = 0.09 and Par. 5: τ = 0.31 s, ω_{nm} = 9.06 rad/s, ζ_{nm} = 0.08 - Par. 8: τ = 0.32 s, ω_{nm} = 10.03 rad/s, ζ_{nm} = 0.06), and this has been ignored in the weighting identification step. While the extent to which individual differences could be quantified with the cost function weightings has been found to be substantial, it does not capture the full breadth of inter-personal cybernetic parameter variation, as evidenced by the participants with the same weightings.

It could be concluded based on these results that predicting individualized cost function weightings have blunted the differences observed between participants, even though the $K1$ and $K2$ values have been discretized finely (discretization step size of 0.001). Although a logical outcome from these results could be that the cost function weightings do not fully capture the individual differences observed in the cybernetic parameters, whether or not the uniformity in the weightings causes a drawback could be more effectively concluded with the next analysis steps, i.e., the cost function weightings could still be effective for generating realistic "simulated participants" for offline simulation studies. Additionally, the uniformity observed in the $K1$ and $K2$ values further builds up on the groupings previously seen in the parameter variation plots in subsection V.A: the set of participants for which the $K1$ and $K2$ values are the same show distinct features in their equalization values (e.g., low-gain & high-lead time constant). This suggests that categorization of HCs could be useful to observe individual differences and that certain differences are ignored due to over-generalization, while trying to encompass a broad range.

C. Step 3: Predicting Cybernetic Parameters

As mentioned earlier in subsection IV.D, the set of parameters that results in the lowest cost (see Eq. (4)) for each participant, and in each optimization case (see Table 2), are collected as results. These are then displayed in box plots, with each plot representing a parameter and each box representing a different optimization case. For cases in which a parameter is not predicted, the corresponding column is shaded and the assumed constant value is marked. A box showing the original parameter value distribution was also added, to enable direct comparison with the original, "realistic" reference values. Figure 11 shows the prediction results for (I), Figure 12 for (II), and Figure 13 for (III). The dashed lines manifest the ±30% deviation-from-the-mean range considered in subsection V.A. Plus, the same plots for the individual case (as explained in subsection IV.D) could be found in report Appendix D, where the similarity in results is seen.

Figures 11 to 13 show that this method could only partially replicate the realistic cybernetic parameter distribution. Prediction distribution of K_v and T_L values (when only they are predicted) have covered similar ranges as the original parameter distribution, as the locations and extents of the boxes are congruent (Wilcoxon signed-rank tests have resulted in an average p-value of 0.056). However, the below-average K_v - above-average T_L group of cases have not been covered extensively for (II). This is the expected result as these K_v and T_L values have been the only real data inputs that have been used in the prediction. The introduction of T_I slightly disturbs prediction accuracy for (III); predicted T_I values are consistently lower (44.28% on average) than the original range, and this has in turn resulted in the K_v and T_L predictions to be lower as well (29.29% and 18.70% on average, respectively), implying that the parameters are related and any inaccuracy in one causes inaccuracies in the others too, which is expected.

Predictions including the "physical limitation" parameters are significantly less accurate: In many cases (such as for τ and ζ_{nm} whenever predicted, and for ω_{nm} when all are predicted in (I) and (III)) the optimization's first results corresponds to a constraint (upper limit for ζ_{nm} and ω_{nm}, lower limit for τ). Similar cases could be seen in (II) too; although τ avoids the limit value and ζ_{nm} and ω_{nm} show some variation, the generated values remain unrealistic when put side by side with the experimental values. On average, the deviations from the experimental values are 56.06% (τ), -94.43% (ω_{nm}), and -170.34% (ζ_{nm}). This is also seen with the black dashed lines previously determined to show a

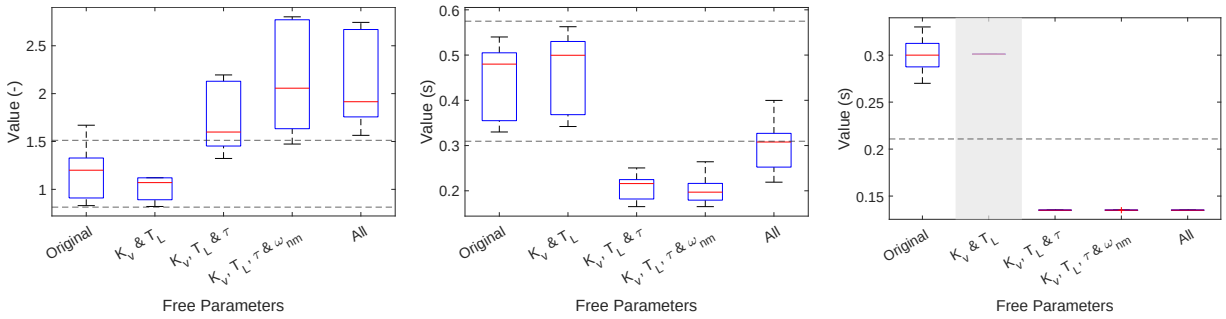

(a) Prediction plots for K_v **(b) Prediction plots for T_L** **(c) Prediction plots for τ**

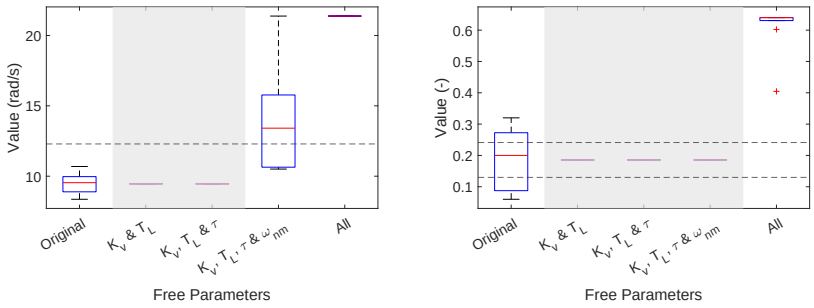

(d) Prediction plots for ω_{nm} **(e) Prediction plots for ζ_{nm}**

Fig. 11 Prediction plots for Exp. (I)

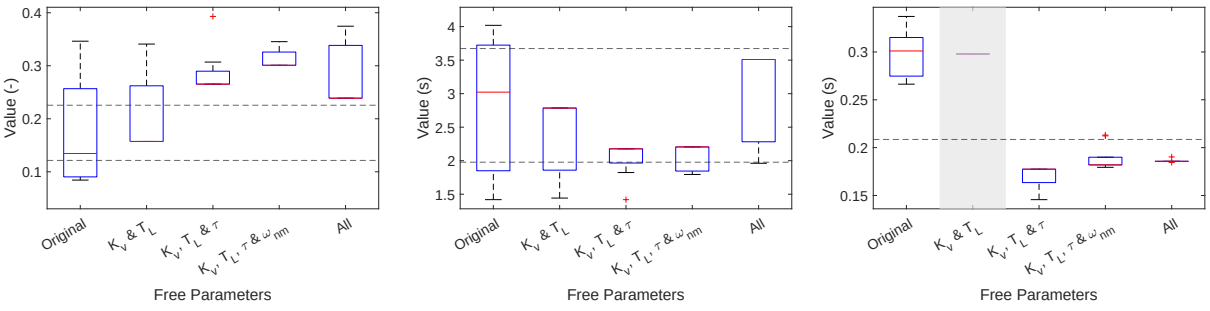

(a) Prediction plots for K_v **(b) Prediction plots for T_L** **(c) Prediction plots for τ**

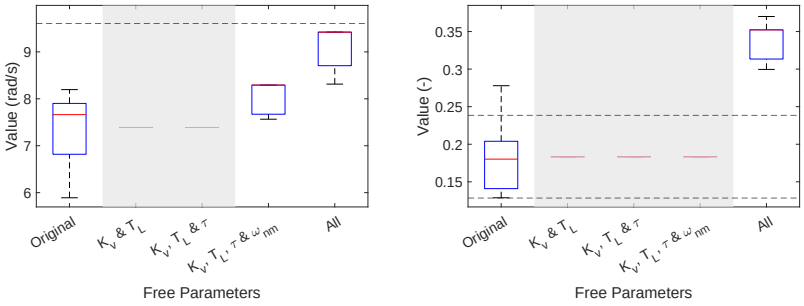

(d) Prediction plots for ω_{nm} **(e) Prediction plots for ζ_{nm}**

Fig. 12 Prediction plots for Exp. (II)

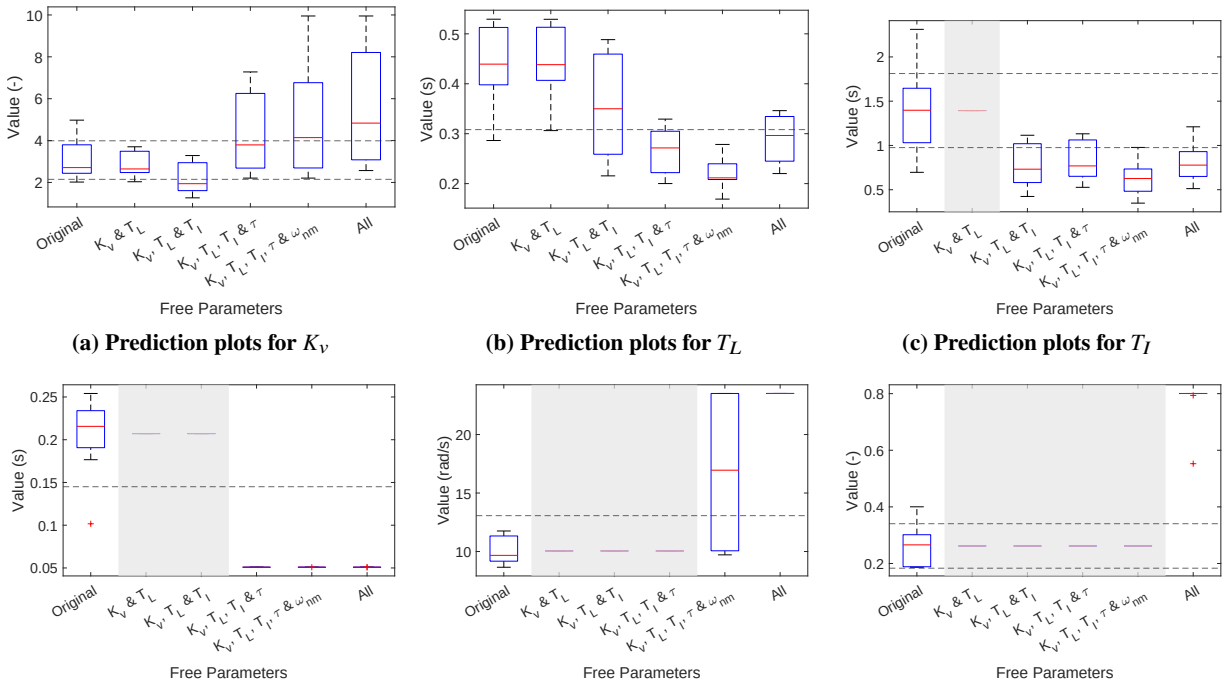

(a) Prediction plots for K_v **(b) Prediction plots for T_L** **(c) Prediction plots for T_I**

(d) Prediction plots for τ **(e) Prediction plots for ω_{nm}** **(f) Prediction plots for ζ_{nm}**

Fig. 13 Prediction plots for Exp. (III)

realistic deviation range (±30% from average). As explained previously, this causes a domino effect that results in other parameters being inaccurately predicted as well. In order to understand these results, the earlier findings that show how the "physical limitation" parameters impact the cost function components in Figure 7 must be examined. Even though the predicted values to way beyond the realistic ±30% range considered, sensitivity trends observed in Figure 7 give an idea on why the optimization results are such. The sensitivity analysis shows that τ, ζ_{nm}, and ω_{nm} have a less significant impact on the σ_e, σ_u, and $\sigma_{\dot{u}}$ values; it is apparent that reducing τ and increasing ζ_{nm} and ω_{nm} lead to a much lower σ_e and hence a lower overall cost function value. This is because the aforementioned changes in each value reduce all components (σ_e, σ_u, and $\sigma_{\dot{u}}$) of the cost function without having any consequences in terms of stability and thus for the cost function it is optimal to have τ, ζ_{nm}, and ω_{nm} as extreme as possible. A result that could be drawn from this is that the cost function weightings are not effective in predicting physical limitations parameters.

An outcome that needs to be addressed is the uniformity in the predicted parameter values. In the optimization cases where K_v, T_L, τ (and ω_{nm}) are predicted, the boxes for K_v (Figure 12a) and T_L (Figures 11b and 12b) are unusually small. The expectation was for these parameters to have the most variation, but the predictions results do not display this case. This could in turn be attributed to the uniformity in the $K1$ and $K2$ values in these data sets. A significant portion of participants (5/9 (I), 6/9 (II)) have very close (if not the same) identified cost function weightings. This results in very similar conditions being optimized, especially as the number of parameters increase. The extreme levels reached in the "physical limitations" could also have an impact on this situation: the small variation observed in the predicted K_v and T_L are on the extreme ends of the experimentally observed range. Thus it could be said that extremities in τ (and ω_{nm}) result in the "optimal" equalization values to be extreme as well. Moreover, it is known that changes in K_v and T_L have opposite effects on e and u, and hence extreme values in physical limitations could further limit the variation in finding the "optimal" solution. It is due to a variety of reasons that the predictions remain in a limited range of anomalous values, and analyses (such as those conducted in Steps 3 & 4) exploring these extreme conditions are necessary to observe the precise behavior of these parameters.

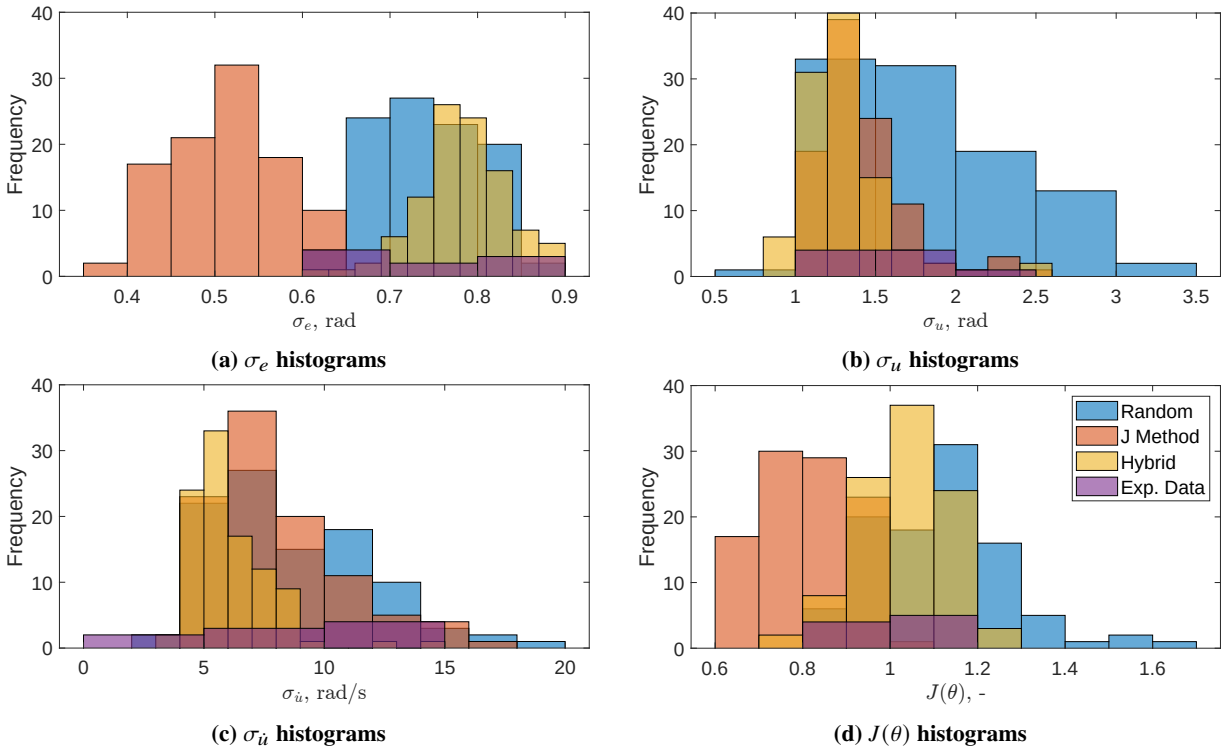

(a) σ_e **histograms** **(b)** σ_u **histograms**

(c) $\sigma_{\dot{u}}$ **histograms** **(d)** $J(\theta)$ **histograms**

Fig. 14 σ_e**,** σ_u**, and** $\sigma_{\dot{u}}$ **histograms comparing data augmentation methods - Exp. (I)**

D. Step 4: Cybernetic Data Augmentation

The histograms showing how the σ_e, σ_u, and $\sigma_{\dot{u}}$ values obtained using various data augmentation methods are presented in this section. For all histograms, four types of data are shown: fully random data, cost function method (J) data, hybrid method data, and the experimental data (see subsection IV.E). For the first three cases, 100 sets of cybernetic parameters are generated each, although the number of data plotted in histograms are less if a parameter set results in the system being unstable. The experimental data only contains results from 9 participants and therefore the corresponding bins in the histogram are much smaller compared to the others. This data is used to validate the *range* of values, and not necessarily the *distribution*. Figure 14 depicts the histograms for experiment (I). The histograms for (II) and (III) can be seen in Figures 16 and 17 in the Appendix. Unstable sets of parameters were expected (especially in the fully randomized case), although in (I) none of the generated "simulated participants" ended up causing an unstable system. However, 43/100 fully randomized "simulated participants" resulted in an unstable system in (II), and this number was 4/100 in (III) (These could be seen as the "gaps" in Figures 16 and 17). None of the "participants" simulated using other methods caused an unstable system in any experiment.

These results are consistent with the takeaways from the previous step: the cost function method indeed optimizes the cybernetic parameters beyond realistic boundaries, as the σ_e values for the cost function method is much lower (mean = 0.51 rad) than the real values (mean = 0.75 rad). The random (mean = 0.74 rad) and the hybrid (mean = 0.78 rad) methods give a more realistic range of σ_e in this case (see Figure 14a). The difference in σ_e values explain why the total cost values for the cost function method are lower than the others (see Figure 14d), since the cost function method does not perform better than the others in σ_u and $\sigma_{\dot{u}}$ metrics (see Figures 14b and 14c). This indicates that the "performance" aspect (the task objective) is the most critical component in the cost function. How the σ_e component in particular is much lower could be explained by the generated cybernetic parameters: the discrepancy between the cost function and the hybrid methods point out to the "physical limitations", as those are not fully optimized in the hybrid case.

It is observed in the cybernetic data (see report Appendix E) that for all the "simulated participants" generated using the cost function (J) method, the "physical limitation" parameter values are equal to the set parameter bounds (as was also seen in Figure 11). Furthermore, since the limits were set so broadly (lower limit at half the minimum value,

and upper limit at double the maximum value), it is practically impossible to obtain values that are even close in the randomized or experimental data. The differences (exp. means: τ = 0.3011 s, ω_{nm} = 9.4556 rad/s, ζ_{nm} = 0.1856 (-) - opt. means: τ = 0.1358 s, ω_{nm} = 20.7914 rad/s, ζ_{nm} = 0.6110 (-), see Figure 11) between the optimized and randomized physical limitation parameters explain why the σ_e histogram for the cost function method is shifted to the left. This explains how the cost function method optimizes parameters beyond the intrinsic limitations.

Supporting this are the corresponding phase margin and crossover frequency data. While the average phase margins for all four cases are similar (exp.: 58.18° , random: 51.76°, cost function: 53.69°, hybrid: 63.60°), the average crossover frequency for the cost function method is almost 1.5 times higher than that observed in the experimental data set (2.98 rad vs. 2.03 rad). Even though an increase in crossover frequency and a decrease in the phase margin is expected, such a large difference is unusual. Achieving a high level of performance while maintaining the phase margin at a comfortably stable level and increasing the crossover frequency could only be explained by the unrealistic delay values reached with the cost function method.

In the σ_u histogram, the randomly generated data has more outlier cases, although the average resembles the experimental data better. The cost function method having lower σ_u values overall supports the claim that the optimization results in a "superhuman" behavior where better performance is achieved with less effort than humanly possible. Another interesting finding is that the hybrid approach results in a comparatively high σ_e (hybrid mean = 0.78 rad, exp. mean = 0.75 rad) and low σ_u (hybrid mean = 1.30 rad, exp. mean = 1.60 rad). This could be explained by the discrepancy in the $K1$ weightings: the randomly generated $K1$ values have a mean (0.1082 1/rad) that is 33% higher than that of the experimental $K1$ values (0.0813 1/rad). This could be because $K1$ values are generated uniformly while the experimental values are skewed towards the lower values. This results in the hybrid optimization focusing much more on getting a lower σ_u value than the participants of the experiment, as it is a more important component in the overall cost function. Even though the σ_u values for the experimental case are higher, they still contribute less in the cost function when adjusted with the weightings (average $K1 * \sigma_u$ values: 0.098 (-) vs 0.1464 (-)). Such difference in $K1$ values is because $K1/K2$ values are sampled from a uniform distribution whereas the limited experimental data in experiment (I) is not uniformly distributed.

Finally, the hybrid method results show the narrowest range in the $\sigma_{\dot{u}}$ (see Figure 14c), as 95% of the values are within the interval between 4 and 9 This could be another indicator that the cost function procedure does not fully encompass the diversity in HCs: the range it considers as "optimal" is only a portion of the range that humans consider as "optimal". Just like the σ_u plot, the cost function method is to the left of the random method and the hybrid method is to the left of both.

While it is sensical that the fully randomized cases have higher σ values, as the other two methods have included explicit minimization based on the cost function, the difference between the cost function and the hybrid methods is nontrivial. Since the hybrid approach only selects the optimal K_v and T_L values and that these values have conflicting impacts on e and u (see subsection V.A), the hybrid approach seems to "sacrifice" the σ_e component of the cost function in order to improve the total cost value via the "effort" components. This is also fortified by the findings in Figure 15, where how the cost function components add up and compare could be seen. (See Figures 18 and 19 in the Appendix for the other two experiments.) It is shown in Figure 15 that the average total cost values (indicated with the black line) for the experimental and hybrid data sets are almost identical, the average σ_e value is lower in the experimental data (0.75 vs. 0.78 rad), while the sum of the "effort" components ($K1 * \sigma_u + K2 * \sigma_{\dot{u}}$) is lower in the hybrid data (0.27 vs. 0.25 -). Finally, by mitigating the unrealistic values observed in both the random and cost function methods, the hybrid method resembles the real range of σ values the most closely overall. The hybrid method is thus the most accurate and feasible for data augmentation purposes.

VI. Discussion

This paper focuses on the importance of personalized HC models, to understand and describe individual differences in the HC balancing of performance and effort when performing manual control compensatory tracking tasks. Previous studies have outlined a need for personalized support in human-machine systems, and individual cybernetic data is of critical importance to realize this [3, 10]. Even though it is possible to use various techniques to identify the personal parameters in cybernetic HC models, the availability of this data is constrained by the availability of participants, and the experiments being done already. Thus, a demand for predicting individual parameters is identified. It had been shown previously [16, 20, 21, 38] that the equalization component of the cybernetic HC model carries greater relevance to individual differences compared to the other parameters generally labeled as "physical limitations". These were validated in this study, as it was confirmed that the equalization parameters show greater variation between participants

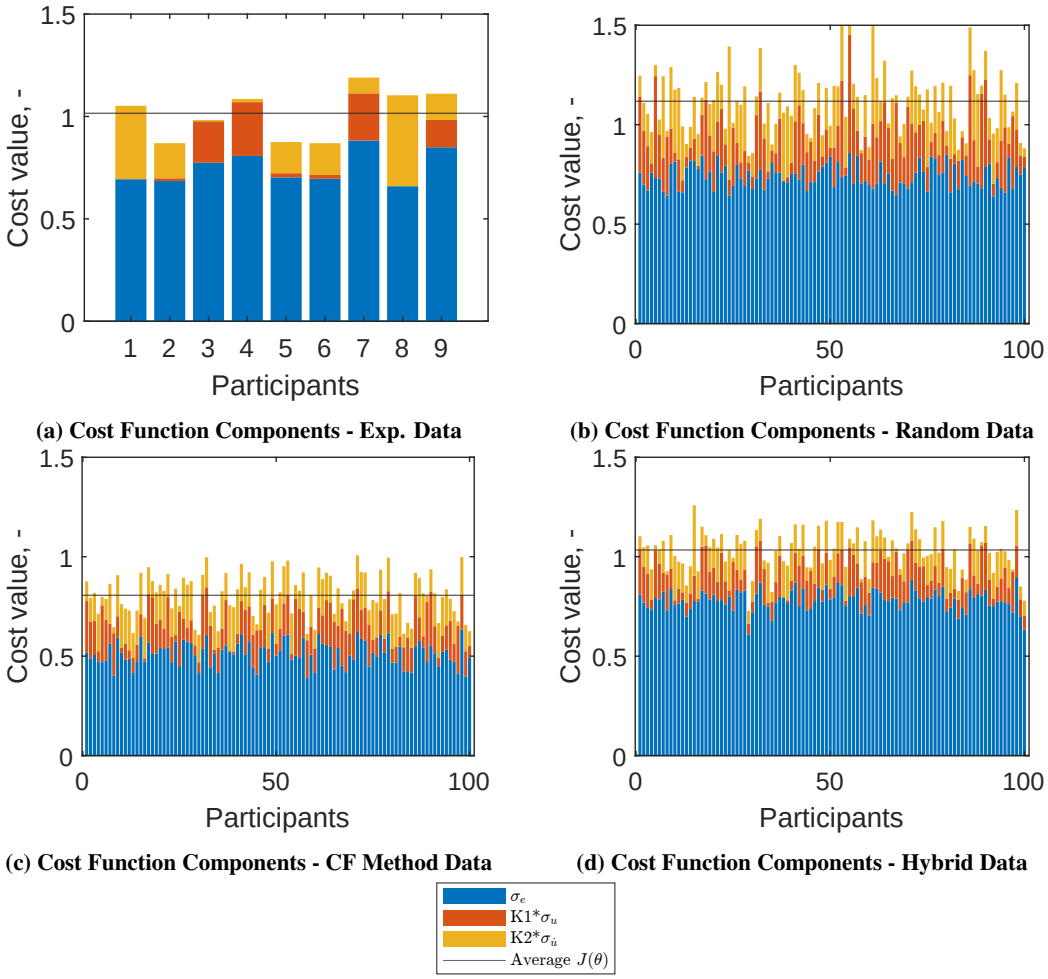

(a) Cost Function Components - Exp. Data

(b) Cost Function Components - Random Data

(c) Cost Function Components - CF Method Data

(d) Cost Function Components - Hybrid Data

Fig. 15 Cost function component breakdown - (I)

than the limitation parameters, while these variations also cause a greater impact in the tracking error and the control input signals. The three experiments considered in this paper all affirm this conclusion.

It has been formulated to utilize the input and output signals of the HC (representing "performance" and "effort") in order to define a "human controller cost function" (HCCF). This cost function can quantify the HC attitude towards the control task and how the HC would balance the "performance" and "effort" terms would be achieved by weightings. Given the inherent nature of the physical limitation parameters, previous work used the HC equalization parameters to predict these weightings [21]. However, this was limited to the "average" controller, and this paper outlined a method to identify individual cost function weightings. While this identification procedure was successful for most participants, certain groups of participants with similar characteristics (e.g., low gain, high lead) was not identified effectively and estimates were made. These estimates caused a notable drawback as the estimated individual cost function weightings were much alike (if not identical) and eroded the diversity. Thus, it is concluded that it is not possible to fully characterize individual HCs using the cost function weightings, at least for the cost function formulation used in this paper and earlier [12–24]. In other words, the HCCF, in its current formulation, does not allow for individualization.

The ineffectiveness of the used cost function method only for participants of similar traits suggest that perhaps an earlier classification of HCs would be useful. Categorizing HC into binary options (e.g., skilled vs. unskilled) have been common, and these categories have been associated with the equalization: pilot gain [37], or its proposed alternative, pilot bandwidth [38]. The analysis in this paper has also showed that there's a significant correlation between the equalization parameters. This supports the pilot bandwidth concept first presented by Doman [16], and then propounded by Mitchell and Klyde [38, 39], implying that the relationship between the equalization parameters

must not be neglected. Nonetheless, the analysis here has shown that the personalization of the remaining parameters should also be taken into consideration, as they have both considerable inter-dependencies and a notable impact on the system output. These findings suggest that further research on classification/clustering HC is necessary to understand individual differences. This would also provide support for research on HQR, where HCs are effectively categorized (e.g., Cooper Harper and Bedford scales) [26]. Given the use of HCCFs in this field before [25, 27], such work on HC classification would also provide insights into how the cost function could be most effectively formulated, in order to align it with the HQR scales. Moreover, data analysis techniques (e.g., k-means clustering) could be used to group HCs and these groupings could also provide insights for personalization.

This research made use of data from three previous experiments and based on the results, it is safe to say that using multiple data sources is crucial for studying individual differences. While in some parts of the paper the results seemed redundant (e.g., Step 4), acquiring results for three different data sets highlighted aspects that are common and must be paid attention to (e.g., high variation in equalization parameters) and other aspects that are observed only for a certain controlled element (e.g., 6/9 participants having the same weightings in (II)). Therefore, it is recommended for similar studies to analyze multiple sources of data, as biases cannot be eliminated even for a "perfect" experiment. Nevertheless, studying too many experiments could be repetitive. It can be seen in this paper that some results overlap and the different experiments considered reiterate conclusions. Moreover, having additional experiments to analyze could also cause certain points to be missed, and therefore it is safe to say that there is negligible marginal benefit for this research from more data. For future work that also aims to establish a novel method in cybernetics, it is recommended to examine data that have considerably different controlled elements, causing different magnitudes in the cybernetic parameters, to avoid statistical biases.

The prediction step used in this study effectively worked as a validation technique, to see if the cost function method could replicate its cybernetic parameter inputs via the cost function weightings. The results indicate a deficiency in predicting the physical limitation parameters even though the approach followed in this study simply used the input (e) and the output (u) of the HC, and this should in theory capture the characteristics. It could have been speculated from the initial results that there wouldn't be much to predict in the physical limitation parameters (i.e., changing physical limitation parameters would not impact the cost function considerably), because their impact on the components of the cost function is limited, especially within a realistic range of parameter variation. Albeit small, the variation in these parameters has still been found to have considerable impact on σ_e, σ_u, and $\sigma_{\dot{u}}$ when left as free optimization parameters. Thus, the values end up at unrealistic extremes when these parameters' values are picked to minimize the cost function, while surprisingly maintaining a stable system. This means that if the HC was indeed to minimize a weighted sum of σ_e, σ_u, and $\sigma_{\dot{u}}$, the physical limitation parameters would diverge. The experimental data clearly shows that this is not the case. It must be noted that this drawback would remain, if an average (not individualized) model is to be used with the cost function, despite previous findings [20, 21]. Another research decision that could be reflected upon is the use of standard deviations instead of variances in the cost function: as demonstrated in preliminary analysis, this change is only expected to *amplify* the outcomes, making the disparity between the experimental and simulated results more apparent. Thus, if further research was to build up on the cost function theory [12], the cost function would require terms that capture the intrinsic variations and constraints in the physical limitation parameters.

Based on the findings in this paper, several recommendations for how the HCCF should be formulated is made. Reflecting back at the literature, a simple phase margin/crossover frequency term could be tested. For example, Bachelder et al. [25] have incorporated a phase margin linearization behavior term earlier. Even though the results in the last step show that phase margin itself also does not capture the variation in "physical limitations", the phase margin linearization behavior (i.e., indicating *workload* via the phase margin [25]) could be a more intricate yet effective addition. A simpler recommendation would be the crossover frequency, however, as it's shown considerable deviation between the cases, and as a basic, fundamental term of the cybernetic theory. Nonetheless, it must be noted that the crossover frequency is also highly dependent on the equalization, and the observability of the physical limitation parameters from it must be assessed. More complicated terms such as the peak open loop neuromuscular amplitude have also been suggested [26], and while this term would be influenced by a number of cybernetic parameters, this could be useful for observing individual differences. However, for the purposes considered in this research, prediction and data augmentation, simpler methods are preferred.

Finally, the performance of the HCCF method as a data augmentation tool further highlights the drawbacks of the assumption that HCs "pick" all their control behavior parameters to minimize a weighted sum of σ_e, σ_u, and $\sigma_{\dot{u}}$. The distribution of these values that result in the generated "synthetic" participants depict "superhuman" control behavior, as a better performance rating is achieved with lower "effort", suggesting that the HCCF utilized in this paper neglects certain hindrances of the HC. The best results were obtained for a hybrid case, where the positives of the cost function

method devised in this paper remain with the equalization predictions, but the "physical limitations" are randomly generated to capture the stochastic nature of HCs. While this method provides a better alternative than randomly generating parameter sets, from an objective point of view, this method does not sufficiently replicate the cybernetic parameter distributions accurately enough to be used as an augmentation tool. Based on the advancements in artificial intelligence, machine learning and generative AI techniques are recommended to be investigated as an effective way to replicate cybernetic parameters. Even though these methods utilize black box models that lack explainability, they could be useful for purely data augmentation purposes.

VII. Conclusion

In this research, individualized weightings defining HCs' balancing of performance and effort were used to capture individual differences in manual control, in order to predict and generate personalized cybernetic parameter sets. The equalization parameters show greater between-participant variation compared to the physical limitations (33.84% higher on average), and have greater impact on the signals that precede and succeed the HC model, e and u. Clear groupings were observed as the equalization parameters showed significant relation, and these groupings were confirmed with when the individual cost function weightings were determined, as groups of (3/9 in (I), 6/9 in (II), 3/12 in (III)) participants with similar equalization values were not identified adequately. The HC model parameter predictions that followed from these weightings yielded unrealistic parameter values, leading to substantial deviations of 56.06% (τ), -94.43% (ω_{nm}), and -170.34% (ζ_{nm}) observed in the physical limitation parameters on average, when contrasted with the experimental values. This concludes that the HC does not optimize for the used cost function, as the cost function fails to take the physical limitations into account. The data augmentation attempt supports these judgments, pointing to a hybrid approach with randomized physical limitations and cost-function-generated equalization, where the σ_e, σ_u. and $\sigma_{\dot{u}}$ values are kept within 15% of the experimental values on average. The findings of this research underline the need for a cost function that captures individual cybernetic parameter variations better moving forward, in order to advance personalization in human-machine systems.

References

[1] Koppen, O. C., "Airplane Stability and Control from a Designer's Point of View," *Journal of the Aeronautical Sciences*, Vol. 7, No. 4, 1940, pp. 135–140. https://doi.org/10.2514/8.1060, URL https://arc.aiaa.org/doi/10.2514/8.1060.

[2] McRuer, D., and Jex, H., "A Review of Quasi-Linear Pilot Models," *IEEE Transactions on Human Factors in Electronics*, Vol. HFE-8, No. 3, 1967, pp. 231–249. https://doi.org/10.1109/THFE.1967.234304, URL http://ieeexplore.ieee.org/document/1698271/.

[3] Mulder, M., Pool, D. M., Abbink, D. A., Boer, E. R., Zaal, P. M. T., Drop, F. M., van der El, K., and van Paassen, M. M., "Manual Control Cybernetics: State-of-the-Art and Current Trends," *IEEE Transactions on Human-Machine Systems*, Vol. 48, No. 5, 2018, pp. 468–485. https://doi.org/10.1109/THMS.2017.2761342, URL https://ieeexplore.ieee.org/document/8088358/.

[4] McRuer, D. T., "Mathematical Models of Human Pilot Behavior," *Agardograph*, , No. 188, 1974.

[5] McRuer, D., and Weir, D., "Theory of Manual Vehicular Control," *IEEE Transactions on Man Machine Systems*, Vol. 10, No. 4, 1969, pp. 257–291. https://doi.org/10.1109/TMMS.1969.299930, URL http://ieeexplore.ieee.org/document/4081909/.

[6] Li, Y., Tee, K. P., Chan, W. L., Yan, R., Chua, Y., and Limbu, D. K., "Continuous Role Adaptation for Human–Robot Shared Control," *IEEE Transactions on Robotics*, Vol. 31, No. 3, 2015, pp. 672–681. https://doi.org/10.1109/TRO.2015.2419873, URL http://ieeexplore.ieee.org/document/7097058/.

[7] Soliveri, P., "Learning manual pursuit tracking skills in patients with Parkinson's disease," *Brain*, Vol. 120, No. 8, 1997, pp. 1325–1337. https://doi.org/10.1093/brain/120.8.1325, URL https://academic.oup.com/brain/article-lookup/doi/10.1093/brain/120.8.1325.

[8] Oishi, M. M. K., TalebiFard, P., and McKeown, M. J., "Assessing Manual Pursuit Tracking in Parkinson's Disease Via Linear Dynamical Systems," *Annals of Biomedical Engineering*, Vol. 39, No. 8, 2011, pp. 2263–2273. https://doi.org/10.1007/s10439-011-0306-5, URL http://link.springer.com/10.1007/s10439-011-0306-5.

[9] Hess, R., and Modjtahedzadeh, A., "A control theoretic model of driver steering behavior," *IEEE Control Systems Magazine*, Vol. 10, No. 5, 1990, pp. 3–8. https://doi.org/10.1109/37.60415.

[10] van der El, K., Pool, D. M., van Paassen, M. M., and Mulder, M., "Modeling driver steering behavior in restricted-preview boundary-avoidance tasks," *Transportation Research Part F: Traffic Psychology and Behaviour*, Vol. 94, 2023, pp. 362–378. https://doi.org/10.1016/j.trf.2023.02.017, URL https://linkinghub.elsevier.com/retrieve/pii/S1369847823000505.

[11] Hess, R., Moore, J. K., and Hubbard, M., "Modeling the Manually Controlled Bicycle," *IEEE Transactions on Systems, Man, and Cybernetics - Part A: Systems and Humans*, Vol. 42, No. 3, 2012, pp. 545–557. https://doi.org/10.1109/TSMCA.2011.2164244, URL http://ieeexplore.ieee.org/document/6151180/.

[12] Kleinman, D., Baron, S., and Levison, W., "An optimal control model of human response part I: Theory and validation," *Automatica*, Vol. 6, No. 3, 1970, pp. 357–369. https://doi.org/10.1016/0005-1098(70)90051-8, URL https://linkinghub.elsevier.com/retrieve/pii/0005109870900518.

[13] Baron, S., Kleinman, D., and Levison, W., "An optimal control model of human response part II: Prediction of human performance in a complex task," *Automatica*, Vol. 6, No. 3, 1970, pp. 371–383. https://doi.org/10.1016/0005-1098(70)90052-X, URL https://linkinghub.elsevier.com/retrieve/pii/000510987090052X.

[14] Phatak, A. V., and Kessler, K. M., "Modeling the Human Gunner in an Anti-Aircraft Artillery (AAA) Tracking Task," *Human Factors: The Journal of the Human Factors and Ergonomics Society*, Vol. 19, No. 5, 1977, pp. 477–494. https://doi.org/10.1177/001872087701900504, URL http://journals.sagepub.com/doi/10.1177/001872087701900504.

[15] Phatak, A., Weinert, H., Segallii, I., and Day, C. N., "Identification of a Modified Optimal Control Model for the Human Operator*t," ????

[16] Doman, D., "Optimal control pilot modeling for resolving Cooper-Harper rating discrepancies," *24th Atmospheric Flight Mechanics Conference*, American Institute of Aeronautics and Astronautics, Portland,OR,U.S.A., 1999. https://doi.org/10.2514/6.1999-4091, URL https://arc.aiaa.org/doi/10.2514/6.1999-4091.

[17] Scibilia, A., Pedrocchi, N., and Fortuna, L., "Human Control Model Estimation in Physical Human–Machine Interaction: A Survey," *Sensors*, Vol. 22, No. 5, 2022, p. 1732. https://doi.org/10.3390/s22051732, URL https://www.mdpi.com/1424-8220/22/5/1732.

[18] Franceschi, P., Pedrocchi, N., and Beschi, M., "Inverse Optimal Control for the identification of human objective: a preparatory study for physical Human-Robot Interaction," *2022 IEEE 27th International Conference on Emerging Technologies and Factory Automation (ETFA)*, IEEE, Stuttgart, Germany, 2022, pp. 1–6. https://doi.org/10.1109/ETFA52439.2022.9921553, URL https://ieeexplore.ieee.org/document/9921553/.

[19] Baron, S., and Kleinman, D., "The Human as an Optimal Controller and Information Processor," *IEEE Transactions on Man Machine Systems*, Vol. 10, No. 1, 1969, pp. 9–17. https://doi.org/10.1109/TMMS.1969.299875, URL http://ieeexplore.ieee.org/document/4081850/.

[20] Lu, T., "Objective evaluation of human manual control adaptation boundaries using a cybernetic approach," Ph.D. thesis, Delft University of Technology, 2018. https://doi.org/10.4233/UUID:A9409495-DCB4-43FB-BF2D-64341056654D, URL http://resolver.tudelft.nl/uuid:a9409495-dcb4-43fb-bf2d-64341056654d.

[21] Butijn, M. C., Lu, T., Pool, D. M., and Van Paassen, M. M., "Assessment of Maximum Unnoticeable Added Lag-Lead or Lead-Lag Dynamics with a Cybernetic Approach," *AIAA Scitech 2019 Forum*, American Institute of Aeronautics and Astronautics, San Diego, California, 2019. https://doi.org/10.2514/6.2019-1229, URL https://arc.aiaa.org/doi/10.2514/6.2019-1229.

[22] Davidson, B., and Schmidt, K., "Modified Optimal Control Pilot Model for Computer-Aided Design and Analysis," ????

[23] Bacon, B. J., and Schmidt, D. K., "An Optimal Control Approach to Pilot-Vehicle Analysis and the Neal-Smith Criteria," 1984.

[24] Hosman, R., *Pilot's Perception and Control of Aircraft Motions*, Delft University Press, 1996. URL https://books.google.nl/books?id=PJRaAAAACAAJ.

[25] Bachelder, E., and Aponso, B., "A Theoretical Framework Unifying Handling Qualities, Workload, Stability and Control," *Proceedings of the 77th Annual Forum*, The Vertical Flight Society, Virtual, 2021, pp. 1744–1763.

[26] Bachelder, E. N., Aponso, B. L., and Berger, T., "A Theoretical Basis for Predicting Pilot Performance, Workload, and Handling Qualities," *AIAA SCITECH 2023 Forum*, American Institute of Aeronautics and Astronautics, National Harbor, MD & Online, 2023. https://doi.org/10.2514/6.2023-1369, URL https://arc.aiaa.org/doi/10.2514/6.2023-1369.

[27] Bachelder, E. N., Hess, R. A., Godfroy-Cooper, M., and Aponso, B. L., "Linking the Pilot Structural Model and Pilot Workload," *2018 AIAA Atmospheric Flight Mechanics Conference*, American Institute of Aeronautics and Astronautics, Kissimmee, Florida, 2018. https://doi.org/10.2514/6.2018-0533, URL https://arc.aiaa.org/doi/10.2514/6.2018-0533.

[28] Mulder, M., Pool, D., Abbink, D., Boer, E., and van Paassen, M., "Fundamental Issues in Manual Control Cybernetics," *IFAC-PapersOnLine*, Vol. 49, No. 19, 2016, pp. 1–6. https://doi.org/https://doi.org/10.1016/j.ifacol.2016.10.429, URL https://www.sciencedirect.com/science/article/pii/S240589631632016X, 13th IFAC Symposium on Analysis, Design, and Evaluation ofHuman-Machine Systems HMS 2016.

[29] Tuzhilin, A., "Personalization: The state of the art and future directions," *Business computing*, Vol. 3, No. 3, 2009, pp. 3–43.

[30] Guozhen Zhao, and Changxu Wu, "Mathematical Modeling of Driver Speed Control With Individual Differences," *IEEE Transactions on Systems, Man, and Cybernetics: Systems*, Vol. 43, No. 5, 2013, pp. 1091–1104. https://doi.org/10.1109/TSMC.2013.2256854, URL http://ieeexplore.ieee.org/document/6573359/.

[31] Hasenjager, M., and Wersing, H., "Personalization in advanced driver assistance systems and autonomous vehicles: A review," *2017 IEEE 20th International Conference on Intelligent Transportation Systems (ITSC)*, IEEE, Yokohama, 2017, pp. 1–7. https://doi.org/10.1109/ITSC.2017.8317803, URL http://ieeexplore.ieee.org/document/8317803/.

[32] Feng, J., and Donmez, B., "DESIGNING FEEDBACK TO INDUCE SAFER DRIVING BEHAVIORS: A LITERATURE REVIEW AND A MODEL OF DRIVER-FEEDBACK INTERACTION," 2013.

[33] Hess, R. A., "Simplified approach for modelling pilot pursuit control behaviour in multi-loop flight control tasks," *Proceedings of the Institution of Mechanical Engineers, Part G: Journal of Aerospace Engineering*, Vol. 220, No. 2, 2006, pp. 85–102. https://doi.org/10.1243/09544100JAERO33, URL http://journals.sagepub.com/doi/10.1243/09544100JAERO33.

[34] de Winter, J., and Happee, R., "Modelling driver behaviour: a rationale for multivariate statistics," *Theoretical Issues in Ergonomics Science*, Vol. 13, No. 5, 2012, pp. 528–545. https://doi.org/10.1080/1463922X.2010.546437.

[35] de Winter, J., "Why person models are important for human factors science," *Theoretical Issues in Ergonomics Science*, Vol. 15, No. 6, 2014, pp. 595–614. https://doi.org/10.1080/1463922X.2013.856494.

[36] Rothengatter, T., "Drivers' illusions—no more risk," *Transportation Research Part F: Traffic Psychology and Behaviour*, Vol. 5, No. 4, 2002, pp. 249–258. https://doi.org/https://doi.org/10.1016/S1369-8478(03)00004-4, URL https://www.sciencedirect.com/science/article/pii/S1369847803000044.

[37] Simm, A., "Technical and Psychological Aspects of Pilot Gain," 2012.

[38] Mitchell, D. G., and Klyde, D. H., "This Is Pilot Gain," *AIAA Scitech 2019 Forum*, American Institute of Aeronautics and Astronautics, San Diego, California, 2019. https://doi.org/10.2514/6.2019-0562, URL https://arc.aiaa.org/doi/10.2514/6.2019-0562.

[39] Mitchell, D. G., and Klyde, D. H., "Defining Pilot Gain," *Journal of Guidance, Control, and Dynamics*, Vol. 43, No. 1, 2020, pp. 85–95. https://doi.org/10.2514/1.G004426, URL https://arc.aiaa.org/doi/10.2514/1.G004426.

[40] Pool, D. M., Zaal, P. M. T., Damveld, H. J., Van Paassen, M. M., Van der Vaart, J. C., and Mulder, M., "Modeling Wide-Frequency-Range Pilot Equalization for Control of Aircraft Pitch Dynamics," *Journal of Guidance, Control, and Dynamics*, Vol. 34, No. 5, 2011, pp. 1529–1542. https://doi.org/10.2514/1.53315, URL https://arc.aiaa.org/doi/10.2514/1.53315.

[41] De Jong, M. J., Pool, D. M., and Mulder, M., "Cybernetic Data Augmentation for Neural Network Classification of Control Skills," *IFAC-PapersOnLine*, Vol. 55, No. 29, 2022, pp. 178–183. https://doi.org/10.1016/j.ifacol.2022.10.252, URL https://linkinghub.elsevier.com/retrieve/pii/S2405896322022790.

[42] van der El, K., Pool, D. M., van Paassen, M. R. M., and Mulder, M., "Effects of Target Trajectory Bandwidth on Manual Control Behavior in Pursuit and Preview Tracking," *IEEE Transactions on Human-Machine Systems*, Vol. 50, No. 1, 2020, pp. 68–78. https://doi.org/10.1109/THMS.2019.2947577.

[43] Pool, D. M., Harder, G. A., and van Paassen, M. M., "Effects of Simulator Motion Feedback on Training of Skill-Based Control Behavior," *Journal of Guidance, Control, and Dynamics*, Vol. 39, No. 4, 2016, pp. 889–902. https://doi.org/10.2514/1.G001603, URL https://arc.aiaa.org/doi/10.2514/1.G001603.

[44] Zolner, H., Pool, D., Damveld, H., van Paassen, M., and Mulder, M., *The Effects of Controlled Element Break Frequency on Pilot Dynamics During Compensatory Target-Following*, American Institute of Aeronautics and Astronautics, 2010. https://doi.org/10.2514/6.2010-8092, URL https://arc.aiaa.org/doi/abs/10.2514/6.2010-8092.

Appendix

Participant Data

Table 5 Participants' parameter sets - (I)

Participant #	K_v (-)	T_L (s)	τ (s)	ω_{nm} (rad/s)	ζ_{nm} (-)	PM (deg)	CF (rad/s)
1	1.59	0.34	0.27	9.54	0.20	44.04	2.58
2	1.24	0.48	0.29	9.33	0.12	57.58	2.35
3	0.96	0.54	0.30	8.38	0.27	65.57	1.79
4	0.83	0.52	0.31	9.95	0.25	71.64	1.43
5	1.20	0.5	0.31	9.06	0.08	57.47	2.34
6	1.20	0.5	0.32	10.03	0.06	57.77	2.30
7	0.85	0.41	0.33	8.36	0.28	63.70	1.36
8	1.67	0.33	0.28	10.69	0.09	44.39	2.65
9	0.93	0.36	0.30	9.76	0.32	61.47	1.44

Table 6 Participants' parameter sets - (II)

Participant #	K_v (-)	T_L (s)	τ (s)	ω_{nm} (rad/s)	ζ_{nm} (-)	PM (deg)	CF (rad/s)
1	0.13	3.72	0.27	8.20	0.23	31.66	2.80
2	0.32	1.56	0.27	7.85	0.14	25.58	2.93
3	0.09	4.02	0.32	7.56	0.14	42.21	2.00
4	0.35	1.42	0.29	7.77	0.13	22.05	2.93
5	0.08	3.74	0.34	6.88	0.18	42.91	1.69
6	0.14	3.02	0.28	7.66	0.19	38.66	2.26
7	0.09	3.37	0.31	5.89	0.18	45.20	1.57
8	0.24	1.95	0.32	8.05	0.28	21.25	2.56
9	0.13	2.63	0.30	6.63	0.18	40.18	1.86

Table 7 Participants' parameter sets - (III)

Participant #	K_v (-)	T_L (s)	T_I (s)	τ (s)	ω_{nm} (rad/s)	ζ_{nm} (-)	PM (deg)	CF (rad/s)
1	3.81	0.52	1.67	0.22	11.59	0.19	42.01	3.35
2	3.78	0.50	1.62	0.21	11.64	0.19	47.23	3.23
3	2.69	0.41	0.99	0.21	9.68	0.27	49.93	2.86
4	2.42	0.46	1.34	0.22	8.66	0.31	93.57	1.13
5	4.98	0.53	2.31	0.20	10.05	0.19	42.36	3.34
6	2.02	0.42	1.07	0.22	9.66	0.29	96.24	0.98
7	2.45	0.39	1.38	0.25	11.07	0.37	84.16	1.00
8	3.06	0.29	0.70	0.10	8.73	0.21	48.08	3.12
9	2.63	0.52	1.81	0.24	9.44	0.40	88.61	0.97
10	2.73	0.51	1.57	0.25	11.76	0.19	94.91	1.24
11	3.96	0.41	1.42	0.18	8.98	0.26	41.79	3.12
12	2.29	0.33	0.86	0.18	9.36	0.28	91.96	1.43

Data Augmentation Histograms - Exps. (II), (III)

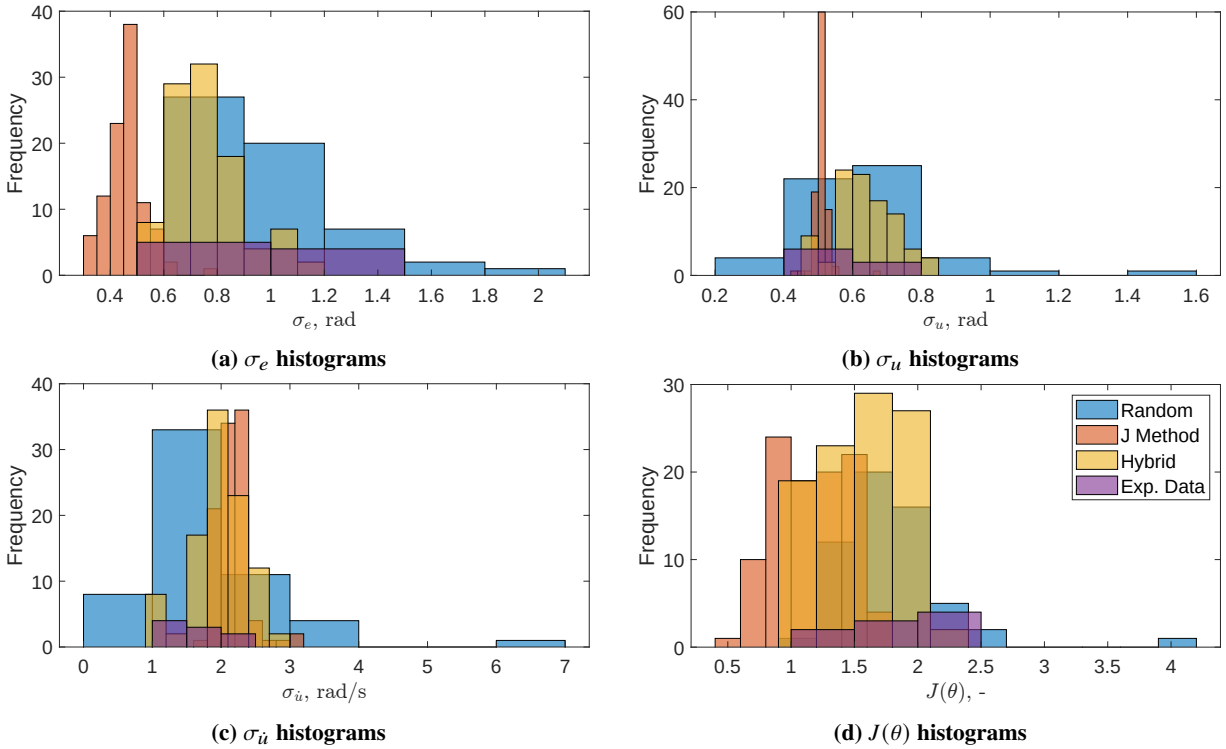

(a) σ_e histograms **(b) σ_u histograms**

(c) $\sigma_{\dot{u}}$ histograms **(d) $J(\theta)$ histograms**

Fig. 16 σ_e, σ_u, and $\sigma_{\dot{u}}$ histograms comparing data augmentation methods - Exp. (II)

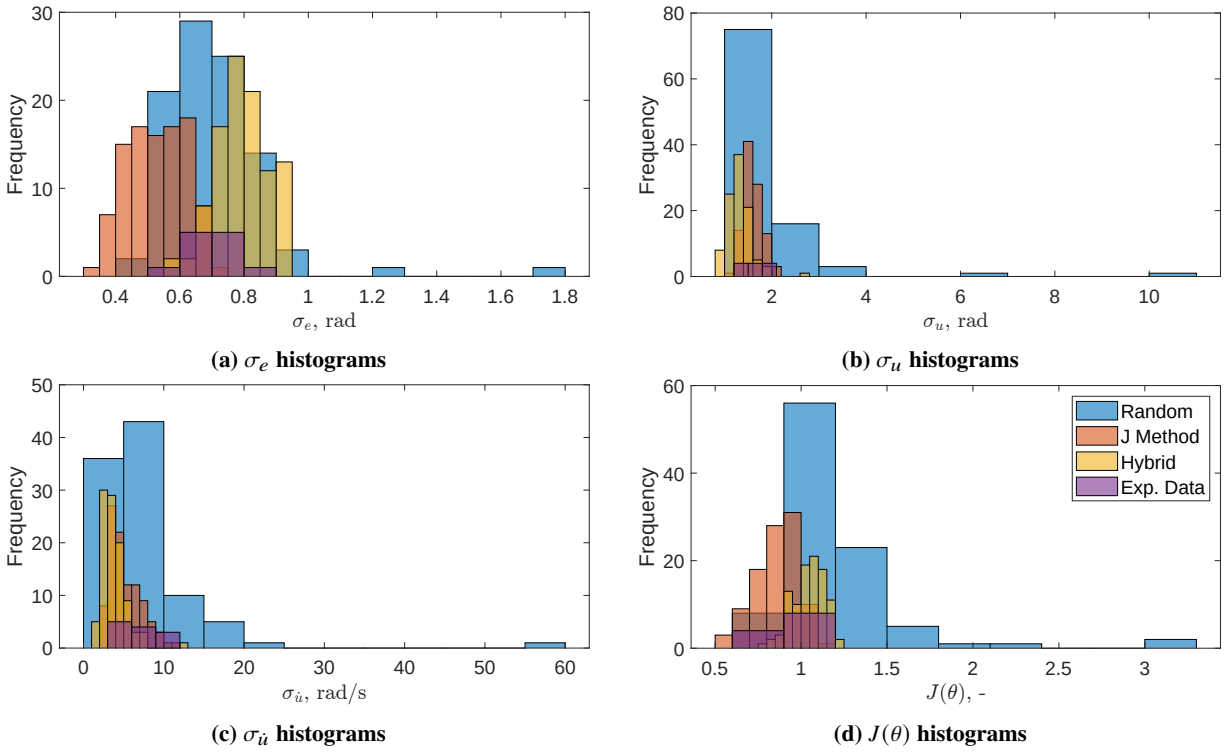

(a) σ_e **histograms**

(b) σ_u **histograms**

(c) $\sigma_{\dot{u}}$ **histograms**

(d) $J(\theta)$ **histograms**

Fig. 17 σ_e, σ_u, **and** $\sigma_{\dot{u}}$ **histograms comparing data augmentation methods - Exp. (III)**

Cost Function Components - Exps. (II), (III)

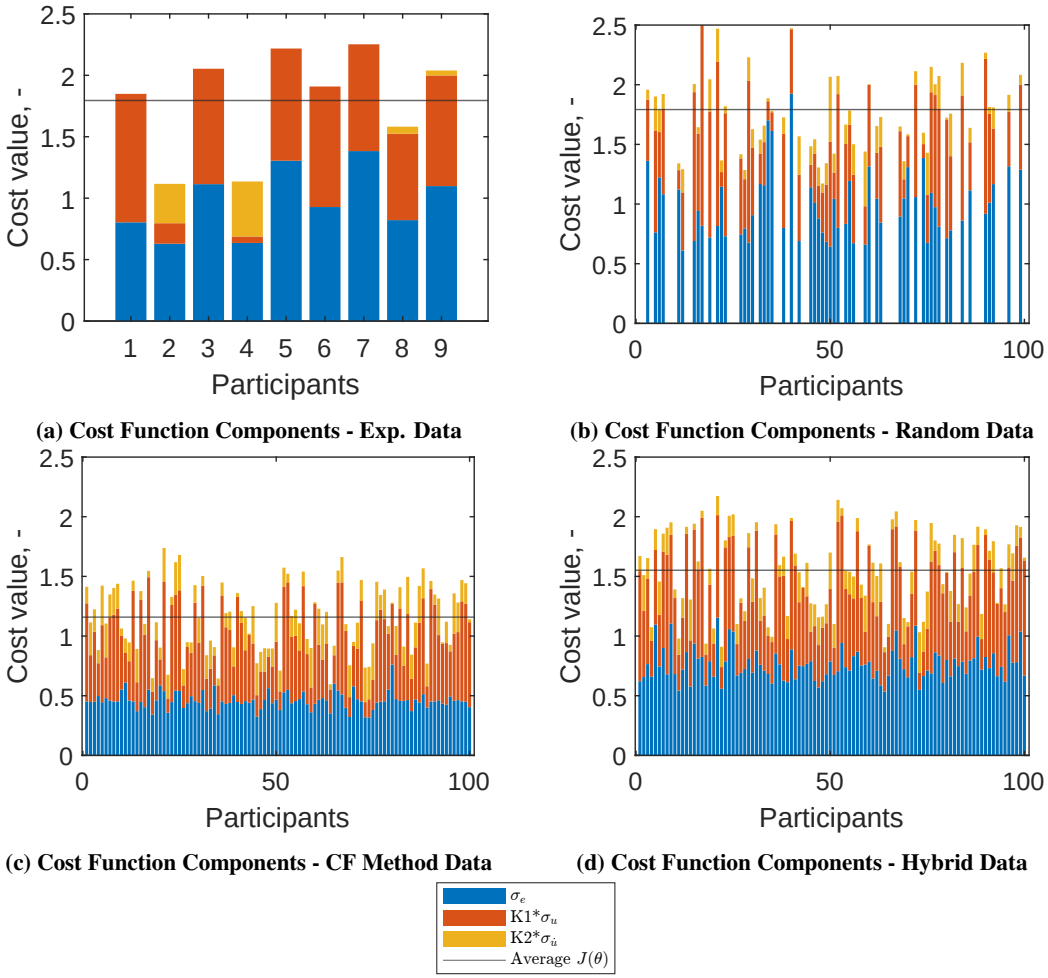

(a) Cost Function Components - Exp. Data

(b) Cost Function Components - Random Data

(c) Cost Function Components - CF Method Data

(d) Cost Function Components - Hybrid Data

Fig. 18 Cost function component breakdown - (II)

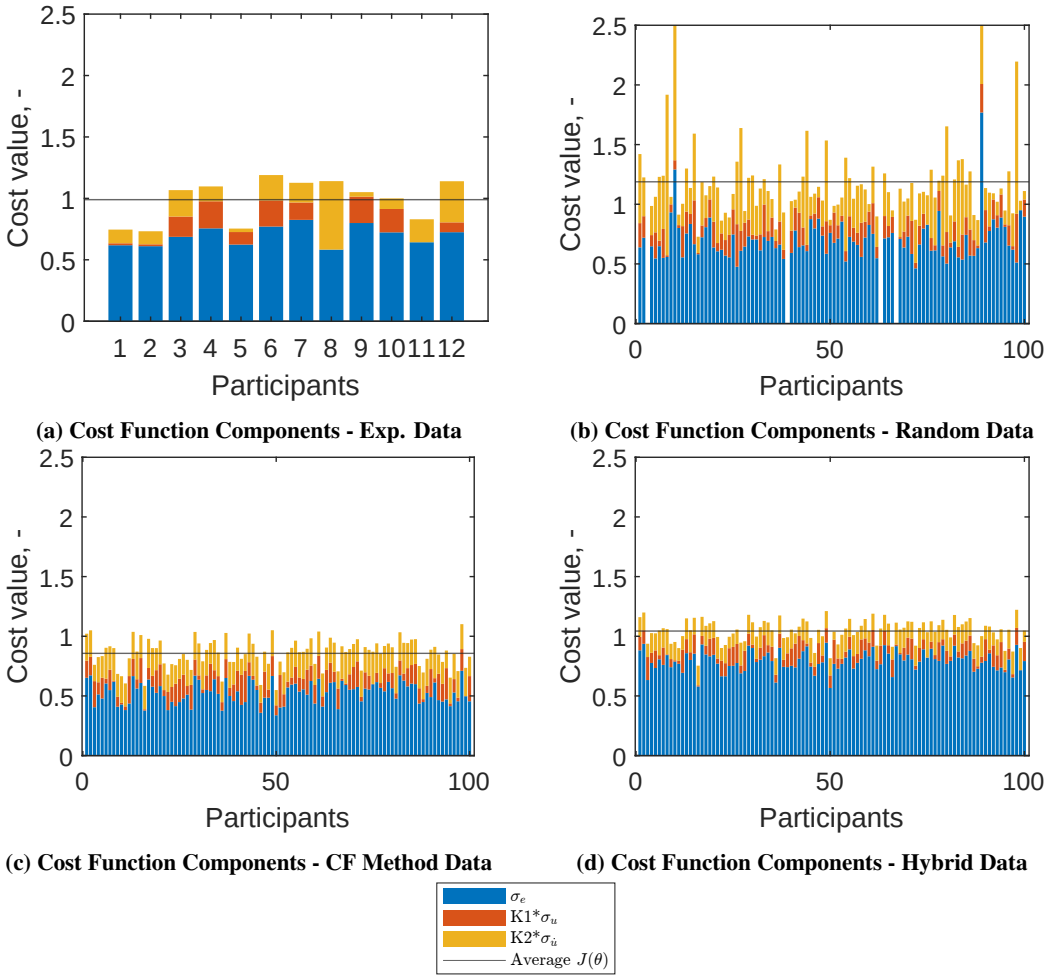

(a) Cost Function Components - Exp. Data

(b) Cost Function Components - Random Data

(c) Cost Function Components - CF Method Data

(d) Cost Function Components - Hybrid Data

Fig. 19 Cost function component breakdown - (III)

Part II

Preliminary Report

*This part has been assessed for the course AE4020 Literature Study.

1

Introduction

Interaction is an essential aspect of the human life, as humans interact with themselves and other beings in their environment for a variety of reasons. Among those needs are the cognitive and practical needs, as humans instinctively seek out to learn more and to acquire and hone skills, in order to solve problems and to achieve goals. While what humans have considered as viable and useful to interact with has changed over the course of humanity, it is safe to say that in present day, devices and machines that deploy modern technology are critical to fulfill these human needs. Therefore, it is important to understand the behavior underlying how humans interact with machines, and control them to accomplish tasks. Such a multidisciplinary field entails various different approaches, and a prominent technical approach to studying human control behavior is manual control cybernetics, which utilizes mathematical models to describe how humans control vehicles and devices. [1]

Cybernetics is the study of the human controller using an approach rooted in mathematical systems theory. The crossover model developed by McRuer and Jex in the 1960's, describing human control dynamics, [2] forms the basis of the "cybernetic approach". This theory, originating in aerospace, has been commonly applied in other fields such as robotics [3], medicine [4, 5], automotive [6, 7], and other vehicles [8]. Even though cybernetics has been considerably effective in explaining human control behavior, it is still incapable of reflecting the full scope of the topic, despite several efforts to update and advance the theory [1]. A limitation in current manual control cybernetics that calls for progress is the lack of "personalized support" [1]; much of the work done has been for an "average" human, although the individual differences between humans in manual control also need attention.

There has been extensive research on the "goal" of the human when performing a control task, and how differences in task performance (especially for pilots) could be explained with the cybernetic theory. However, a quantitative framework outlining the differences in "attitude" of humans to a manual control task is lacking. Defining a cost function that weighs the performance and effort using individualized weightings could then be useful to explore personalization in cybernetics. Therefore, the main question tackled in this research is: *To what extent can individual differences in cybernetic parameters be predicted by using a cost function, that describes human controllers' relative weighting of task performance and required effort in compensatory tracking tasks?*

This research project aims to contribute by introducing a novel method for predicting individual differences. Existing research gaps, such as the lack of a clear definition for the human cost function and the absence of a established method for finding personal weightings will be addressed. These weightings are integral to reach the ultimate aim of predicting individual cybernetic parameters. By doing so, the project generate more accurate participant data for simulations compared to existing methods such as generating parameters randomly or by matching the tracking run data from real experiments, which has been considered deficient [9]. Validly generating cybernetic parameter data for individuals would be a significant improvement, as it would eliminate the need for extensive human-subject experiments and allow for the "generation" of participants.

First three chapters of this report summarize the literature study conducted to identify research gaps and contextualize the research. Chapter 2 provides a broad overview on the topic of individual differences, starting from how it is defined in psychology and neuroscience, and then focusing on engineering and cybernetics specifically. The next chapter, Chapter 3 explains the cybernetic theory in depth, with an

emphasis on the pilot model that depicts the human controller. Then, Chapter 4 introduces the idea of the human cost function and explains different ideas related to cybernetics that have been used for examining individual differences. Following the literature study is the preliminary analysis presented in Chapter 5, where data from previous studies are scrutinized to gain insights. Finally, Chapter 6 presents the research plan that outlines how the remaining part of the project will be proceeded, thus concluding the preliminary phase of thesis.

2

Individual Differences

This chapter will follow a multidisciplinary approach to investigate existing research on individual differences and explain how personalization could be useful in human-machine interaction. This chapter begins by briefly explaining what individual differences mean and where they arise from, in a biological and psychological sense. Later, how these reflect into the need personalization in a modern, individualized, and technological society will be elaborated on.

2.1. Definition

Individual differences refer to the variation in characteristics and traits of individuals which make them distinguishable from each other [10]. These differences in psychological characteristics of humans could be seen in many aspects; personality, physical traits, attitude, cognition, etc. Moreover, due to having such a large filed of impact, individual differences has been approached by multiple disciplines ranging from psychology and economics to engineering and neuroscience.

Due to this wide range of application, what could be considered as “individual differences” is loosely defined. For studies in psychology, for example, a basic and common set of individual differences could include gender, age, interest, motivation, and self-efficacy [11]. However, individual differences could be much more specific for deeper and more technical studies.

Albeit being addressed from many different perspectives, one statement that all can agree upon is that individual differences are crucial to the society. Literature in psychology has outlined both social and practical advantages of paying attention to the ways individuals differ. For the social aspect, it has been argued that attending individual differences is a sign of evolutionary success [12]. On the other hand, there are consequences of ignoring such differences; resource depletion and damage to reputation could be given as such examples.

Understanding individual differences enhances diversity, by acknowledging the needs and strengths of individuals. For example, studies on cognition have revealed that considering individual differences could lead to significant improvements for learning and performance in a control task [13]. Furthermore, there has been attempts to link individual task performances to “cognitive resources” as well as to intellectual abilities [14]. The relation between resource allocation and task performance is devised for different tasks as the case for learning and adaptation is made. Figure 2.1 demonstrates that performance becomes less and less resource-dependent for consistent tasks “as automatic processes develop” [14].

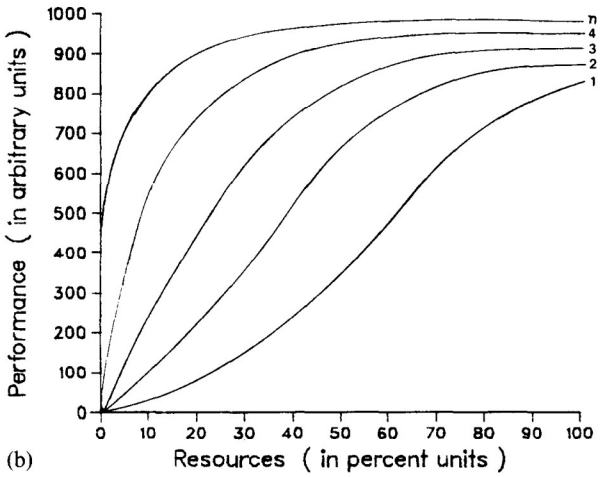

Figure 2.1: The Performance-Resource Function for a consistent task [14]

Individual differences are qualitative in nature, and it has been proposed that quantifying the level or amount of individual differences is not logical [15]. Evaluation of individual differences is usually done by categorizing behavior into one of the fields, without any vagueness. Furthermore, there is no established framework for how individual differences are observed, although two methods are commonly used for assessment. The most standard and accurate ways to measure individual differences centred on self-report or performance metrics. The latter relies on tests (or test-like situations), in an attempt to judge variation between individuals.

2.2. Towards Cybernetics

Personalization, from the engineering point of view, refers to designing and tailoring works and products in order to meet the demands of individuals [16]. It is therefore essential to understand and define individual differences well for personalization. While personalization has always played a role in human history, it is evident that there has been a significant surge in interest over the past three decades, primarily due to the advancements in internet technology [17]. Thus, in the foreseeable future, engineering design is expected to make use of personalization to develop devices and tools that better fit the skills and attitudes of individuals, both to make effective use of existing skills and to train other useful skills.

Even though the topic of personalization could be approached in numerous ways, human-machine interaction stands out as a discipline of considerable importance. As a study of making technology more usable and effective for people, understanding personalization through the perspective of human-machine interaction could significantly improve people's experiences with novel devices and vehicles. It is crucial to understand just how differently humans interact with devices and how devices could be adjusted to assist the individual, in order to have safer, more comfortable, and more efficient technologies.

Within this regard, the study of human controllers in various task-specific contexts, such as drivers or pilots, has attracted significant attention in research and various methods have been used to try to model the human operator [18, 19]. Although there has been attempts to incorporate individual differences in these driver models [20], most models still depict the "average" driver and lack personal adaptation [21]. Lack of personalized driver models remains an issue and a difficult task that calls for further research, in pursuance of "more human-like" and tailored driver assistance systems [7]. An example human controller model has been given in Figure 2.2. The corresponding mathematical formulation of the controller, containing personalizable parameters is then given in Eq. (2.1).

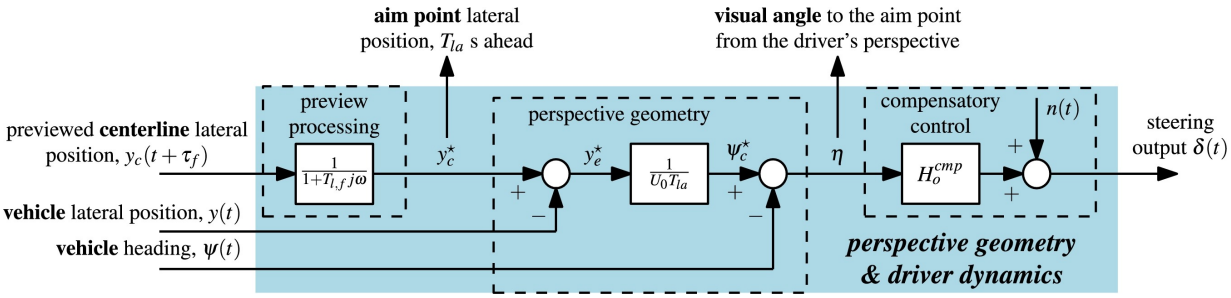

Figure 2.2: An example human controller (driver steering) model [7]

$$H_o^{comp}(j\omega) = K_{e^\star}(1 + T_{L,e^\star} j\omega) e^{-\tau_\nu j\omega} \frac{\omega_{nms}^2}{(j\omega)^2 + 2\zeta_{nms}\omega_{nms} j\omega + \omega_{nms}^2} \tag{2.1}$$

While there are multiple methods that could be used in identifying individual differences and personalizing human models, manual control cybernetics could be named as an effective way to characterize and explore how humans perform tasks. Manual control cybernetics follows a human-centred approach rooted in control theory to understand how humans control vehicles and devices [22]. Cybernetics has been useful for exploring human behavior in various complex systems due to its mathematical framework and system-theoretical approach [1], such as in the example presented above with Figure 2.2 and Eq. (2.1). Building up on what has been explained earlier, the need of providing personalized support as opposed to having interfaces for the "average" human has also been described as a key issue in the field of manual control cybernetics [23]. Therefore, cybernetics provide a crucial and objective approach to study individual differences in human controllers. The cybernetic theory and how individual differences could be observed through different aspects of the cybernetic model will be explained in the next chapter.

2.3. Conclusion

As a project focusing on individual differences, it was important to define the topic well and consider what other fields and previous research have mentioned. While it could be agreed that individual differences refer to how different attributes and features of individuals vary to make them identifiable, it was seen that this definition is stretched towards the characteristics of each field that tackles this concept. It was also observed that the trade-off between "performance" and "resources" could be used to study individual differences in learning and task performance, and this approach could be adopted. Attention was then narrowed down to how individual differences shape modern engineering in the form of personalized devices and vehicle systems. Research in fields that study human behavior when controlling vehicles has especially outlined a need for increased personalized support, with plenty of work being designed for the "average". This suggests that individualizing the cybernetic model via its components is a necessary step moving forward.

3

Manual Control Cybernetics

This chapter explains the main approach that forms the basis of this research, manual control cybernetics. Cybernetic theory is used to explain human behavior via mathematical models and is therefore considered particularly useful to assess differences in individual control behaviour, especially in aerospace. McRuer's foundations of the cybernetic theory and pilot models will be briefly explained first, followed by the state-of-the-art. Key components of the pilot model will be elaborated on to conclude with the precise approach taken for this research.

3.1. Foundations

While the question of how humans control aircraft has been a part of scientific research since the inception of airplanes, the cybernetic theory and the mathematical pilot models developed by McRuer [2, 24, 25] is considered a groundbreaking piece of work in the field. This approach to investigate human behavior to control vehicles is rooted in control theory, as the human and the vehicle is modelled together in a complex dynamical system. The fundamental human-vehicle system describing the elements and the variables that it comprises of as well as their relations is depicted in Figure 3.1.

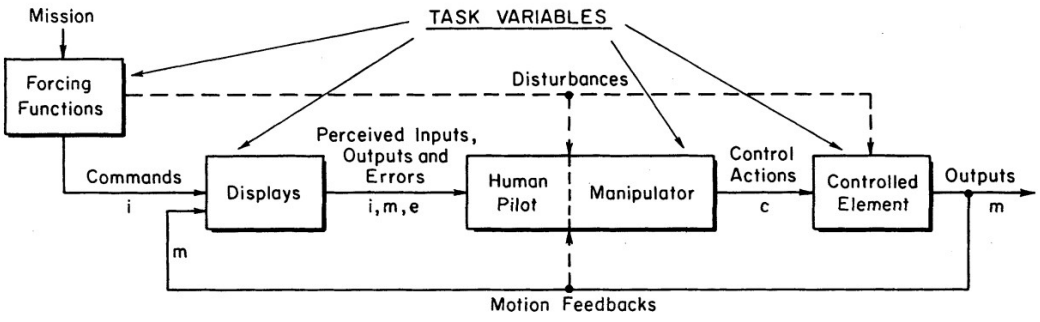

ENVIRONMENTAL VARIABLES:	OPERATOR-CENTERED VARIABLES:	PROCEDURAL VARIABLES:
In-Flight vs. Fixed-Base	Motivation	Instructions
Vibration	Stress	Practice
G-Level	Workload	Experimental Design
Temperature	Training	Order of Presentation
Atmospheric Conditions	Fatigue	Etc.
Etc.	Etc.	

Figure 3.1: The pilot-vehicle system as modeled by McRuer [2]

The feedback loop representation of this system is driven by the *forcing functions*, which represent the control mission, and presented to the *human pilot* via a *display*. The *human pilot* then takes action through a *manipulator* to provide an input to the *controlled element*. The output of the *controlled element* is also fed back into the *display* to complete the loop.

In order to accurately represent applicable pilot-vehicle situations, McRuer and Jex worked with *compensatory* tracking tasks, in which the human controller (HC) exerts control based on the error between the target command input and the actual command output [2]. Dynamics of the human pilot and the controlled element are represented through transfer functions, $H_p(s)$ and $H_c(s)$ respectively. The *crossover model* defines several key capabilities for the HC, most notably the ability to adjust and equalize behavior to provide a desired response while keeping the system stable. In control theory terms, this is represented by the open loop transfer function, $|H_{OL}| = |H_p H_c|$, showing integrator-like dynamics (-20 dB per decade slope) at frequencies in the crossover region (near ω_c, where $|H_{OL}| = 0\ [dB]$). The stability and performance requirements are then represented through the input bandwidth (ω_i) being smaller than the crossover frequency (ω_c), and the system having an adequate phase margin (φ_m) that's not too small.

These outlined elements form the basis of the *crossover model*. However, an important limitation of the HC, the effective time delay, must also be included. This time delay represents the inherent slowness of humans in responding to a visual input in the form of a neuromuscular output. With this addition, the *crossover model* is thus defined in Eq. (3.1):

$$H_{OL}(j\omega) = H_p(j\omega)H_c(j\omega) = \frac{\omega_c e^{-j\omega\tau_e}}{j\omega}, \text{ in the crossover region [2]} \tag{3.1}$$

This equation is of fundamental importance because it also makes it possible to estimate the transfer function describing the human pilot control dynamics through Eq. (3.2).

$$H_p(j\omega) = \frac{\omega_c e^{-j\omega\tau_e}}{H_c(j\omega) \cdot j\omega} \tag{3.2}$$

Being able to define a transfer function describing the dynamics of HCs leads the way into investigating various aspects of human control behavior, as identification and analysis of influencing factors could be expressed in mathematical dick terms. Finally, McRuer defines a set of six rules, the so-called *verbal adjustment rules*, to aid in modeling and predicting the pilot model and its behavior. These rules explain several aspects on pilot behavior, as well as provide a guideline on what to expect in certain experimental scenarios. A relevant takeaway that has been theorized in these rules is that the HC first aims to achieve the integrator-like behavior and once that's successful, tries to minimize the mean-squared error. Furthermore, a relation between the error and the system phase margin is defined, thus putting forward the phase margin as a critical parameter for performance [2].

3.2. State-of-the-Art

The state-of-the-art of the cybernetic theory for compensatory tracking tasks is formulated on the basis laid down by McRuer's *crossover model* and *verbal adjustment rules*. This framework uses a quasi-linear model to describe pilot behavior; composed of a linear time-invariant (LTI) component, and a "remnant" as the non-linear component. The so-called "remnant" has drawn considerable interest, and it is worth taking it into account. Ways to simulate the remnant has been developed, and depending on its impact and the fidelity of the developed pilot model, these could be used. Moreover, in addition to the input forcing function, the control task of the HC is also influenced by a disturbance signal, in order to accurately simulate real-life disturbances such as turbulence. With these elements of the system established, the basic control loop that serves as the foundation of current cybernetic theory is given in Figure 3.2.

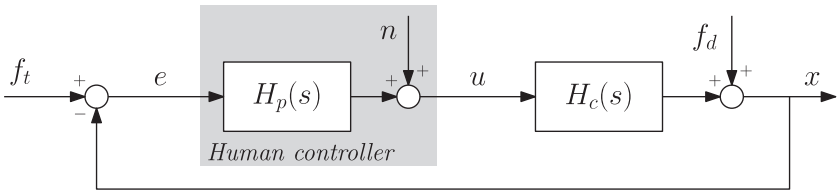

Figure 3.2: The simplified control loop [1]

Following sections outline the two main components of this control loop, the controlled element and the pilot model, as well as providing details on relevant sub-components that form a critical part of the theory underlying this research.

3.3. Controlled Element

The controlled element is the component of the control loop that will be explained first. It represents the dynamics of the vehicle system (or a part of the system) that is being controlled using mathematical models. Mathematically expressing the input-output relationship of a system is critical to assessing the system behavior, as well as the human behavior when tasked with controlling this system. Obtaining the transfer function representation for a controlled element could be done by observing the relationship between inputs and outputs for such system in the frequency domain.

Aerospace applications of this framework usually makes use of specific aircraft dynamics, such as the Cessna Citation I Ce500 [26]. However, since covering the entire breadth of an entire aircraft's dynamics is fairly complicated, transfer functions that describe the relationship between an input and an output, for a set of conditions are used. An example, frequently used in research in TU Delft is the controlled aircraft pitch dynamics, relating elevator input to aircraft pitch attitude using a reduced linear model of the Cessna Citation I Ce500, trimmed at 10000 [ft] and at an airspeed of 160 [kt] [27, 28].

Even though the controlled element dynamics could be in various forms, the open loop behavior described in Eq. (3.1) is expected to hold true regardless of the task. This implies that the pilot model adapts and adjusts based on the controlled element to maintain the required stability and controllability conditions. Therefore, it is important to consider the influence of the controlled element when investigating pilot behavior.

3.4. Pilot Model

As described previously, the pilot model has a LTI component that could be modeled mathematically as a transfer function, and a "remnant" component. The remnant component represents the nonlinear, noisy element of the HC that is independent of the input and the vehicle [29]. Although the remnant also has a notable impact, much of the attention is drawn into the LTI model, which is more relevant for examining human behavior. The *precision model* that was first introduced by McRuer [30] has been accepted as the basis for the pilot model.

The *precision model* comprises of three main parts, as presented in Figure 3.3: delay, neuromuscular dynamics, and equalization. The delay and the neuromuscular dynamics components together are referred to as *physical limitations*, as they reflect certain intrinsic flaws of the human body. Equalization however, is the adaptation of the HC to the specific control dynamics, is mainly to meet the condition given in Eq. (3.1). Therefore the equalization component of the pilot model could take up various forms and show more diversity.

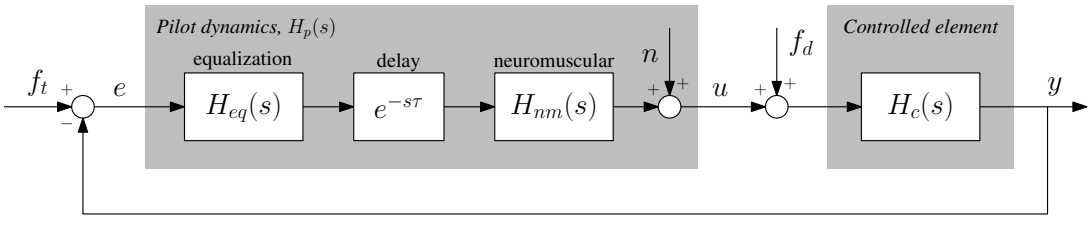

Figure 3.3: The control loop with detailed pilot model

3.4.1. Time Delay

For a compensatory tracking task with only visual input and neuromuscular output (i.e. moving the controller/stick), the delay term, as the name suggests, represents the human inability to respond immediately. Since the HC first perceives the input, makes a decision based on it, and translates this decision into an action (e.g. arm movements), the delay term in the *precision model* reflects the non-negligible albeit little time that this process takes.

3.4.2. Neuromuscular Dynamics

Since the HC provides the control input to the vehicle by muscle movements after the control decision is taken, the neuromuscular system carries great importance in defining human control behavior. The neuromuscular system involves the sensory and motor neurons, and the muscle fibres in the body, thus having a central role in any body movement [31]. In manual control cybernetics, early research has investigated the characteristics of the manipulator and the neuromuscular system together [2, 32], although later research has first looked at full-body movement situations [33], and then on the pilot's arm specifically [34].

Current cybernetic approach models the neuromuscular dynamics as a damped second-order system [1, 35, 36], with the natural frequency and the damping of the system as parameters to be adjusted. The neuromuscular transfer function does not include a gain as the human neuromuscular system is gain-adaptive, meaning that it adjusts the gain it operates at based on the input. The neuromuscular natural frequency, ω_{nm}, represents the cutoff frequency and the damping coefficient, ζ_{nm}, influences the magnitude peak of the transfer function [37, 38]. In more common terms, the damping coefficient could be said to represent the "stiffness" of the neuromuscular system, indicating how "flexed" or "relaxed" the muscles of the HC is when performing the control task.

3.4.3. Equalization

The final part of the pilot model is the equalization, which represents the main adaptation of the human pilot's behavior to the controlled element [1]. Controlled element of various forms require different control behavior from the human operator in order to achieve the crossover condition defined in Eq. (3.1), and while the delay and the neuromuscular system are intrinsically limited in how much they could be varied, equalization covers for this tailoring.

There are three main elements that the equalization comprises of: gain, K_v , lead, T_L, and lag, T_I. The gain term represents how much the sheer magnitude of the human controller's response is amplified relative to the input. Pilot gain have been used as a metric to denote aggressiveness and observe differences between individual pilots [39]. The lead term could be seen as the compensation as the controller anticipates changes to the input to provide an earlier response. Finally, the lag term stand for the delayed response that aims the prevent large oscillations.

Not all terms are always used, and more than a single lead/lag term could be used [1]. Pure lead and lead-lag equalization forms are especially common for pitch attitude tracking tasks, although recent works have suggested that an additional lead term could increase accuracy [27]. The motive for adding the equalization to the pilot model has been to extend the cover of the crossover model as the initial framework only covered for a limited frequency range within the crossover region. Extending the equalization is crucial for observing the bandwidth of the controller, as pilot dynamics outside the crossover region are also relevant. Furthermore, it has been proposed to use the "pilot bandwidth" as a measure of differences between pilots, and to classify and assess them [40].

3.4.4. Summary

To sum up, manual control cybernetics mathematically models the human controller that performs a task with a transfer function. This model could be used to explain key aspects of pilot behavior as the perception, decision-making, and intrinsic limitations of the human form the basis. There are three main parts to the model, namely the equalization, delay, and the neuromuscular dynamics. An example of this pilot model could be seen in Eq. (3.3), where the sections of the model are labeled.

$$H_p(j\omega) = \overbrace{K_v \frac{T_L j\omega + 1}{T_I j\omega + 1}}^{\text{equalization}} \overbrace{e^{-j\omega\tau}}^{\text{delay}} \overbrace{\frac{\omega_{nm}^2}{(j\omega)^2 + 2\zeta_{nm} j\omega + \omega_{nm}^2}}^{\text{neuromuscular dynamics}} \tag{3.3}$$

The parameters that make up this transfer function depend on a variety of factors, such as the control task and the individual controller. This makes it possible to observe and analyze individual differences between human controllers through these parameters. Even though sometimes average pilot models are used [35, 8], predicting individual controller models is outlined as a critical need for personalized support [7, 1].

3.5. Conclusion

To sum up, this chapter explains the literature search on the cybernetic theory, which forms the basis for modeling human behavior in manual control. The cybernetic model comprises of several parameters that vary in terms of how much they differ between individuals. Previous research has outlined the equalization part as a more person-dependent component of the model, although this claim needs validation. Studying how the cybernetic model parameters change from person to person is key to understanding individual differences in manual control, and examining controller data and simulating various conditions would be helpful in this regard. Furthermore, the control loop shows that the human controller is located between the tracking error and the control input signals and these could be used to examine the differences between individual human controllers. Finally, it could be said that much of the attention has been on the LTI component of the pilot model and thus it would also be beneficial to assess the impact of the remnant its relevance to individual differences.

4

Human Aim

This chapter will bind together the previous chapters by examining literature that continues upon the cybernetic theory and focuses on individual differences. First, a key element for this research, the human cost function, will be explained. Later, aerospace-specific applications of the topic, such as handling quality ratings and pilot gain will be explained.

4.1. Human Cost Function

In this section, the human cost function, or more precisely the cost function that the human operator minimizes during a control task, will be explained. This cost function is considered as a key indicator of the attitude with which the control task is taken on by the human controller. A brief origins of the cost function will be provided, as well as current developments and ideas on the topic.

4.1.1. Origins

The history of a cost function describing human controllers' approach to a control task could be traced back to the Optimal Control Model (OCM) devised by Kleinman et al. [32]. The foundation for the cost function lies in the key assumption that the human "chooses" a control input to provide as a response when performing a tracking task, and that this choice is made based on the solution that minimizes a cost function.

The human controller is tasked with minimizing the mean squared error for tracking. However, it is intrinsically impossible to simply ignore the effort required, and try to get to the best performance. Therefore, the cost function must be composed by using the terms for the error signal and the control input. These are represented with e and u respectively in the control loop depicted in Figure 3.2. There, it could be seen that the system error is formulated as the difference between the system output and the forcing function, also provided as an input to the pilot, and the control input is the resulting signal as the pilot processes the error, and provides as an input to the controlled vehicle.

The basic form of the cost function is the weighted sum of the mean squared values for the system error, control input, and its derivative, see Eq. (4.1). This equation shows how the cost function was originally stated and then simplified in [32] and [41]. Note that the initial formulation of the cost function had the n-vector system state, which is represented by the system error for a compensatory tracking task. Moreover, the mean squared values were formulated as expected values, which was then simplified into variances, and the trivial weighting on the error term is omitted.

$$J(u) = E\left\{\sum_{i=1}^{n} q_i x_i^2 + ru^2 + g\dot{u}^2\right\} = \overline{\sigma_e^2} + r\overline{\sigma_u^2} + g\overline{\sigma_{\dot{u}}^2} \tag{4.1}$$

The human cost function has been adopted in various forms in research mainly in the field of cybernetics [42, 43], but also other related fields such as robotics [3], where it has been adapted to describe the robot objective too. In some versions of the cost function, the "effort" terms, u and $\dot{u}$, have been simplified to just one of them (usually in favor of $\dot{u}$) [32, 44, 45]. Overall, there has been no set guideline on how the cost function should be formulated for a control task and how it should be adjusted based on differences in the

tasks. However, the human cost function remains commonplace in literature and novel cost functions for more specific purposes are being propounded [46], although personalization is still lacking.

4.1.2. Finding the Weightings

Despite all the variation on how the cost function is presented, the goal of the cost function remains: to define and find a numeric weighting between how humans value “performance” and “effort” for a control task. Finding the cost function weightings has been presented as a “nontrivial matter” [32], and multiple methods have been used to try to compute them, based on the application of the cost function.

Due to being closely associated concepts, there have been several attempts to link the weightings in the cost function to the cybernetic pilot model, going as far back as to the original OCM paper [32]. The initial idea was that the weighting on the control input rate would be directly proportional to the first-order neuromuscular lag [41], and this idea has seen recognition, even in recent research [44]. Nevertheless, no framework was established as the second-order representation of neuromuscular dynamics has gained popularity [1] and subjectivity became focused on equalization rather than the physical limitations [47].

Finally, the option of linking the equalization parameters (namely the visual gain, K_v, and the lead time constant, T_L) to cost function weightings was considered, following up on the research conducted by Butijn [48]. A simplified cost function was utilized, as the control input rate term was neglected, resulting in one weighting only (K_u, for σ_u). This paper thus determined the control input weighting for an optimal controller by assuming constant values for the physical limitations and varying the gain and the lead time. The weighting that most closely resembled the reference data for σ_e and σ_u was selected, alongside the corresponding equalization. How the σ_e and σ_u values change as a function of K_v and T_L was plotted as contour maps, and could be seen in Figure 4.1. A significant portion of the plots remain blank as the equalization corresponding to those points lead to unstable control systems.

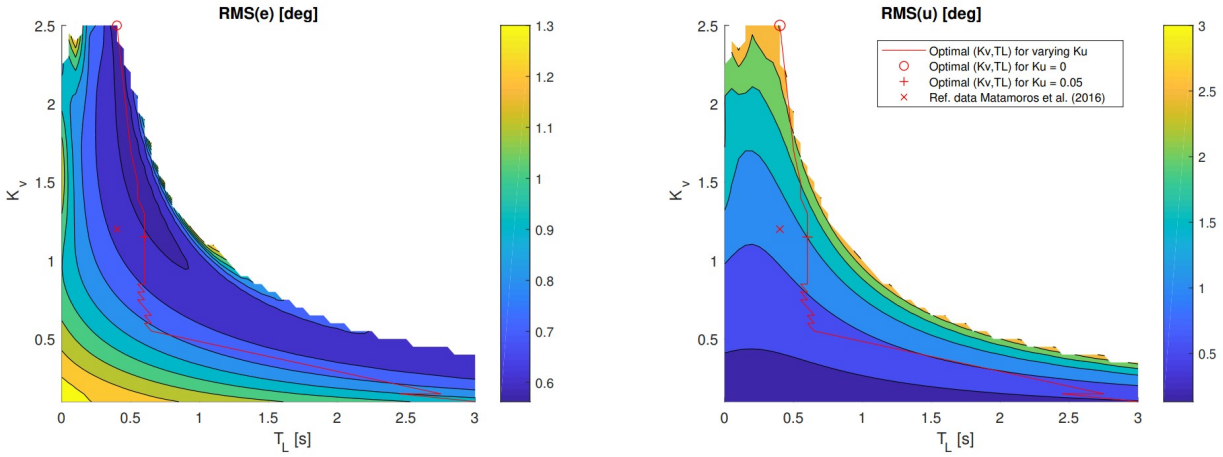

Figure 4.1: Contour maps showing how σ_e and σ_u are influenced by the equalization [48]

The red circle on the plot represents the “ideal” controller, with only the performance (σ_e) term in the cost function ($K_u = 0$). The red line that follows shows the operating conditions for varying values of the control input weighting, K_u, so which equalization parameters the human controller would adapt to when operating with the cost function that corresponds to that weighting. Finally, the cross and the plus mark the reference point from literature, and the point on the line that is the closest to that respectively. The point marked with a plus correspond to $K_u = 0.05$, thus concluding the cost function weighting for the “optimal controller”. This contour maps thus visualizes how σ_e and σ_u values change for different equalization settings and how a correspondence between the cost function weighting and the equalization could be established.

An important aspect of this work that must be mentioned is that it was focused on the human adaptation to changes in the controlled element and the differences between participants were largely ignored for this step. Even though this identifies a research gap, it also highlights the specific context in which these results were found and what needs to be adjusted.

4.2. Pilot Gain & Novel Cost Functions

As one of the most widely known manifestations of human controller's balancing of performance and effort, "pilot gain" refers to how much amplification a controller applies in a control system. It is mainly the ratio between magnitudes of the input provided to an element and its output. Pilot gain is of critical importance to system stability and operator performance, while it also depends on a variety of factors; including the system properties, task requirements, and the pilot's characteristics. Moreover, in a report addressing both the technical and psychological factors that define the concept of pilot gain, it has been said to represent the "individual *aggressiveness* with which a pilot controls" [39].

Pilot gain has traditionally been used as the key distinguishing feature between pilots, although some literature have claimed that this is a "misnomer" [40, 47], and the "bandwidth" of the pilot is what defines differences between pilots. The bandwidth is significantly influenced by the equalization parameters (which include the gain), suggesting that they could mark individual differences. This links back to the equalization component of the cybernetic pilot model, as the range of frequencies covered by the equalization describes the bandwidth.

Closely related to pilot gain is the topic of handling qualities ratings, which are a series of methods of subjectively assessing how pilots perceive the flight characteristics when controlling a vehicle. These ratings are crucial to examine both how well the vehicle and its interface are designed, and also how well a pilot is equipped with guiding such vehicle. Thus, looking at handling qualities ratings and how it relates to pilot gain could be helpful for eliminating pilot errors, such as pilot induced oscillations (PIO).

While handling qualities ratings are sometimes determined by simply using qualitative scales, previous research has looked at using the cybernetic theory to quantify handling qualities [36, 49]. Hess and Bachelder have investigated how the cybernetic analysis and related concepts such as the phase margin could be utilized to have a unified framework that explains pilot control perception in quantitative terms. Furthermore, as part of these works, Bachelder has developed new human cost functions that are formulated to represent handling qualities criteria better. These functions have included terms such as the phase margin [50]; see Eq. (4.2), where the $I_{\dot{e}\dot{e}}$ term is derived to represent the phase margin linearization behavior. Some more abstract terms have also been included, such as the peak open loop neuromuscular amplitude ($|G_{OL,NM}|$), the difference between the actual slope and idealized Crossover Model slope ($|m_{OL} - m_{CM}|$), and the projection of the line formed by conducting a least squares regression on the *workload metric* ($|\mu^{\gamma} - \mu^{\gamma}_{lin}|$) in Eq. (4.3) [46]. Even though these novel human cost functions are still unaccustomed, introduction of new ideas within this area to bridge cybernetics and handling qualities ratings via individual differences is a significant step forwards in research.

$$J = \frac{\sigma_e}{I_{\dot{e}\dot{e}}} \tag{4.2}$$

$$J = \frac{1}{Perf}|G_{OL,NM}|[\Sigma_{\omega=.9\omega_c}^{\omega=1.1\omega_c}|m_{OL} - m_{CM}|][\Sigma|\mu^{\gamma} - \mu^{\gamma}_{lin}|] \tag{4.3}$$

4.3. Conclusion

Overall, the idea of observing human controller attitude via a cost function has been considered in cybernetics for over half a century, At the forefront is the cost function that utilizes the tracking performance and control input, stated in Eq. (4.1). Although other cost functions have been developed recently, this function and its derivatives, with either the control input or its rate omitted, is by far the most commonly used one.

For this research project, Eq. (4.1) is considered as the most viable cost function to explore individual differences upon and predict the individual set of cybernetic parameters from. This is due to multiple reasons, firstly because of its aforementioned extent. Secondly, the weightings and existing research on estimating/predicting these weightings provide a feasible baseline to then study individual differences on. Ease of individualization and link to the cybernetic model are not present in other cost functions which are generally developed for specific purposes such as estimating handling qualities ratings. Finally, the simplicity of Eq. (4.1) suggests that using that would be more suitable initial attempt and based on how this cost function performs, later research can utilize concepts and ideas from the novel cost functions.

5

Preliminary Analysis

Alongside findings from literature, some preliminary analysis was conducted using the data collected in experiments carried out for previous research projects [28, 48]. The goal of performing some analysis early on is to fortify the results of the literature study, and to gain new insights by looking at existing data from a different point of view. Preliminary analyses will also involve replicating conditions from earlier experiments and running simulations to test out the methods proposed for this research. This will help make some research decisions, and show which direction to go towards.

5.1. Setup

The preliminary analysis will be conducted in MATLAB, and the data from Harder's thesis [28] will be the centerpiece of this setup. This dataset was picked to perform preliminary analysis upon due to its availability and extent. The experiment that was conducted as a part of this thesis involved a tracking task performed by 24 participants which were divided into two groups of equal size: training with motion feedback and then test runs without motion and training without motion and testing with motion feedback. Each participant performed 100 runs of training, followed by 75 runs of testing and these runs were split into a total of 7 sessions of 25 runs each. For the preliminary analysis conducted as a part of this project, only the data from the no-motion training is considered, in order to nullify the effects of motion feedback and training and focus purely on the individual differences in the tracking task control.

The experiment consisted of a pitch compensatory tracking task, following the structure given in Figure 3.2. The forcing functions (target and disturbance) were sum of sines signals, with sines having varying amplitudes, frequencies, and phases. For the design of these forcing functions, the method laid out by Damveld et al. has been implemented [51] as 20 different sinusoidal signals each were combined to generate them. Furthermore, the experiments lasted 90 seconds, from which the first 8.08 seconds were discarded as the settling time and the remaining 81.92 seconds were used for measurement. Finally, the reduced-order linearized model for the elevator-to-pitch dynamics of a Cessna Citation I, shown in Eq. (5.1), was used as the controlled element [26].

$$H_c(j\omega) = H_{\theta,\delta_e}(j\omega) = 10.6189\frac{j\omega + 0.9906}{j\omega((j\omega)^2 + 2.576j\omega + 7.612)} \tag{5.1}$$

The measurements that will be used in the preliminary analyses mainly involve the error and control signals, e and u, and the identified cybernetic parameter data. For every run that is performed as part of the experiment, the time traces for the signals are recorded and the cybernetic parameters for the human controller is identified using the model described by Zaal et al. [52]. It must be noted that these recordings and identification methods are prone to errors, with some values beyond the limits of what is considered humanly possible.

5.2. Performance - Effort Plots

The first data that was looked at for the preliminary analysis were the tracking error and the control input signals. The human cost function utilizes root mean squared values of the error and control signals alongside personalized coefficients and thus taking a look into these signals before working with the cost

function could provide beneficial insights. For all 100 runs of the 12 participants in the desired experimental conditions, the standard deviations of the error and control signals were calculated (σ_e and σ_u) and plotted in different ways.

5.2.1. Methodology

Firstly, the individual run data were plotted on σ_e-σ_u axes to see if participants are already distinguishable from the magnitudes of their tracking error and control input. Plotting the σ_e and σ_u could already portray certain differences between individuals: For example, a person with a high control input and high tracking error could be considered as "overcompensating". On the contrary, someone with low values could be viewed as more "effective" or "economical" for this particular task. Similarly, a controller with low input and high error can be seen as more "careless" while the opposite would be said to have "tried harder". All 100 run data for all 12 participants are shown in Figure 5.1 as each color represents a different participant.

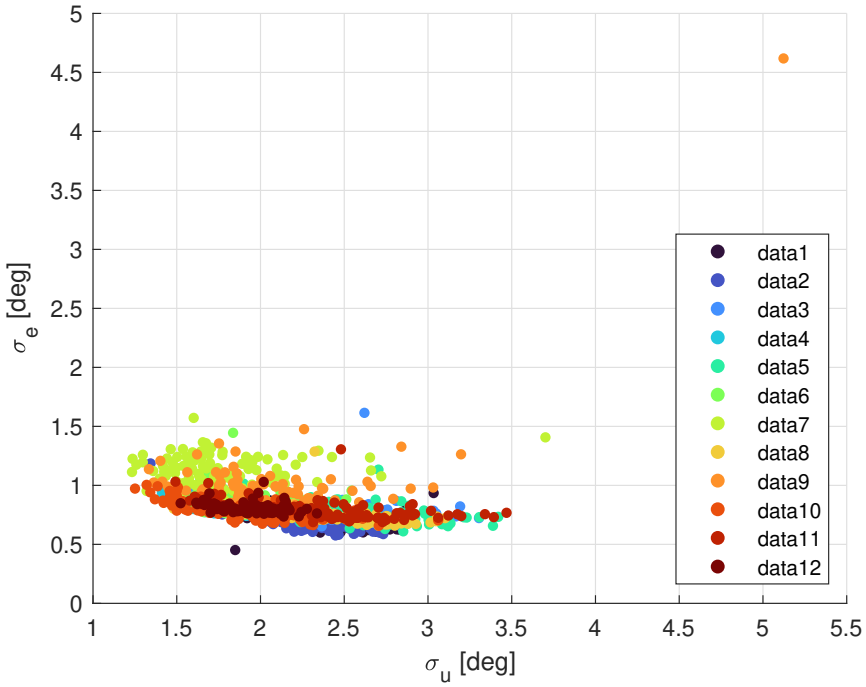

Figure 5.1: All σ_e and σ_u data

Most of the data lies in between the $0.5 < \sigma_e < 1.5$ and $1 < \sigma_u < 3.5$ ranges, except for a few outliers, such as a run of participant 9 with $\sigma_u \approx 5$ and $\sigma_e \approx 4.5$. Furthermore, data were mostly clustered for each individual, meaning that the data points of a participant are located close to each other without mixing much with other participants' data points. Nevertheless, 100 runs could be considered too many to analyze together as skill training and task learning takes place during these. Effects of training and learning influence the control attitude of human controllers and thus affecting the cybernetic parameters as well. Defining individual differences in learning and adaptation on top of the basic characteristic differences could extend the scope of the research project significantly. Therefore, observing how the σ_e and σ_u data progresses through the runs would be a useful first step for the analysis, to narrow down the data if necessary.

5.2.2. Progression

To examine how each participant progresses through the runs with their attitude towards the control task, the plot from Figure 5.1 was split into twelve plots that each feature only one participant's data, seen in Figure 5.2. Furthermore, since it is no longer useful to use different colors to distinguish the participants, a different color coding was used to indicate the run number. The data-points gradually transition from cool to warm colors as the run number increases, e.g. blue in the initial runs, green and then yellow in the intermediate runs and orange-red in the last runs. The plots are all set to have the same axes ranges in

order to compare them effectively.

Supporting this is Figure 5.3, where once again the progression of σ_e and σ_u for individual participants is shown with the lateral axis indicating the run number. The three black vertical lines mark the different sessions; since it would be quite exhausting to perform 100 runs in one go, the participants in this experiment were invited for four sessions of 25 runs each and therefore these distinct sessions are also denoted in the plot. In this figure, trends in the control input and tracking error values as the controller trains could be observed. Compared to Figure 5.2, Figure 5.3 more clearly displays the changes in magnitude as the two values are plotted separately.

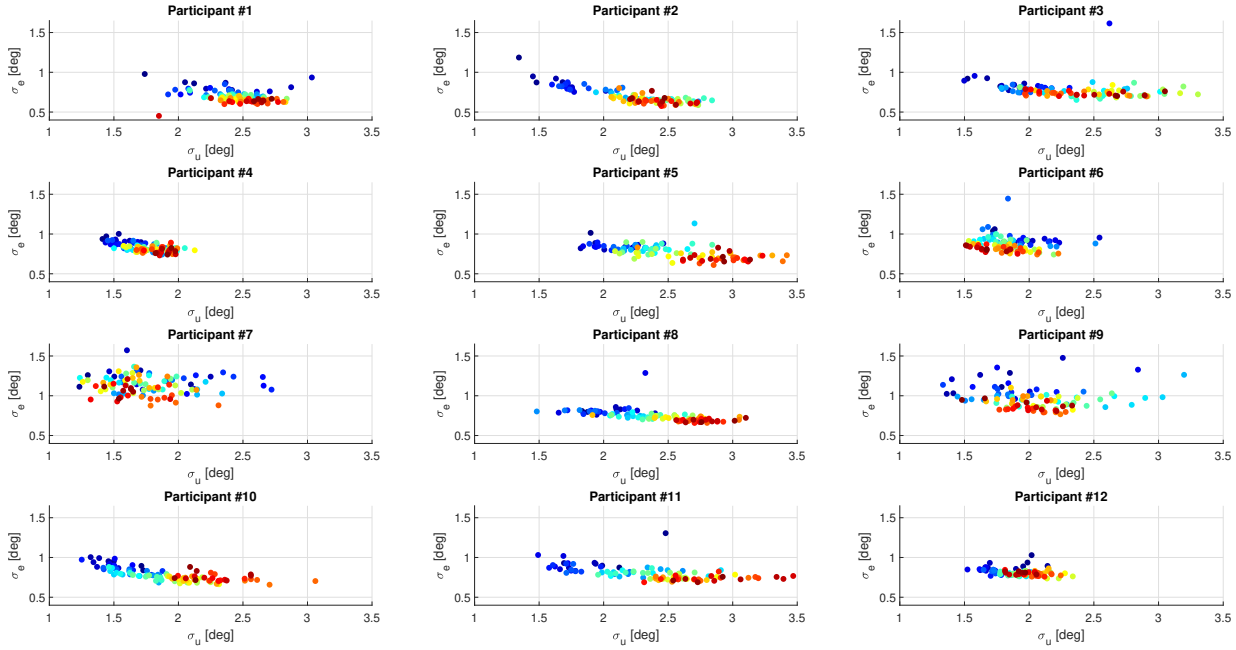

Figure 5.2: Progression of σ_e and σ_u

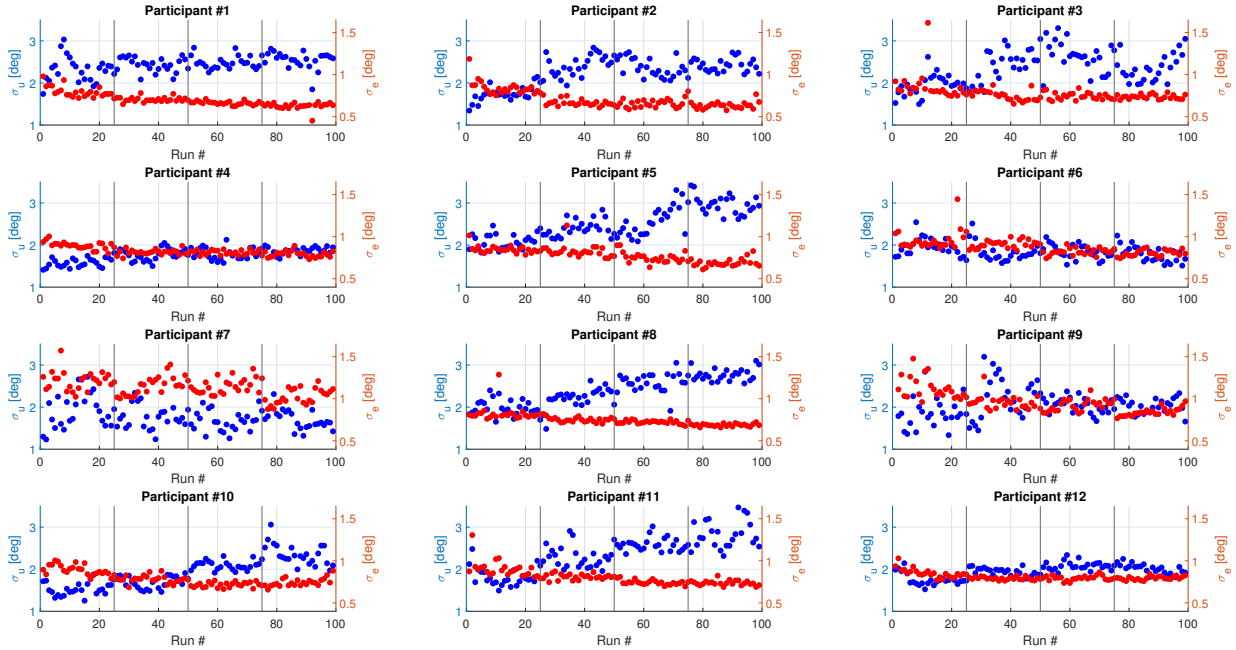

Figure 5.3: Change of σ_e and σ_u through the runs

These plots show how the σ_e and σ_u values of each individual changed as they became more familiar with the task and points out differences in learning/adaptation styles: some participants (such as participants 7 and 9) show great variation in their data through the runs and some other participants (such as participants 4 and 12) are very limited in that aspect. Naturally, when participants perform more runs of the control task, their tracking errors decrease, even though by different margins. Plus, it could be clearly seen for many participants that as they become more and more "skilled" in this control task, they tend to increase their control input. Exceptions to this are participants 6 and 7 who have also seen a decrease in the control input alongside the decrease in the tracking error.

Another thing to comment on based on these plots is the difference in the magnitudes of σ_e and σ_u: participants have had characteristically different ranges of values throughout the runs. For instance, participant 4 has exceeded $\sigma_u = 2$ twice while participant 5 has fallen behind this value on very few occasions. On the other hand, these participants have had very similar σ_e values, thus depicted that individual differences could be traced in σ_e and σ_u values.

Finally, this dataset was reduced to contain just the last 25 runs, which could be considered as the "skilled" period. The σ_e and σ_u values averaged from the last 25 runs were plotted against each other in Figure 5.4, with the opaque data-points marking the average and the ellipses showing the variation in these values, within those runs. The ellipses were drawn with the assumption that the data-points are distributed normally around the average and the 95% confidence interval is covered by the extent of the ellipses. The sizes of the ellipses depict the differences in variation between individuals; some of participants' data is more consistent around the average, resulting in smaller ellipses while some other participants' data changes considerably from run to run, with much larger ellipses. Moreover, less data makes the data that remains more clearly visible and thus the differences between the participants are more easily identifiable. This suggests that data from numerous runs is redundant when observing individual differences through σ_e and σ_u and that focusing on the "skilled" phase of participants could give a better indication on individual differences, as these differences will be "sharper" after training is complete and personal traits are more evident.

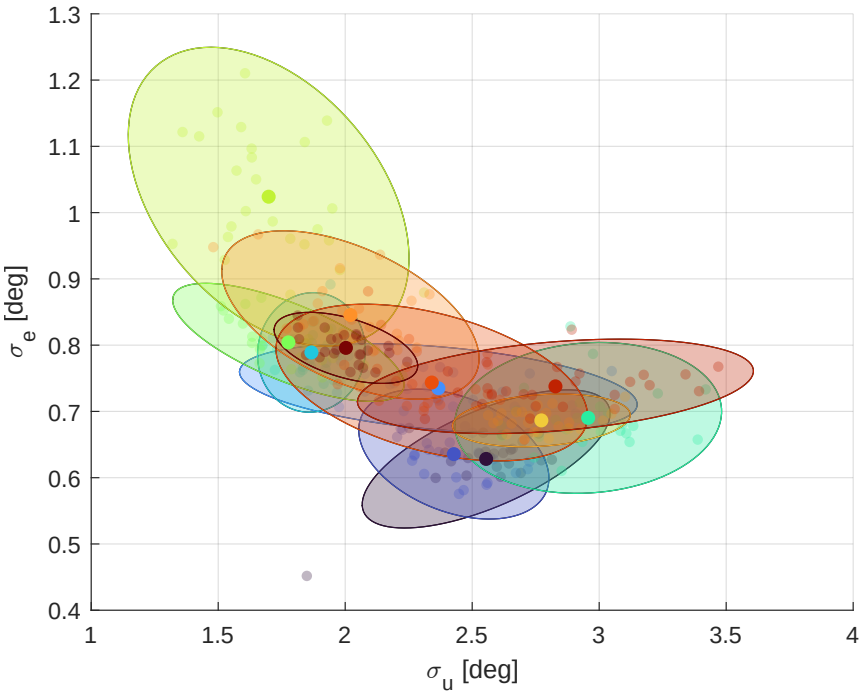

Figure 5.4: Average σ_e and σ_u values and variation

This plot gives a clearer view on where the individual "operating points" in terms of σ_e and σ_u are at, and how consistent each individual is with it. The points are distributed along a curved line of inverse relationship between σ_e and σ_u, suggesting that controllers pick their operating points based on how much effort they're willing to put in, in order to perform better. However, the shape also implies that with each

additional increment of effort, the amount of improvement in performance decreases, hinting at intrinsic limitations. The size and shape of the ellipses show that individual differences between task attitude consistency also exist and that inconsistencies could be in either of σ_e or σ_u, or both.

5.3. Cybernetic Parameters

In addition to the analysis on the σ_e and σ_u values, a look into identified cybernetic parameters from Harder's experiment was taken. As explained earlier, the cybernetic parameters are useful for observing individual differences in manual control. Thus, a sensitivity analysis on just how much these parameters vary between individuals and to what extent changes in these parameters impact σ_e, σ_u, and $\sigma_{\dot{u}}$ will provide valuable insights. Since these values make up the human cost function, it is important to see which parameters in particular drive these values and if there are certain parameters that are completely unrelated.

The cybernetic parameter data is available already in Harder's dataset and therefore no processing is needed. As a part of the research [28], the cybernetic parameters have been identified for every run of every participant. Once again, only the last 25 runs (the "skilled" period) will be used for this analysis as the parameters are more stable within that period. The identified parameters from these runs are averaged (no significant outliers were present) to define the characteristic set of cybernetic parameters for each participant. The pilot model used in Harder's experiment was defined as given in Eq. (5.2), resulting in six cybernetic parameters: $K_v, T_L, T_I, \tau, \omega_{nm}, \zeta_{nm}$. These parameters are named: the visual gain, the lead-time constant, the lag-time constant, the time delay, the neuromuscular natural frequency, and the neuromuscular damping coefficient, respectively.

$$H_p(j\omega) = K_v \frac{(T_L j\omega + 1)^2}{T_I j\omega + 1} e^{-j\omega\tau} \frac{\omega_{nm}^2}{(j\omega)^2 + 2\zeta_{nm} j\omega + \omega_{nm}^2} \tag{5.2}$$

5.3.1. Between-Subject Parameter Variation

Before getting to the main section of the sensitivity analysis, where how "sensitive" σ_e, σ_u, and $\sigma_{\dot{u}}$ values are to the variation in the cybernetic parameters will be examined, how much these parameters actually vary needs to be assessed. This will not only provide an idea on which parameters are more susceptible to changes from person to person but also a range to look into in the sensitivity analysis itself. Hence, the variation in each of the six cybernetic parameters for the twelve participants were shown in a box plot in Figure 5.5, with the average values of the parameters given in Table 5.1.

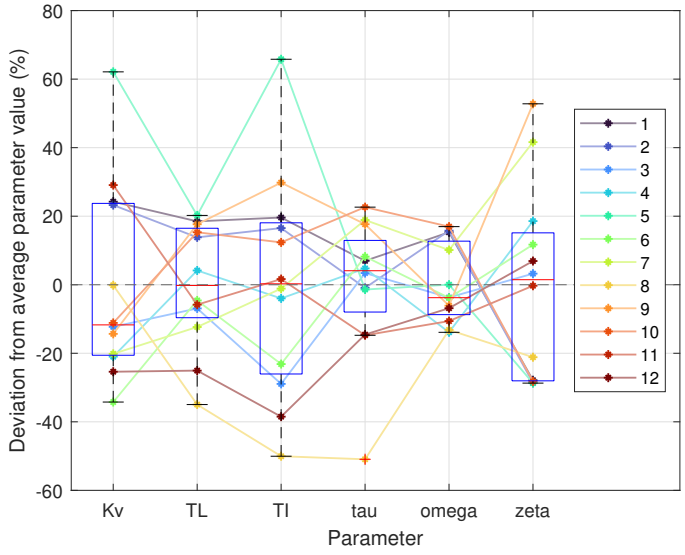

Figure 5.5: Variation box plots, overlapped with individual data

Table 5.1: Average parameter values

Parameter	Average Value
K_v	3.069
T_L	0.440
T_I	1.394
τ	0.207
ω_{nm}	10.05
ζ_{nm}	0.262

This figure states that for all parameters the interquartile range is around $\pm 20\%$ of the average value. However, for parameters such as the visual gain, K_v, and the lag-time constant, T_I, the variation beyond

this range is considerably more than that of the other parameters. The time delay and the neuromuscular natural frequency vary the least between participants, which is in accordance with the expectations from literature that these parameters (alongside the neuromuscular damping coefficient) represent the intrinsic limitations of the human body and are less person-dependent: with the sole exception of a participant with a very low time delay, all participants' τ and ω_{nm} values remain within a range of 40 percentage points. This increases to 60, 100, and 120 percentage points for T_L, K_v, and T_I respectively, thus making the values of these parameters more person-dependent.

5.3.2. Performance & Effort Sensitivity Analysis

Taking the interquartile range of average $\pm 20\%$, the sensitivity analysis could be conducted. For the sensitivity analysis, an average controller model is made first by taking the averages of all six cybernetic parameters for the twelve participants that there is data for. From this model, simulations replicating the control task represented in the control loop in Figure 3.2 are run and the σ_e, σ_u, and $\sigma_{\dot{u}}$ values are computed. These simulations will be explained in more detail in the next section. The simulations for the sensitivity analysis involve changing the value of a cybernetic parameters within the average $\pm 20\%$ range and comparing how much the resulting σ_e, σ_u, and $\sigma_{\dot{u}}$ get influenced by this change in a parameter. This sensitivity analysis is conducted for these three values independently and for the six cybernetic parameters, for a total of 18 conditions and the results are given in Figure 5.6.

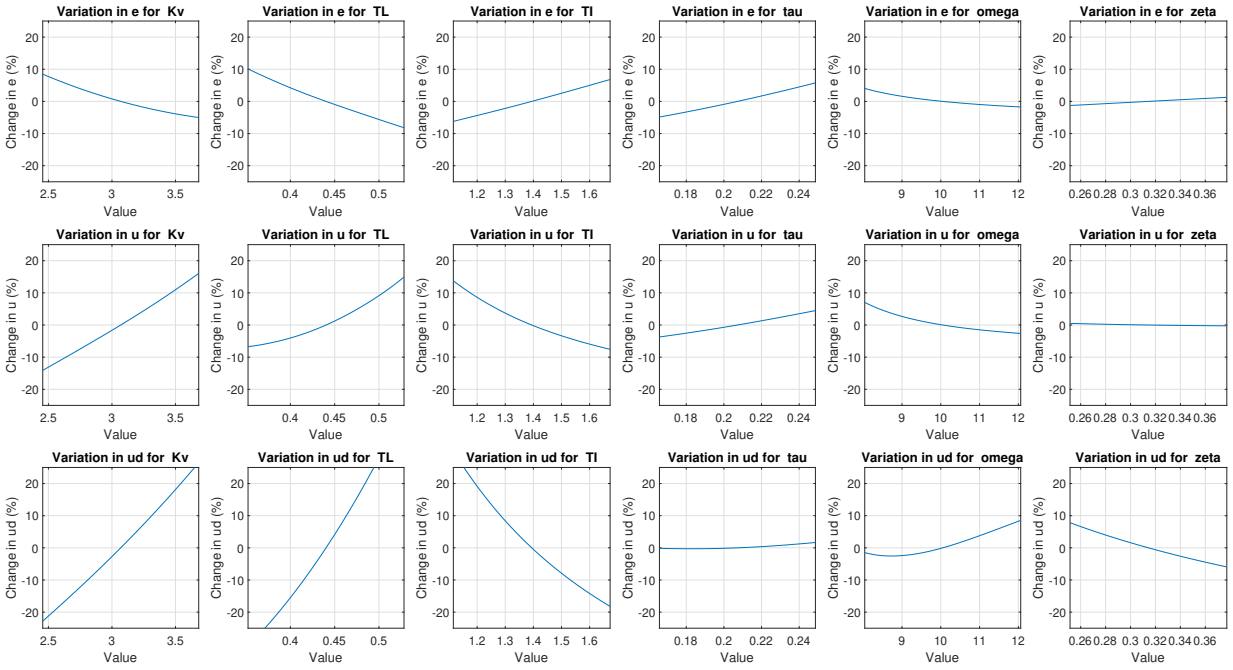

Figure 5.6: Sensitivity of σ_e, σ_u, and $\sigma_{\dot{u}}$ on the cybernetic parameters

These results show that the equalization parameters (K_v, T_L, T_I) have a much more significant impact on the error and control signals, as these signals are more *sensitive* to the equalization compared to the physical limitations. The σ_e, σ_u, and $\sigma_{\dot{u}}$ values rapidly change for different equalization parameters while these values are mostly invariant for changes in the physical limitation parameters ($\tau, \omega_{nm}, \zeta_{nm}$). For both σ_u, and $\sigma_{\dot{u}}$, the ranges of variation in K_v, T_L, and T_I result in a total of at least 20% difference (difference between positive and negative changes) compared to the average while for σ_e this value nearly approaches 20% for the three parameters. For the other parameters, this is below 10% for almost all cases, with the sole exception being the variation in $\sigma_{\dot{u}}$ for changes in ζ_{nm}.

While this confirms that the human cost function could be closely tied to the equalization part of the pilot model only, it also raises the question on whether the cost function could be used to observe individual differences in the time delay and the neuromuscular dynamics. Moreover, this sensitivity analysis only looks at the case where the parameters are changed independently of each other, and looking at how

sensitive the error and control signals are to *combinations* of parameters could also provide interesting outcomes.

5.4. Control Task Simulations

Although the available experimental data gives perspective for the research project, it is still constrained by the conditions and circumstances of the experiment, e.g. it is limited to the specific control task, participants, and controlled element used. In order to investigate how results would be different for more custom cases, such as a hypothetical controller with a specific set of cybernetic parameters, the experimental conditions could be replicated in a simulation. Simulations conducted for this purpose focus on how different cybernetic parameters would influence the σ_e, σ_u, and $\sigma_{\dot{u}}$ values that make up the cost function. Therefore, the simulations are set up with the forcing functions (f_t and f_d) and the controlled element dynamics (elevator-to-pitch dynamics of a Cessna Citation I, Eq. (5.1)) exactly the same, the pilot model following the same structure as in Eq. (5.2) but the parameters as independent variables, and the σ_e, σ_u, and $\sigma_{\dot{u}}$ as the outcomes of the simulation. In short, how different sets of cybernetic parameters result in different values for σ_e, σ_u, and $\sigma_{\dot{u}}$ are studied using simulations. These simulations are then primarily aimed to link the human cost function and the cybernetic parameters, extending on the approach taken by Butijn [48], where the equalization parameters were linked to the cost function weighting.

5.4.1. Methodology

As explained in Chapter 4, previous research has assumed that the human controller picks and adjusts a control attitude based on a cost function that takes into account the performance and the effort, and operates at the point at which this cost function is minimal. Butijn has built up on this assumption to find the equalization that would correspond to the operating point. This was done by exploring ranges of gain and lead-time constant values, computing the σ_e and σ_u values corresponding to each equalization point, and finding the point that most closely resembles the experimental data [48]. This was visualized with the *cost maps* in Figure 4.1. However, this link between the cost function and the equalization was only for an average controller and personalization was simply ignored.

Furthermore, it must be noted that Butijn's experiment utilized different controlled element dynamics and as a result the equalization component of the pilot model was adjusted accordingly. This pilot model featured a single lead-time component instead of a double-lead and a lag (as was the case in Harder's experiment) alongside the gain, given in Eq. (5.3).

$$H_p(j\omega) = K_v(T_L j\omega + 1)e^{-j\omega\tau}\frac{\omega_{nm}^2}{(j\omega)^2 + 2\zeta_{nm}j\omega + \omega_{nm}^2} \tag{5.3}$$

This also means that varying the visual gain and the lead-time constant only covers to complete extent of the equalization as there is no lag-time constant. Plus, the cost function considered in Butijn's research included only σ_e and σ_u terms (no $\sigma_{\dot{u}}$). Different options will be explored in Section 5.4.3, but a broad form including both the control input and the control input rate term was used in the preliminary analyses (Eq. (5.4)).

$$J = \sigma_e + K1 \cdot \sigma_u + K2 \cdot \sigma_{\dot{u}} \tag{5.4}$$

Thus, this process was repeated using Harder's data, to find the individual cost function weightings that correspond to each participant's equalization point. The visual gain and the lead-time constant were varied in an extensive range and the σ_e, σ_u, and $\sigma_{\dot{u}}$ values were computed for each combination. For now, the other cybernetic model parameters were kept at the average value for every participant, although the advantages and disadvantages of using average values for the rest of the model need to be weighed carefully in later analyses.

5.4.2. Cost Maps

The σ_e, σ_u, or $\sigma_{\dot{u}}$ values were displayed on three contour plots (one for each signal), where the color indicated the value while the visual gain and the lead-time constant values were set on the axes. The total cost map is then basically a sum of these three maps, with the σ_u and $\sigma_{\dot{u}}$ plots scaled with the cost function weightings.

The cost function weightings were identified similarly to the method Butijn followed; the equalization combinations that correspond to the minimum cost function value for every discrete step of cost function weightings were marked. The points closest to the identified equalization values for each participant were taken as the cost function weightings that the participant operated at. Example cost maps for two of the participants are shown in Figure 5.7 and Figure 5.8.

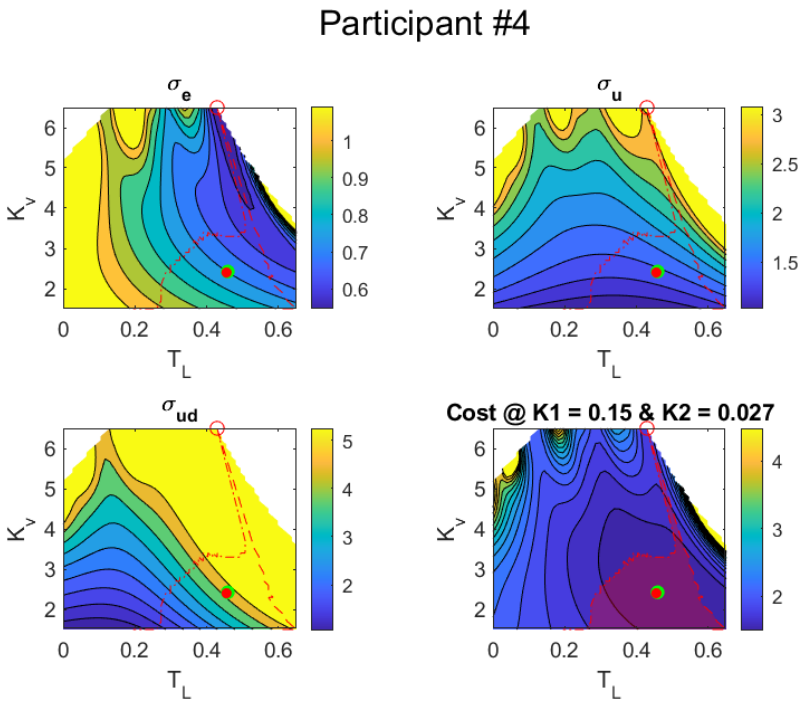

Figure 5.7: Cost map of participant 4

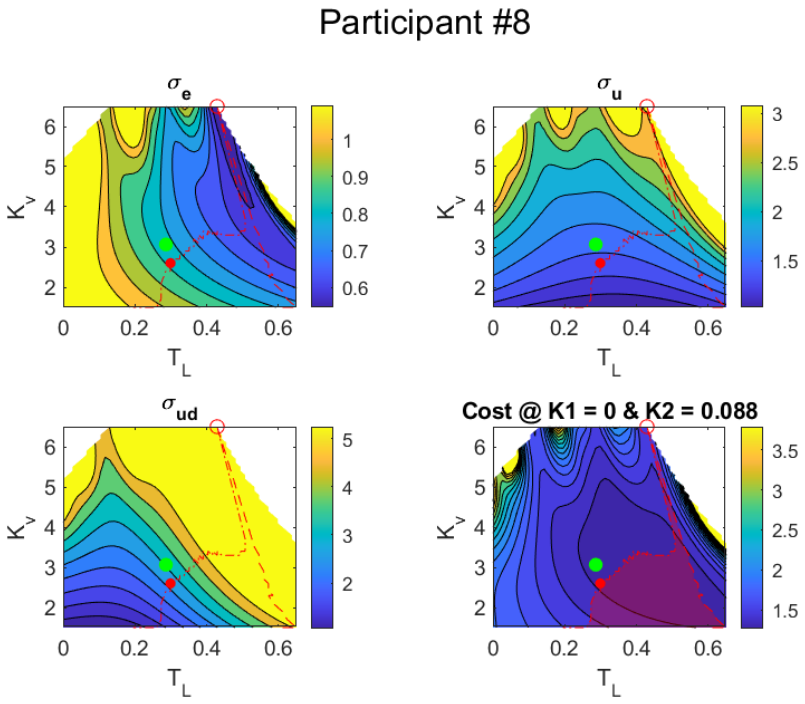

Figure 5.8: Cost map of participant 8

The red circle indicates the minimum cost function point for when both cost function weightings are zero (minimum tracking error), and the dashed lines indicate the operating points for when either of the σ_u or $\sigma_{\dot{u}}$ weightings are set to zero. The red highlighted area in between these lines covers the range of values that could be reached by a combination of the weightings (exact match) while the K_v and T_L combinations that are outside cannot be precisely predicted with the cost function weightings. As seen in the figures, this is the case for participant 8 although for 8/12 participants the equalization could be found using the cost function weightings on the average controller model. While this suggests that individualizing K_v and T_L only could be used to predict the cost function weightings to a considerable extent, it must be investigated how these weightings could in turn be used to predict the cybernetic parameters.

5.4.3. Cost Function Comparison

To conclude the preliminary analyses, different forms of the cost function will be weighed out. How the human cost function is defined is also critical to the analysis, as the cost function weightings will form the centerpiece of the method to predict individual parameters. Literature search has provided a broad definition on the human cost function and the form including both σ_u or $\sigma_{\dot{u}}$ has been used accordingly. However, possible simplifications could be investigated, similar to how Butijn has used a cost function without the $\sigma_{\dot{u}}$ term. Therefore, three cost function options were considered: error and control input only, error and control input rate only, and error and both control input and its rate. These functions are shown below.

$$J = \sigma_e + K \cdot \sigma_u \quad (5.5) \qquad J = \sigma_e + K \cdot \sigma_{\dot{u}} \quad (5.6) \qquad J = \sigma_e + K1 \cdot \sigma_u + K2 \cdot \sigma_{\dot{u}} \quad (5.7)$$

The basis for comparing these cost functions and defining which one is better is the “distance” metric. This metric essentially measures how far the estimate point of the cost function is to the actual identified equalization point. It is calculated as the absolute percentage difference in both K_v and T_L from the original value, summed up. The distance measures for the three cost functions’ estimations of the twelve participants were compared on a box plot in Figure 5.9.

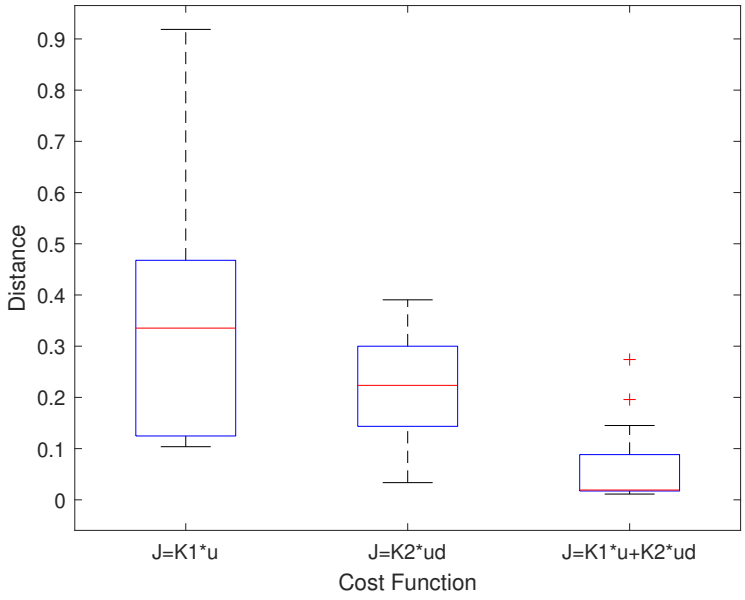

Figure 5.9: Cost function comparison

Figure 5.9 shows that the two simpler cost functions are considerably less effective than the third one, as the distance metrics are much higher. The median distance scores for the cost functions are: 0.335, 0.223, 0.019. The upper adjacent of the third cost function has a value comparable to those of the other cost functions’ 25^{th} percentiles (at around 0.14), meaning that the cases where the third cost function performs particularly worse, it is still as effective as the cases where other cost functions well.

It is also worth noting that a deeper look into the distance values for the first cost function are remarkably divided in two groups, with one group having much higher values compared to the other. Finally, as

discussed in the previous subsection, the distance value is near zero for 8/12 participants with the third cost function, since these participants' equalization lie within the red zone. This puts forth the cost function with all three terms as the most effective one, and implies that simplifying the cost function hampers the accuracy greatly.

5.5. Conclusion

The conclusions that could be drawn from the preliminary analyses begin with how the σ_e and σ_u terms compare between the participants of an experiment. The work conducted on the sample dataset suggests that these values vary considerably between individuals through the course of 100 runs and it is possible to observe individual differences using them. Next, attention was turned into how the identified cybernetic parameters of these participants vary and it was seen that the equalization parameters (K_v, T_L, and T_I) vary and impact the σ_e, σ_u, and $\sigma_{\dot{u}}$ signals to a greater extent compared to the physical limitation parameters (τ, ω_{nm}, and ζ_{nm}). However, the importance of the latter set of parameters is still non-negligible and while they are expected to be less "observable" via a cost function utilizing error and control input signals, the methodology should include a way to predict them using the cost function as well.

The cost maps were generated later, concluding that the cost function weightings could be tuned individually to match with the K_v and T_L value of each participant. The development of these cost maps was a crucial step in this research as it visualized the extent to which the weightings could be identified using the equalization parameters. Following this step would be to in turn predict the complete individual controller model parameters from the identified cost function weightings.

Finally, comparing the three options used for the cost function concluded that the cost function with both σ_u, and $\sigma_{\dot{u}}$ terms perform much better than the other two that lack either term. Moreover, the cost function performed very well (exact match for 8/12 participants) in identifying the cost function weightings and therefore provide a good initial method to then predict cybernetic parameters from. This means that other cost function options could be put aside for now, and novel ideas stemming from those could be interpreted later, based on how effective the current cost function is for prediction.

6

Research Plan

In this chapter concluding the report, an overall plan for the research project will be given. First, major implications from the literature study explained in the previous chapters will be restated alongside the findings from the preliminary analyses. Next, the methodology that builds upon these results will be explained, as the scientific work that will be done as part of this thesis work. Finally, the contributions that the research project is expected to provide will be presented.

6.1. Preliminary Results

The key takeaways from the literature study and the preliminary analyses could be summarized as follows:

- Individual differences is a multidisciplinary field and the trend of personalized products and personalized support in vehicles call for increased attention to individual differences in human-machine systems. (Chapter 2)
- This is reflected on manual cybernetics via the parameters in the pilot model. These parameters have either been assumed for an average controller, or experimental data need to be identified to obtain individualized values. (Chapter 3)
- Different components of the cybernetic human controller model have different implications for individual differences: physical limitations are constrained within a smaller range compared to the equalization, which is viewed as more person-dependant. This idea has been stated in literature and validated in preliminary analyses. (Chapter 3, 5)
- A human cost function to describe how humans balance performance and effort while performing a control task has been suggested although it is not clearly defined. It has also been proposed that the weightings that mathematically represent this balance are personal, but attempts to observe individual differences using such cost functions have been limited. (Chapter 4)
- Research in cybernetics have also inspected the differences between controllers through handling qualities ratings and studies on pilot gain, and linking these to a cost function have been worked on. (Chapter 4)
- The cost function weightings could be connected to the equalization parameters in the cybernetic model although this connection has been established for limited conditions, e.g. limited numbers of participants and controlled elements. Moreover, extending this connection to the other cybernetic parameters is necessary in order to personalize fully, as their impact is non-negligible, although it is yet unknown if this is possible. (Chapter 4, 5)
- Predicting individual sets of cybernetic parameters using the human cost function could be useful in research for generating new, accurate “participant” data. Data generated using individual cost function weightings could provide more realistic human controller models compared to generating cybernetic data randomly or by matching real tracking run data. (Chapter 5)

6.2. Research Questions

The findings from the preliminary part of the research project point towards a need to estimate individual sets of cybernetic parameters and identify the human cost function as a viable tool to install this connection.

Thus main research objective for this project could be stated as: *To predict individual differences in cybernetic parameters by using a cost function, that describes human controllers' relative weighting of task performance and required effort in compensatory tracking tasks*

In addition to the objective, several supporting research questions are also formulated:

- *To what extent do each cybernetic parameter vary between individual human controllers, and how do these variations impact the overall system?* An initial check of which parameters really vary from person to person is necessary. Plus, the impact of such variation in the parameters on the overall control system is also significant, and this could be observed through the performance and control signals that are the input and output of the human controller model respectively.
- *Could a cost function comprising of task performance and required effort, with personalized relative weightings be used to accurately encompass human control attitude?* It is useful to investigate if the original formulation of the cost function is sufficient to establish a connection with the cybernetic model. If not, the components missing in the cost function should be identified. Existing models have pointed out that equalization parameters in particular are useful in this context but it has not yet been tested for comparing individual controllers.
- *Are the relative weightings of performance and effort in the cost function sufficient to predict the set of cybernetic parameters for a controller?* The previous question mainly concerns if a link between the cybernetic model and the cost function could be established at all, while this question builds up on that to assess the effectiveness of the weightings in the cost function for predicting model parameters. It is critical to see which parameters could be predicted and how well these predictions fare for different sets of parameters. The baseline for the success inquired with this question would be the existing methods for generating cybernetic parameter data.
- *To what extent do these assessments of the previous research questions hold true for different controlled element conditions?* Finally, the consistency of the results must be examined to see if a conclusion is valid for a specific case only or if it's a general property. This would provide the scope on how effective the methodology pursued in this research project.

6.3. Methodology

In this section, the methodology that will be followed for the rest of the thesis project will be explained. A brief overview of this methodology could be seen in Figure 6.1, where the scope of the project is illustrated.

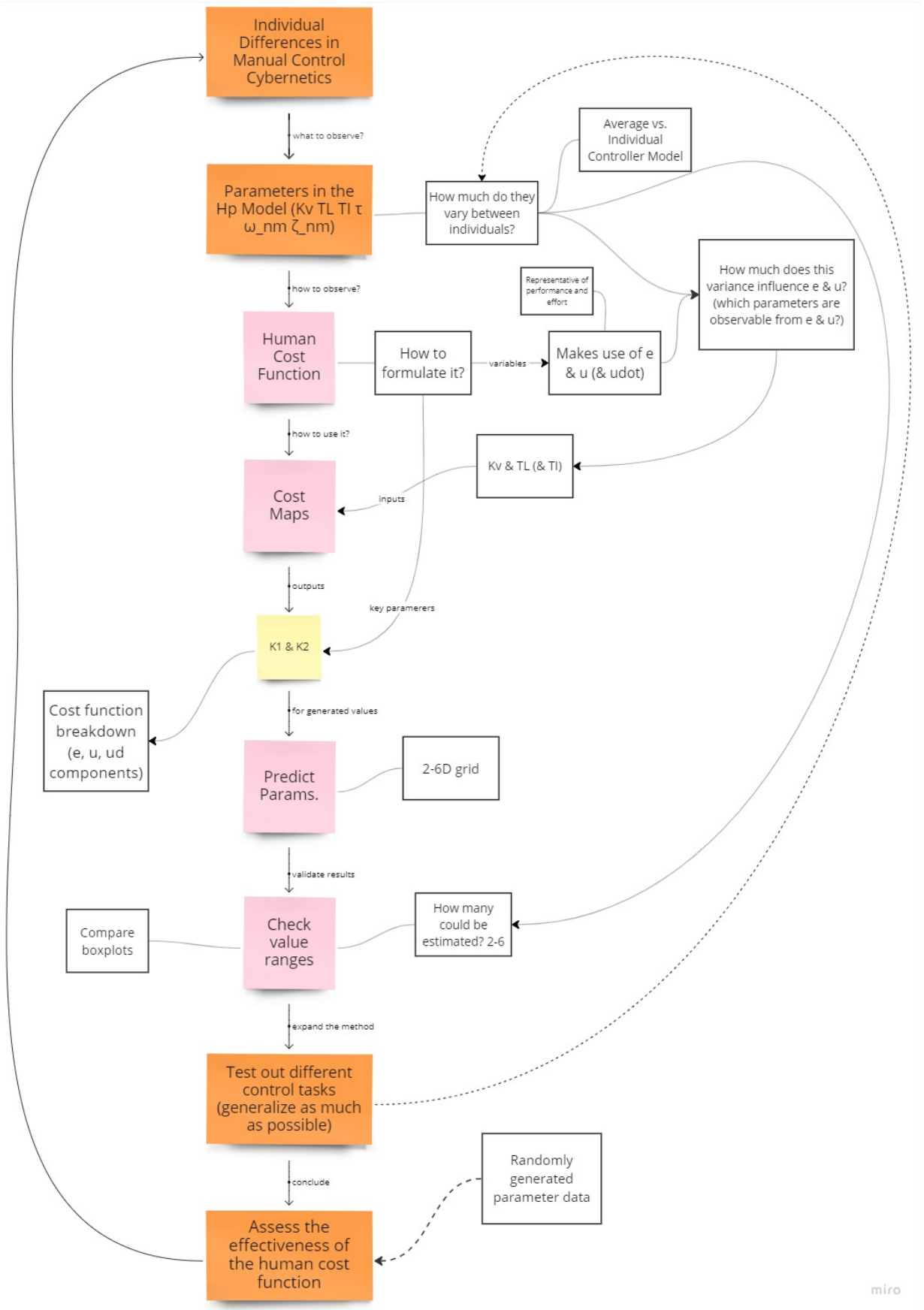

Figure 6.1: Project flowchart

The project explores individual differences in manual control cybernetics and the pilot model parameters are thus the main feature. The human cost function has also been identified as a key concept that individual differences in cybernetics could be observed upon. How this cost function is formulated is nontrivial, as some components are occasionally omitted and recently the addition of more abstract, task-specific terms are proposed to increase fidelity. Nevertheless, the error and control input (also control input rate) signals are certain to form the core of it. In the preliminary analysis section, data from previous experiments were looked at to see how much cybernetic parameters vary between people and how much these variations impact the aforementioned signals, to gain insights into how a cost function based on them could portray individual differences. Based on literature and initial findings, an attempt to link the gain and lead-time constant of the cybernetic pilot model to the cost function was made, as visualized in the cost maps. These cost maps concluded that individualized cost function weightings could indeed be obtained from controller equalization.

Next steps will work with this connection between the cost function and the cybernetic model, to see if independent cost function weightings could be used to predict individual cybernetic parameters ($K_v, T_L, T_I, \tau, \omega_{nm}, \zeta_{nm}$). For this purpose, the predictions will begin with just the equalization parameters (K_v and T_L first, T_I later), and then expanded step by step to involve the other parameters ($\tau, \omega_{nm}, \zeta_{nm}$), as the cost map grid will be extended from two dimensions to six.

These predictions will be validated by comparing the ranges of the values to real-life data (from [48, 53]), to check if the distributions are similar. With additional data, the use of this cost function to predict cybernetic parameters will be tested out in various controlled tasks in order to see how much it could be generalized. This is why the experiments in [48, 53] are considered: double integrator and low order equivalent system dynamics are preferred to encompass a variety of bandwidths and difficulties in the control task, as well as to observe cases where the magnitudes of the equalization parameters are expected to be different. Finally, these results will be compared to simply randomly generating cybernetic parameters data in order to assess how much more effective the cost function predictions actually are.

6.4. Expected Contributions

This project is expected to contribute by introducing a novel method to predict individual differences and to accurately account for them when setting up simulations (e.g. analyses using Monte Carlo methods). This procedure will make progress to fill in certain gaps in research, for example regarding the human cost function, which has been a concept that has lacked clear definition albeit applied for various uses. Already when introduced, the cost function weightings were mentioned to be individualized, although no method for finding such personal weightings using the cybernetic model has been established [32]. Recent research has linked the cost function weightings to the equalization, yet this was done for an average controller [48]. Moreover, ideas from newly developed cost functions for e.g. predicting handling qualities ratings [46] could then be adopted to improve upon the weaknesses of the current methodology.

In addition, predicting individual cybernetic parameters using the cost function could also help generate more accurate participant data to be used in simulations. Generating cybernetic parameter data based on matching real tracking runs were attempted and it was concluded that such method is feeble [9]. Having a more accurate predictor for individual cybernetic data could be helpful for generating extra participant data without having to conduct human-subject experiments and identifying the resulting data. This could provide new insights into individual differences in manual control cybernetics by showing how several parameters could be related (as well as the degree of relation). This research could also perhaps help reinforce/debunk controller “types” (e.g. high gain - low gain or high bandwidth - low bandwidth) or establish new ones if clear groupings between individual controllers are found.

References

[1] Max Mulder et al. “Manual Control Cybernetics: State-of-the-Art and Current Trends”. en. In: *IEEE Transactions on Human-Machine Systems* 48.5 (Oct. 2018), pp. 468–485. DOI: 10.1109/THMS.2017.2761342. URL: https://ieeexplore.ieee.org/document/8088358/ (visited on 04/03/2023).

[2] D.T. McRuer et al. “A Review of Quasi-Linear Pilot Models”. en. In: *IEEE Transactions on Human Factors in Electronics* HFE-8.3 (Sept. 1967), pp. 231–249. DOI: 10.1109/THFE.1967.234304. URL: http://ieeexplore.ieee.org/document/1698271/ (visited on 04/03/2023).

[3] Yanan Li et al. “Continuous Role Adaptation for Human–Robot Shared Control”. en. In: *IEEE Transactions on Robotics* 31.3 (June 2015), pp. 672–681. DOI: 10.1109/TRO.2015.2419873. URL: http://ieeexplore.ieee.org/document/7097058/ (visited on 04/03/2023).

[4] P Soliveri. “Learning manual pursuit tracking skills in patients with Parkinson’s disease”. In: *Brain* 120.8 (Aug. 1997), pp. 1325–1337. DOI: 10.1093/brain/120.8.1325. URL: https://academic.oup.com/brain/article-lookup/doi/10.1093/brain/120.8.1325 (visited on 04/03/2023).

[5] Meeko M. K. Oishi et al. “Assessing Manual Pursuit Tracking in Parkinson’s Disease Via Linear Dynamical Systems”. en. In: *Annals of Biomedical Engineering* 39.8 (Aug. 2011), pp. 2263–2273. DOI: 10.1007/s10439-011-0306-5. URL: http://link.springer.com/10.1007/s10439-011-0306-5 (visited on 04/03/2023).

[6] R.A. Hess et al. “A control theoretic model of driver steering behavior”. In: *IEEE Control Systems Magazine* 10.5 (1990), pp. 3–8. DOI: 10.1109/37.60415.

[7] Kasper van der El et al. “Modeling driver steering behavior in restricted-preview boundary-avoidance tasks”. en. In: *Transportation Research Part F: Traffic Psychology and Behaviour* 94 (Apr. 2023), pp. 362–378. DOI: 10.1016/j.trf.2023.02.017. URL: https://linkinghub.elsevier.com/retrieve/pii/S1369847823000505 (visited on 04/07/2023).

[8] Ronald Hess et al. “Modeling the Manually Controlled Bicycle”. en. In: *IEEE Transactions on Systems, Man, and Cybernetics - Part A: Systems and Humans* 42.3 (May 2012), pp. 545–557. DOI: 10.1109/TSMCA.2011.2164244. URL: http://ieeexplore.ieee.org/document/6151180/ (visited on 04/03/2023).

[9] Martijn J.L. De Jong et al. “Cybernetic Data Augmentation for Neural Network Classification of Control Skills”. en. In: *IFAC-PapersOnLine* 55.29 (2022), pp. 178–183. DOI: 10.1016/j.ifacol.2022.10.252. URL: https://linkinghub.elsevier.com/retrieve/pii/S2405896322022790 (visited on 06/01/2023).

[10] *Individual differences*. 2023. URL: https://dictionary.apa.org/individual-differences (visited on 03/28/2023).

[11] Yıldız Kuzgun. *Eğitimde bireysel faklılıklar*. Nobel Akademik Yayıncılık, 2017.

[12] David M. Buss et al. “Adaptive individual differences”. In: *Journal of personality* 67.2 (1999), pp. 209–243.

[13] Carolyn H. Declerck et al. “On feeling in control: A biological theory for individual differences in control perception”. en. In: *Brain and Cognition* 62.2 (Nov. 2006), pp. 143–176. DOI: 10.1016/j.bandc.2006.04.004. URL: https://linkinghub.elsevier.com/retrieve/pii/S0278262606000819 (visited on 04/03/2023).

[14] Phillip L. Ackerman. “Individual differences in information processing: An investigation of intellectual abilities and task performance during practice”. In: *Intelligence* 10.2 (1986), pp. 101–139. DOI: https://doi.org/10.1016/0160-2896(86)90010-3. URL: https://www.sciencedirect.com/science/article/pii/0160289686900103.

[15] Ali Simsek. “Individual Differences”. In: *Encyclopedia of the Sciences of Learning*. Ed. by Norbert M. Seel. Boston, MA: Springer US, 2012, pp. 1529–1532. DOI: 10.1007/978-1-4419-1428-6_370. URL: https://doi.org/10.1007/978-1-4419-1428-6_370.

[16] G. Adomavicius et al. “Personalization Technologies: A Process-Oriented Perspective”. In: *Commun. ACM* 48.10 (Aug. 2005), pp. 83–90. DOI: 10.1145/1089107.1089109. URL: https://doi.org/10.1145/1089107.1089109.

[17] Alexander Tuzhilin. “Personalization: The state of the art and future directions”. In: *Business computing* 3.3 (2009), pp. 3–43.

[18] Na Lin et al. “An Overview on Study of Identification of Driver Behavior Characteristics for Automotive Control”. In: *Mathematical Problems in Engineering* 2014 (Mar. 2014). Ed. by Hamid R. Karimi. Publisher: Hindawi Publishing Corporation, p. 569109. DOI: 10.1155/2014/569109. URL: https://doi.org/10.1155/2014/569109.

[19] Wenshuo Wang et al. “Modeling and Recognizing Driver Behavior Based on Driving Data: A Survey”. In: *Mathematical Problems in Engineering* 2014 (Feb. 2014). Ed. by Rongni Yang. Publisher: Hindawi Publishing Corporation, p. 245641. DOI: 10.1155/2014/245641. URL: https://doi.org/10.1155/2014/245641.

[20] Guozhen Zhao et al. “Mathematical Modeling of Driver Speed Control With Individual Differences”. en. In: *IEEE Transactions on Systems, Man, and Cybernetics: Systems* 43.5 (Sept. 2013), pp. 1091–1104. DOI: 10.1109/TSMC.2013.2256854. URL: http://ieeexplore.ieee.org/document/6573359/ (visited on 04/07/2023).

[21] Martina Hasenjager et al. “Personalization in advanced driver assistance systems and autonomous vehicles: A review”. en. In: *2017 IEEE 20th International Conference on Intelligent Transportation Systems (ITSC)*. Yokohama: IEEE, Oct. 2017, pp. 1–7. DOI: 10.1109/ITSC.2017.8317803. URL: http://ieeexplore.ieee.org/document/8317803/ (visited on 04/03/2023).

[22] Norbert Wiener et al. “Cybernetics or Control and Communication in the Animal and the Machine”. In: *Physics Today* 2.5 (1949), pp. 33–34.

[23] M. Mulder et al. “Fundamental Issues in Manual Control Cybernetics”. In: *IFAC-PapersOnLine* 49.19 (2016). 13th IFAC Symposium on Analysis, Design, and Evaluation ofHuman-Machine Systems HMS 2016, pp. 1–6. DOI: https://doi.org/10.1016/j.ifacol.2016.10.429. URL: https://www.sciencedirect.com/science/article/pii/S240589631632016X.

[24] D T McRuer. “Mathematical Models of Human Pilot Behavior”. en. In: *Agardograph* 188 (1974).

[25] D. McRuer et al. “Theory of Manual Vehicular Control”. en. In: *IEEE Transactions on Man Machine Systems* 10.4 (Dec. 1969), pp. 257–291. DOI: 10.1109/TMMS.1969.299930. URL: http://ieeexplore.ieee.org/document/4081909/ (visited on 04/03/2023).

[26] P. M. T. Zaal et al. “Use of Pitch and Heave Motion Cues in a Pitch Control Task”. In: *Journal of Guidance, Control, and Dynamics* 32.2 (2009). _eprint: https://doi.org/10.2514/1.39953, pp. 366–377. DOI: 10.2514/1.39953. URL: https://doi.org/10.2514/1.39953.

[27] D. M. Pool et al. “Modeling Wide-Frequency-Range Pilot Equalization for Control of Aircraft Pitch Dynamics”. en. In: *Journal of Guidance, Control, and Dynamics* 34.5 (Sept. 2011), pp. 1529–1542. DOI: 10.2514/1.53315. URL: https://arc.aiaa.org/doi/10.2514/1.53315 (visited on 04/03/2023).

[28] D. M. Pool et al. “Effects of Simulator Motion Feedback on Training of Skill-Based Control Behavior”. en. In: *Journal of Guidance, Control, and Dynamics* 39.4 (Apr. 2016), pp. 889–902. DOI: 10.2514/1.G001603. URL: https://arc.aiaa.org/doi/10.2514/1.G001603 (visited on 04/03/2023).

[29] William Levison et al. “A Model for Human Controller Remnant”. en. In: *IEEE Transactions on Man Machine Systems* 10.4 (Dec. 1969), pp. 101–108. DOI: 10.1109/TMMS.1969.299906. URL: http://ieeexplore.ieee.org/document/4081885/ (visited on 04/03/2023).

[30] D. McRuer et al. “Human-pilot dynamics in compensatory systems: An abstract of U.S. Government report AFFDL-TR-65–15”. en. In: *IEEE Transactions on Human Factors in Electronics* HFE-6.1

(Sept. 1965), pp. 84–84. DOI: 10.1109/THFE.1965.6591261. URL: http://ieeexplore.ieee.org/document/6591261/ (visited on 04/03/2023).

[31] C.-P. Ko. “Neuromuscular System”. en. In: *International Encyclopedia of the Social & Behavioral Sciences*. Elsevier, 2001, pp. 10595–10600. DOI: 10.1016/B0-08-043076-7/03482-3. URL: https://linkinghub.elsevier.com/retrieve/pii/B0080430767034823 (visited on 04/03/2023).

[32] D.L. Kleinman et al. “An optimal control model of human response part I: Theory and validation”. en. In: *Automatica* 6.3 (May 1970), pp. 357–369. DOI: 10.1016/0005-1098(70)90051-8. URL: https://linkinghub.elsevier.com/retrieve/pii/0005109870900518 (visited on 04/03/2023).

[33] Henry R. Jex. “Problems in Modeling Man-Machine Control Behavior in Biodynamic Environments”. In: *Seventh Annual Conference on Manual Control*. Vol. 281. NASA, 1972, p. 3.

[34] M. M. van Paasen et al. “Model of the Neuromuscular Dynamics of the Human Pilot’s Arm”. en. In: *Journal of Aircraft* 41.6 (Nov. 2004), pp. 1482–1490. DOI: 10.2514/1.14434. URL: https://arc.aiaa.org/doi/10.2514/1.14434 (visited on 04/03/2023).

[35] R A Hess. “Simplified approach for modelling pilot pursuit control behaviour in multi-loop flight control tasks”. en. In: *Proceedings of the Institution of Mechanical Engineers, Part G: Journal of Aerospace Engineering* 220.2 (Feb. 2006), pp. 85–102. DOI: 10.1243/09544100JAERO33. URL: http://journals.sagepub.com/doi/10.1243/09544100JAERO33 (visited on 04/03/2023).

[36] R. A. Hess. “Unified Theory for Aircraft Handling Qualities and Adverse Aircraft-Pilot Coupling”. en. In: *Journal of Guidance, Control, and Dynamics* 20.6 (Nov. 1997), pp. 1141–1148. DOI: 10.2514/2.4169. URL: https://arc.aiaa.org/doi/10.2514/2.4169 (visited on 04/03/2023).

[37] Duane T. McRuer et al. “A Neuromuscular Actuation System Model”. In: *IEEE Transactions on Man-Machine Systems* 9.3 (1968), pp. 61–71. DOI: 10.1109/TMMS.1968.300039.

[38] D. McRuer. “Remarks on some neuromuscular subsystem dynamics”. In: *IEEE Transactions on Human Factors in Electronics* HFE-7.3 (1966), pp. 129–130. DOI: 10.1109/THFE.1966.232653.

[39] Anja Simm. “Technical and Psychological Aspects of Pilot Gain”. de. In: (2012).

[40] David Doman. “Optimal control pilot modeling for resolving Cooper-Harper rating discrepancies”. en. In: *24th Atmospheric Flight Mechanics Conference*. Portland,OR,U.S.A.: American Institute of Aeronautics and Astronautics, Aug. 1999. DOI: 10.2514/6.1999-4091. URL: https://arc.aiaa.org/doi/10.2514/6.1999-4091 (visited on 04/03/2023).

[41] S. Baron et al. “An optimal control model of human response part II: Prediction of human performance in a complex task”. en. In: *Automatica* 6.3 (May 1970), pp. 371–383. DOI: 10.1016/0005-1098(70)90052-X. URL: https://linkinghub.elsevier.com/retrieve/pii/000510987090052X (visited on 04/03/2023).

[42] R. Hosman. *Pilot’s Perception and Control of Aircraft Motions*. Delft University Press, 1996. URL: https://books.google.nl/books?id=PJRaAAAACAAJ.

[43] B. J. Bacon et al. “An Optimal Control Approach to Pilot-Vehicle Analysis and the Neal-Smith Criteria”. en. In: (1984).

[44] Adriano Scibilia et al. “Human Control Model Estimation in Physical Human–Machine Interaction: A Survey”. en. In: *Sensors* 22.5 (Feb. 2022), p. 1732. DOI: 10.3390/s22051732. URL: https://www.mdpi.com/1424-8220/22/5/1732 (visited on 04/03/2023).

[45] Paolo Franceschi et al. “Inverse Optimal Control for the identification of human objective: a preparatory study for physical Human-Robot Interaction”. en. In: *2022 IEEE 27th International Conference on Emerging Technologies and Factory Automation (ETFA)*. Stuttgart, Germany: IEEE, Sept. 2022, pp. 1–6. DOI: 10.1109/ETFA52439.2022.9921553. URL: https://ieeexplore.ieee.org/document/9921553/ (visited on 04/03/2023).

[46] Edward N. Bachelder et al. “A Theoretical Basis for Predicting Pilot Performance, Workload, and Handling Qualities”. en. In: *AIAA SCITECH 2023 Forum*. National Harbor, MD & Online: American

Institute of Aeronautics and Astronautics, Jan. 2023. DOI: 10.2514/6.2023-1369. URL: https://arc.aiaa.org/doi/10.2514/6.2023-1369 (visited on 04/03/2023).

[47] David G. Mitchell et al. “This Is Pilot Gain”. en. In: *AIAA Scitech 2019 Forum*. San Diego, California: American Institute of Aeronautics and Astronautics, Jan. 2019. DOI: 10.2514/6.2019-0562. URL: https://arc.aiaa.org/doi/10.2514/6.2019-0562 (visited on 04/03/2023).

[48] Martin C. Butijn et al. “Assessment of Maximum Unnoticeable Added Lag-Lead or Lead-Lag Dynamics with a Cybernetic Approach”. en. In: *AIAA Scitech 2019 Forum*. San Diego, California: American Institute of Aeronautics and Astronautics, Jan. 2019. DOI: 10.2514/6.2019-1229. URL: https://arc.aiaa.org/doi/10.2514/6.2019-1229 (visited on 06/05/2023).

[49] Edward N. Bachelder et al. “Linking the Pilot Structural Model and Pilot Workload”. en. In: *2018 AIAA Atmospheric Flight Mechanics Conference*. Kissimmee, Florida: American Institute of Aeronautics and Astronautics, Jan. 2018. DOI: 10.2514/6.2018-0533. URL: https://arc.aiaa.org/doi/10.2514/6.2018-0533 (visited on 04/03/2023).

[50] Edward Bachelder et al. “A Theoretical Framework Unifying Handling Qualities, Workload, Stability and Control”. In: *Proceedings of the 77th Annual Forum*. The Vertical Flight Society. Virtual, May 2021.

[51] H. J. Damveld et al. “Design of Forcing Functions for the Identification of Human Control Behavior”. en. In: *Journal of Guidance, Control, and Dynamics* 33.4 (July 2010), pp. 1064–1081. DOI: 10.2514/1.47730. URL: https://arc.aiaa.org/doi/10.2514/1.47730 (visited on 04/03/2023).

[52] P. M. T. Zaal et al. “Modeling Human Multimodal Perception and Control Using Genetic Maximum Likelihood Estimation”. en. In: *Journal of Guidance, Control, and Dynamics* 32.4 (July 2009), pp. 1089–1099. DOI: 10.2514/1.42843. URL: https://arc.aiaa.org/doi/10.2514/1.42843 (visited on 04/03/2023).

[53] Kasper van der El et al. “Effects of Target Trajectory Bandwidth on Manual Control Behavior in Pursuit and Preview Tracking”. In: *IEEE Transactions on Human-Machine Systems* 50.1 (2020), pp. 68–78. DOI: 10.1109/THMS.2019.2947577.

Part III

Appendices

A Additional Results

A.1. Experimental vs. Simulated Results

This plot has been generated during the preliminary analyses, and is therefore only available for Exp. (III).

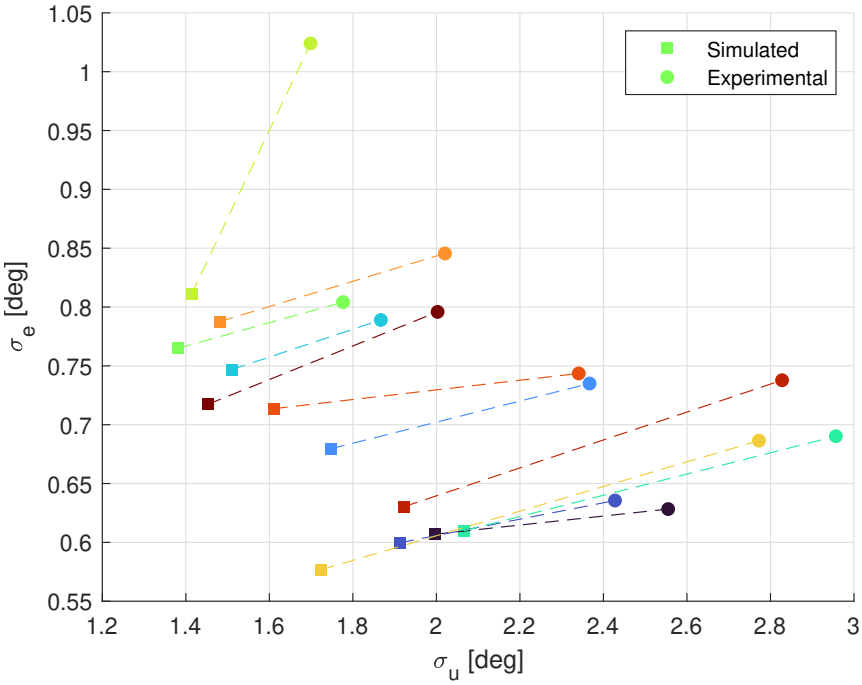

Figure A.1: Experimental vs. Simulated σ_e and σ_u values - Exp. (III)

A.2. Cybernetic Parameter Progression over Runs

This plot has been generated during the preliminary analyses, and is therefore only available for Exp. (III).

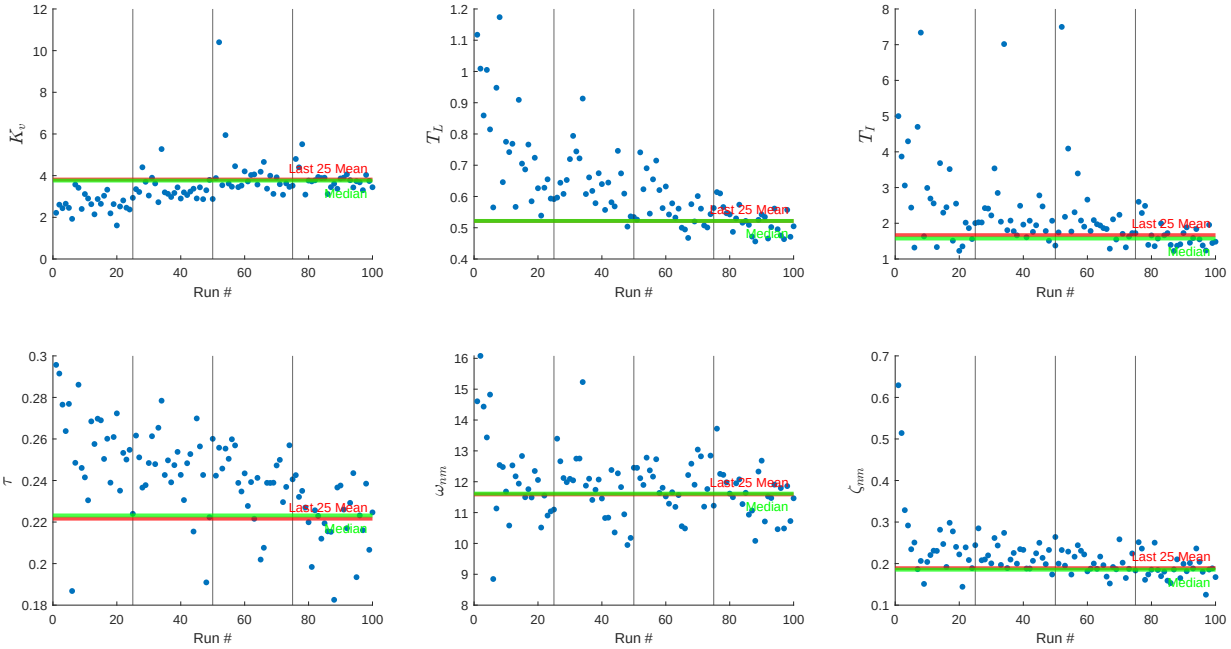

Figure A.2: Parameter Progression for participant 1 - Exp. (III)

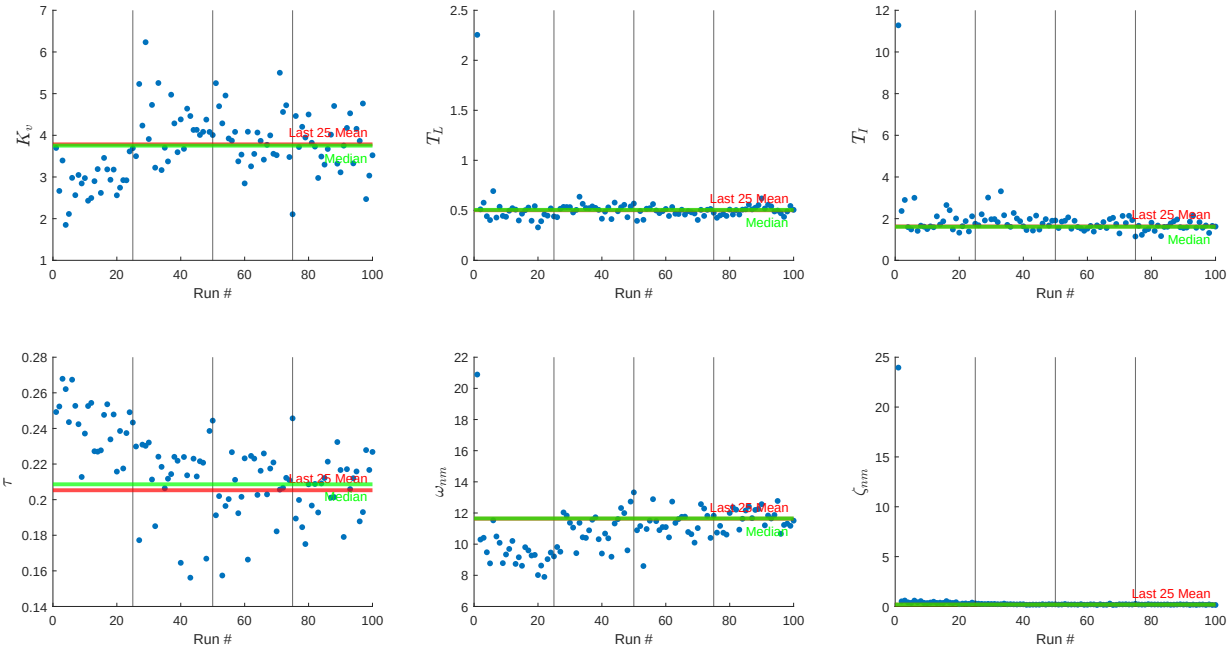

Figure A.3: Parameter Progression for participant 2 - Exp. (III)

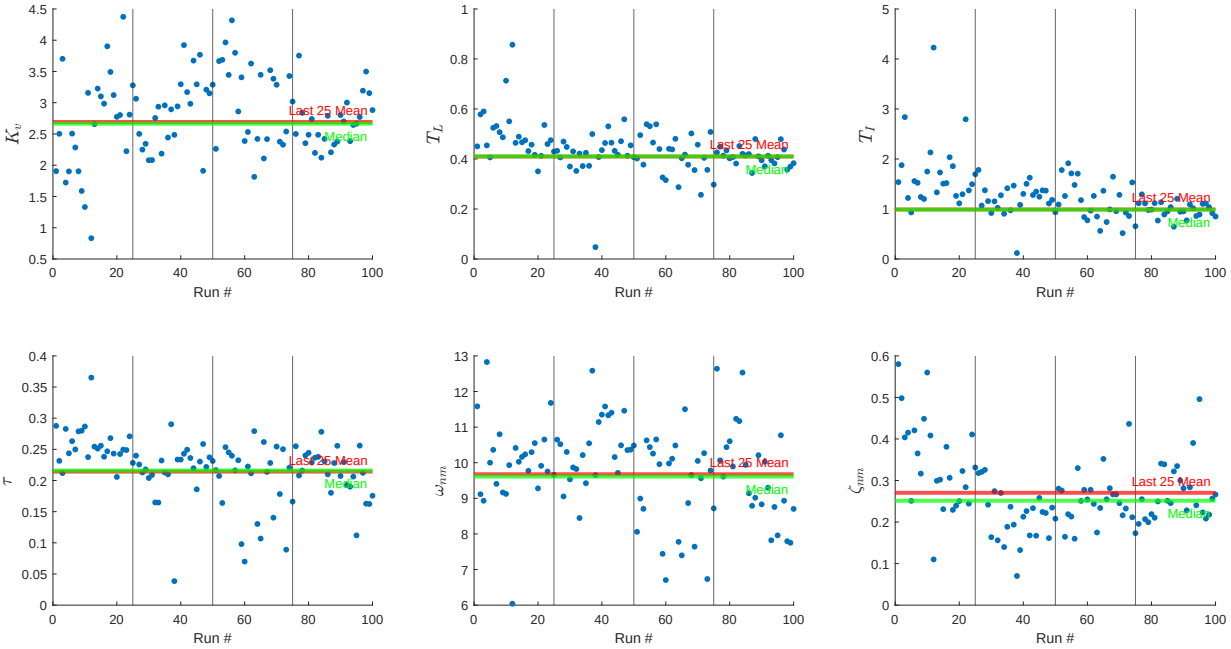

Figure A.4: Parameter Progression for participant 3 - Exp. (III)

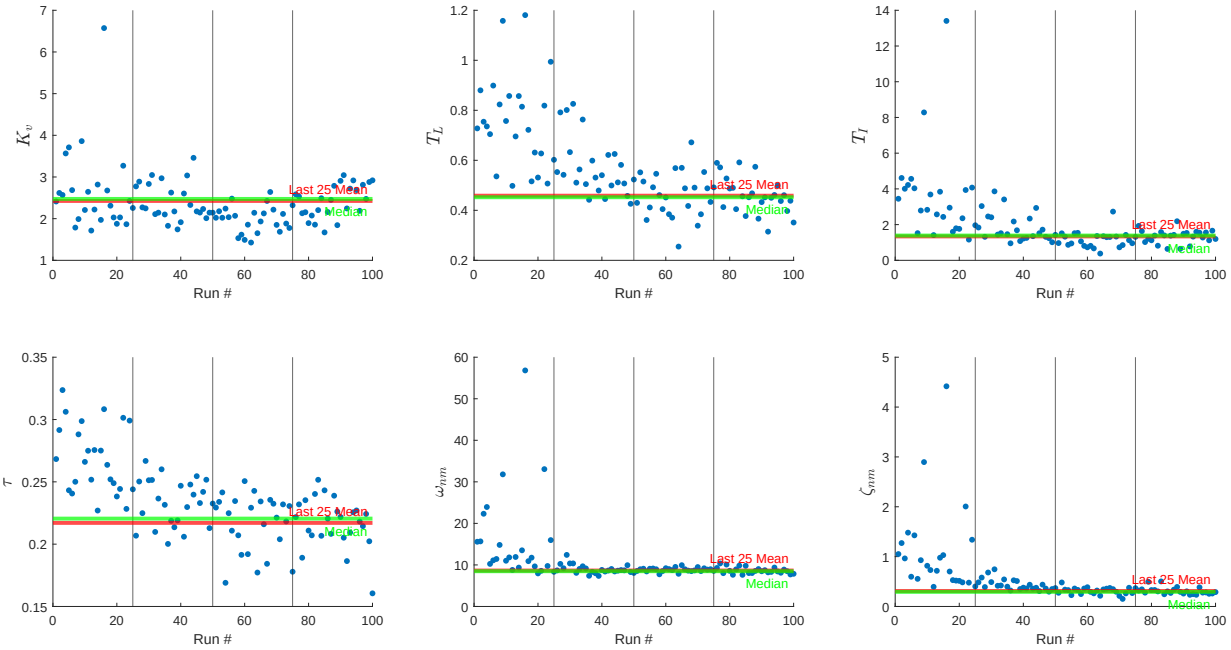

Figure A.5: Parameter Progression for participant 4 - Exp. (III)

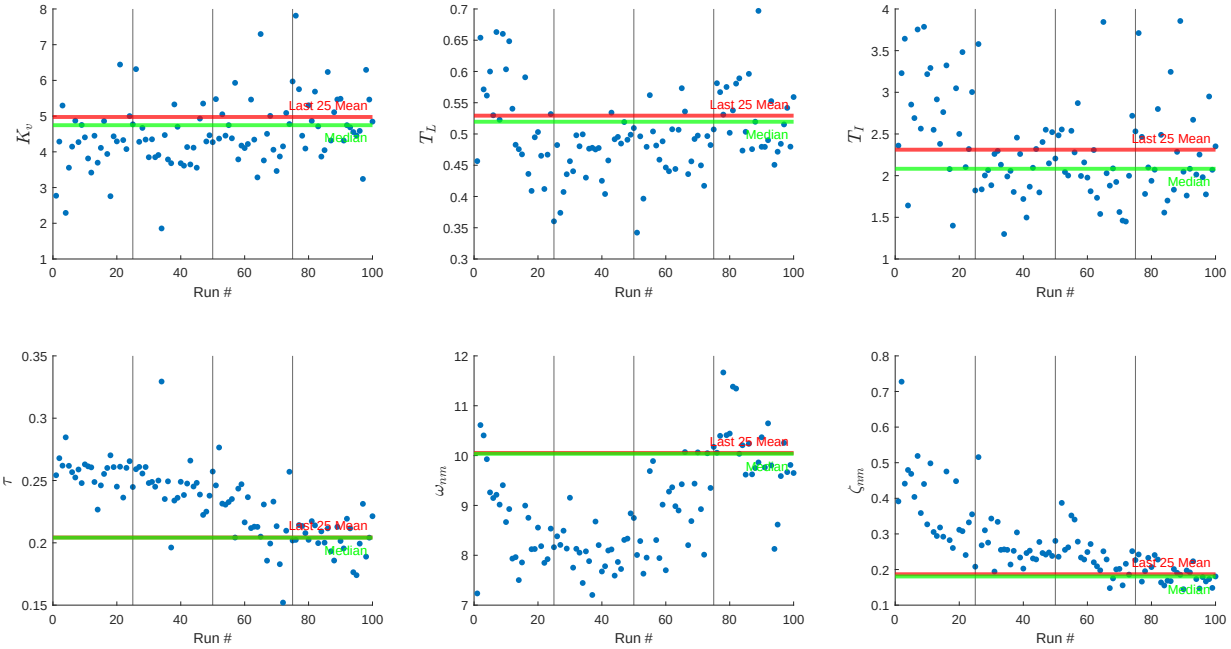

Figure A.6: Parameter Progression for participant 5 - Exp. (III)

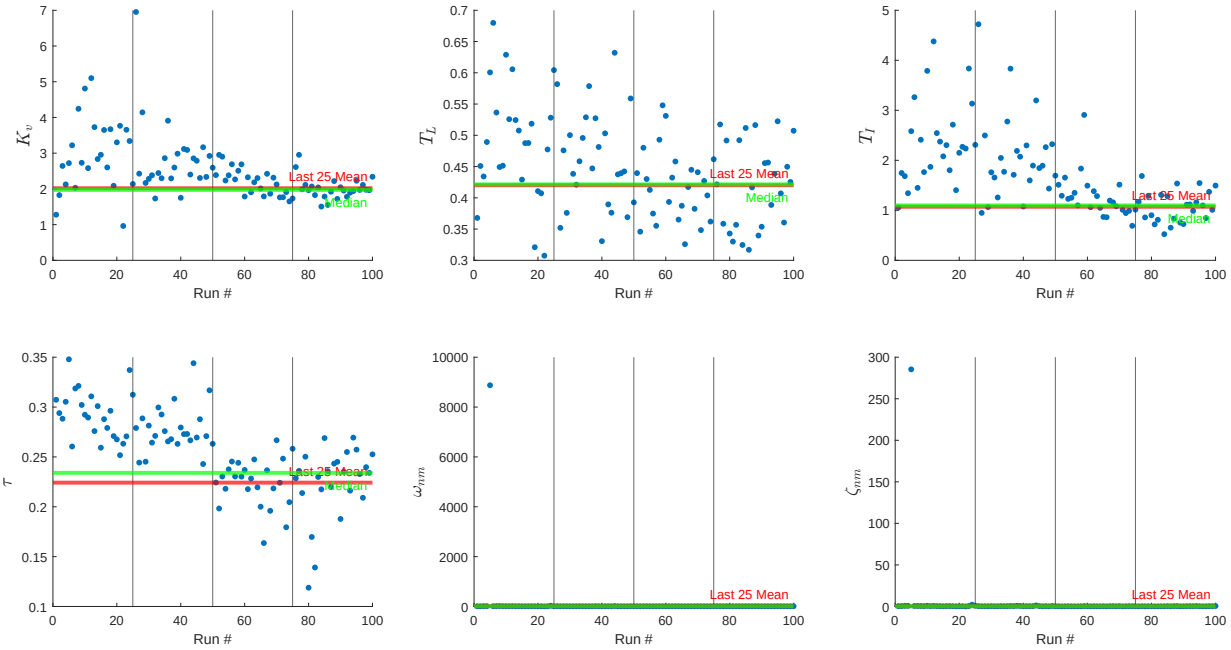

Figure A.7: Parameter Progression for participant 6 - Exp. (III)

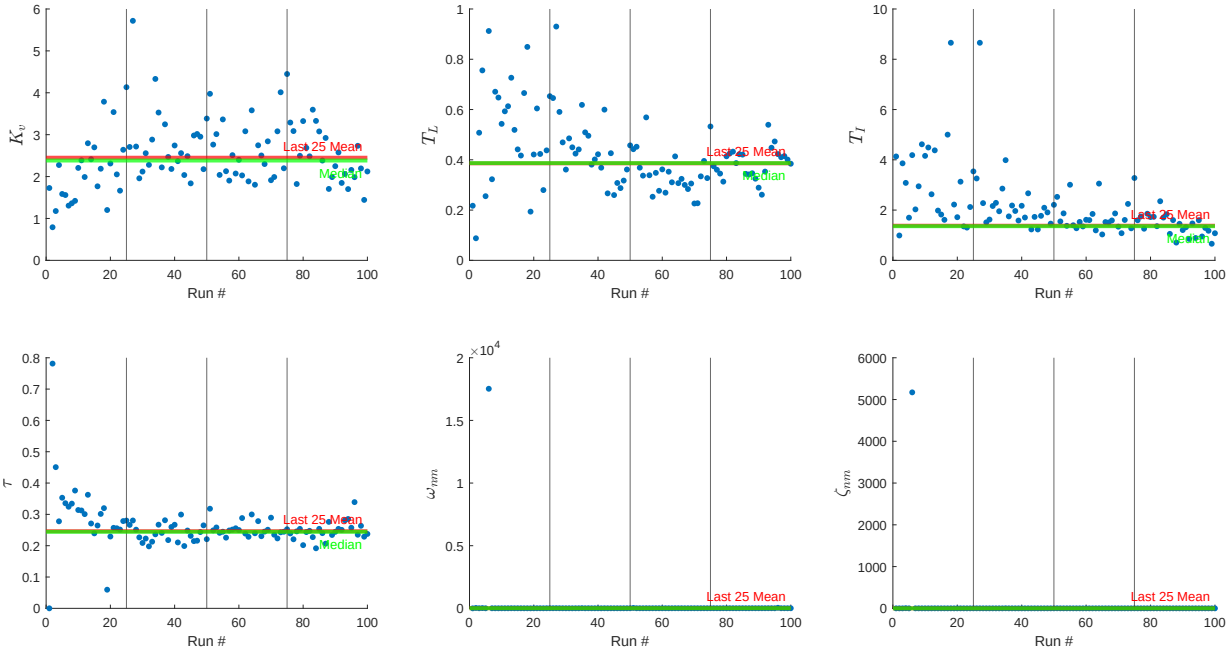

Figure A.8: Parameter Progression for participant 7 - Exp. (III)

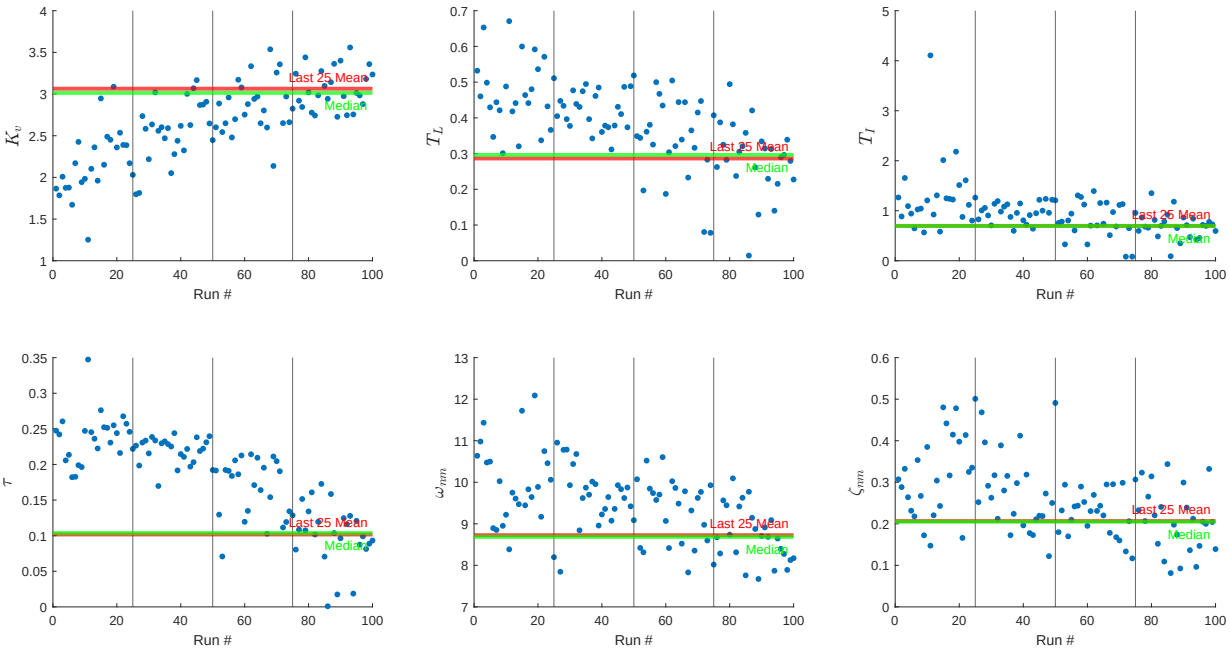

Figure A.9: Parameter Progression for participant 8 - Exp. (III)

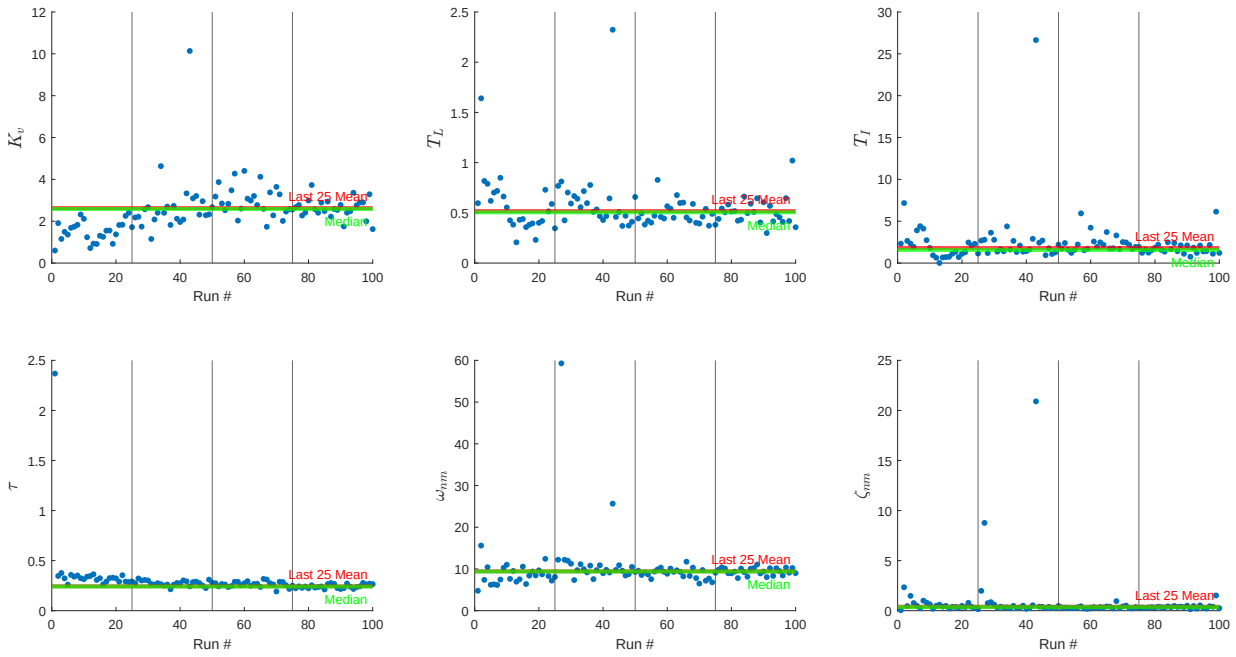

Figure A.10: Parameter Progression for participant 9 - Exp. (III)

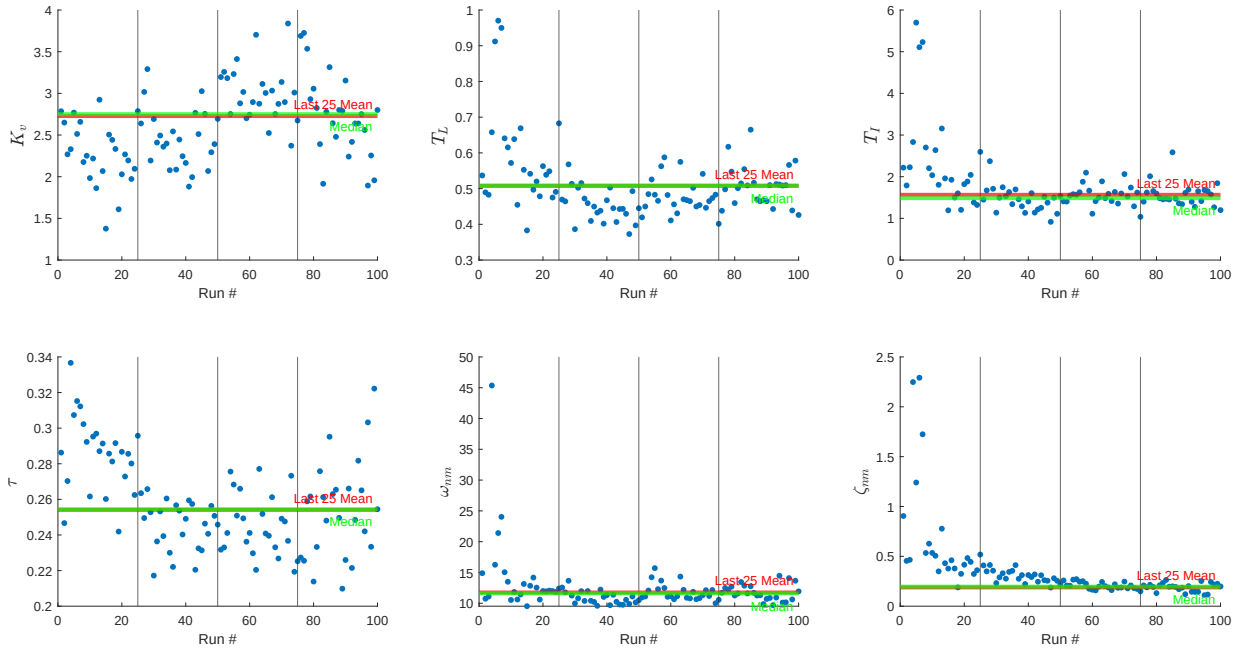

Figure A.11: Parameter Progression for participant 10 - Exp. (III)

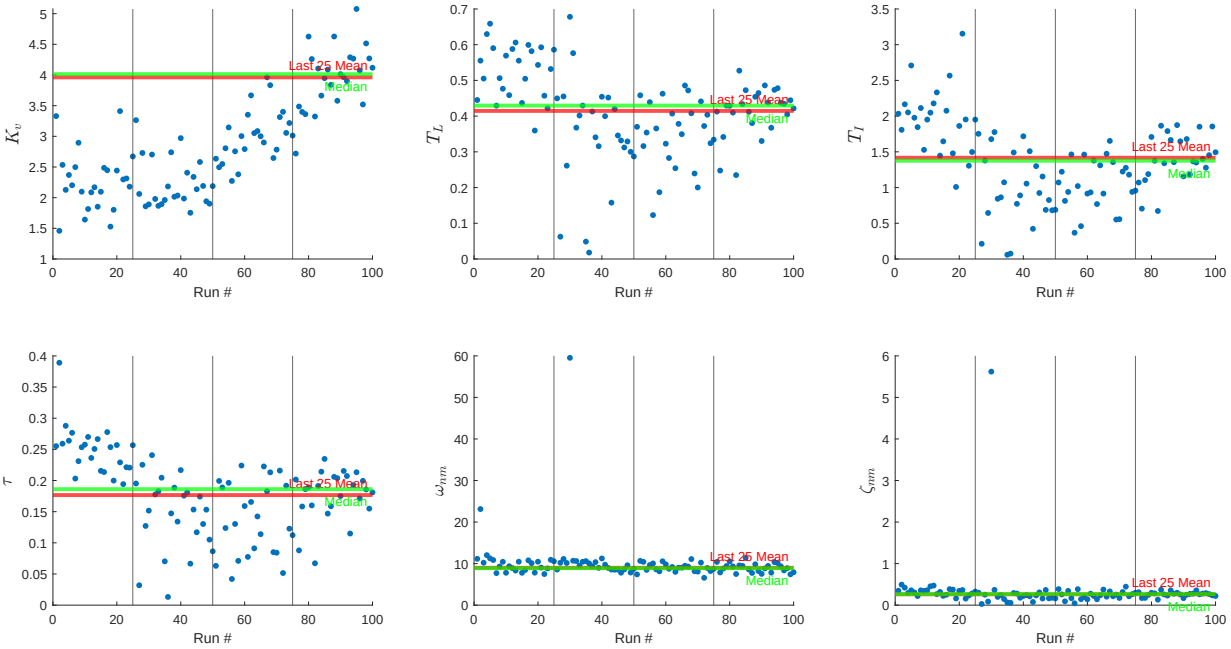

Figure A.12: Parameter Progression for participant 11 - Exp. (III)

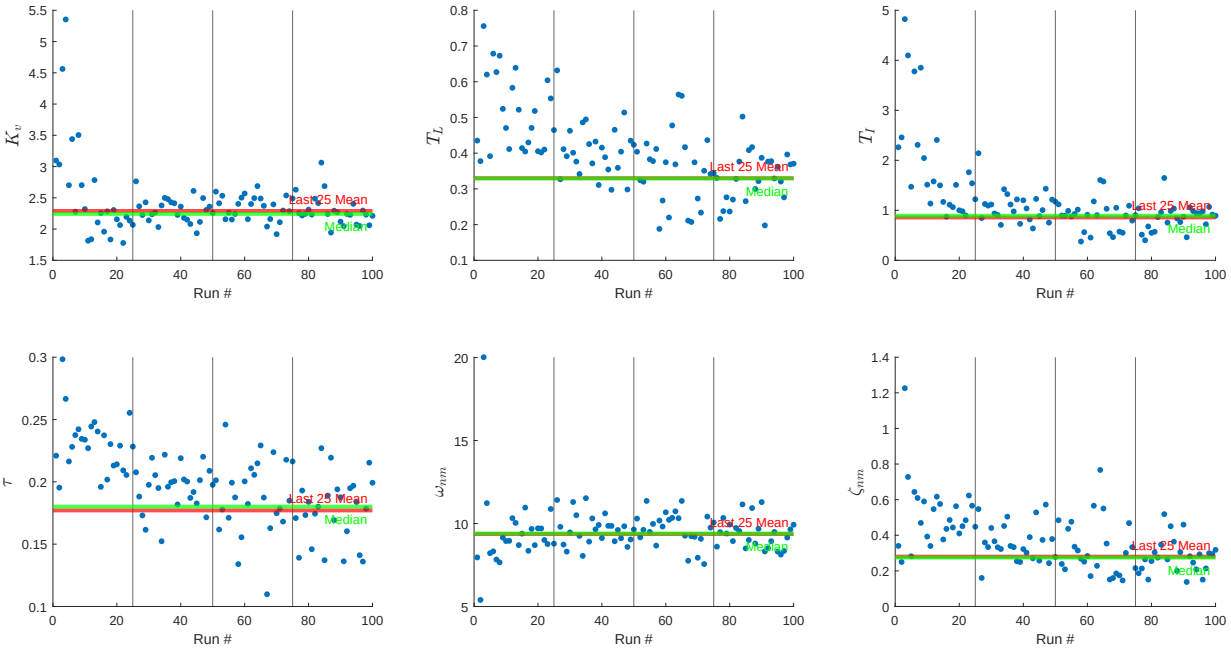

Figure A.13: Parameter Progression for participant 12 - Exp. (III)

A.3. Deviation from the Average Standard Deviation

This plot is not available for Exp. (I), as the time traces of the e and u signals from this data set were not made use of.

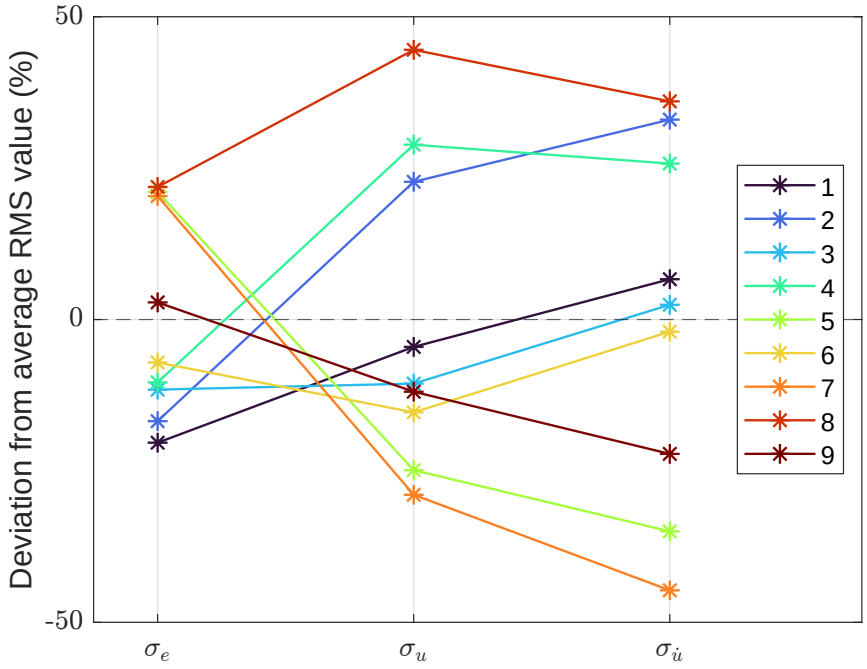

Figure A.14: Deviation from the average σ_e, σ_u, and $\sigma_{\dot{u}}$ values - Exp. (II)

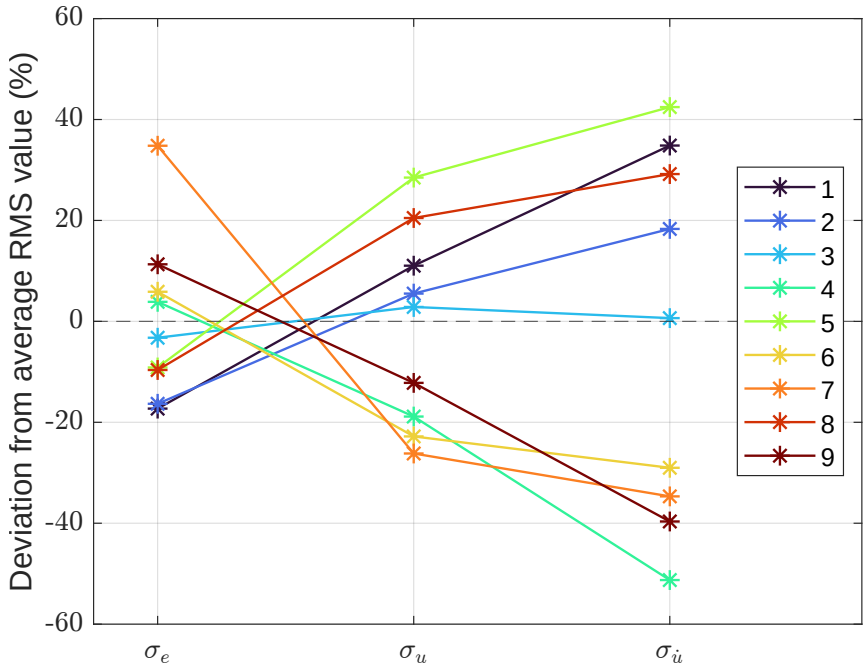

Figure A.15: Deviation from the average σ_e, σ_u, and $\sigma_{\dot{u}}$ values - Exp. (III)

A.4. Cybernetic Parameter Correlations

Table A.1: Parameter Correlations - Exp. (I)

	K_v	T_L	τ	ω_{nm}	ζ_{nm}
K_v	1.000	-0.542	-0.758	0.522	-0.638
T_L	-0.542	1.000	0.516	-0.390	-0.113
τ	-0.758	0.516	1.000	-0.397	0.135
ω_{nm}	0.522	-0.390	-0.397	1.000	-0.427
ζ_{nm}	-0.638	-0.113	0.135	-0.427	1.000

Table A.2: Parameter Correlations - Exp. (II)

	K_v	T_L	τ	ω_{nm}	ζ_{nm}
K_v	1.000	-0.928	-0.478	0.537	-0.207
T_L	-0.928	1.000	0.359	-0.309	0.114
τ	-0.478	0.359	1.000	-0.545	0.096
ω_{nm}	0.537	-0.309	-0.545	1.000	0.229
ζ_{nm}	-0.207	0.114	0.096	0.229	1.000

Table A.3: Parameter Correlations - Exp. (III)

	K_v	T_L	T_I	τ	ω_{nm}	ζ_{nm}
K_v	1.000	0.435	0.659	-0.208	0.212	-0.612
T_L	0.435	1.000	0.880	0.681	0.525	-0.167
T_I	0.659	0.880	1.000	0.509	0.425	-0.138
τ	-0.208	0.681	0.509	1.000	0.545	0.345
ω_{nm}	0.212	0.525	0.425	0.545	1.000	-0.375
ζ_{nm}	-0.612	-0.167	-0.138	0.345	-0.375	1.000

B

Additional Sensitivity Analysis Results

B.1. Parameter Impact at Interquartile Ranges

Table B.1: Impact of each parameter on σ_e, σ_u, and $\sigma_{\dot{u}}$, at their interquartile ranges - Exp. (I)

Parameter	σ_e Deviation (%)		σ_u Deviation (%)		$\sigma_{\dot{u}}$ Deviation (%)	
	at Q1	at Q3	at Q1	at Q3	at Q1	at Q3
K_v	8.45	-2.78	-23.96	19.88	-26.17	21.17
T_L	5.31	-3.06	-11.88	11.43	-19.45	16.70
τ	-2.18	1.74	-1.39	1.23	0.66	-0.26
ω_{nm}	1.07	-0.75	3.44	-2.35	-0.36	1.27
ζ_{nm}	-1.70	1.74	2.51	-1.58	9.78	-7.21

Table B.2: Impact of each parameter on σ_e, σ_u, and $\sigma_{\dot{u}}$, at their interquartile ranges - Exp. (II)

Parameter	σ_e Deviation (%)		σ_u Deviation (%)		$\sigma_{\dot{u}}$ Deviation (%)	
	at Q1	at Q3	at Q1	at Q3	at Q1	at Q3
K_v	40.14	50+	-25.95	50+	-36.98	50+
T_L	26.60	50+	-19.58	50+	-33.33	50+
τ	-2.12	1.68	-6.85	2.55	-5.41	-0.97
ω_{nm}	0.90	-0.44	13.00	-5.68	15.49	-3.52
ζ_{nm}	-1.09	0.52	-0.63	-0.40	3.57	-2.94

Table B.3: Impact of each parameter on σ_e, σ_u, and $\sigma_{\dot{u}}$, at their interquartile ranges - Exp. (III)

Parameter	σ_e Deviation (%)		σ_u Deviation (%)		$\sigma_{\dot{u}}$ Deviation (%)	
	at Q1	at Q3	at Q1	at Q3	at Q1	at Q3
K_v	5.37	-4.27	-9.68	12.61	-15.80	20.83
T_L	2.90	-4.50	-3.01	6.96	-11.12	21.73
T_I	-5.37	4.04	11.25	-5.00	24.80	-11.89
τ	-1.36	2.44	-1.05	1.90	-0.20	0.57
ω_{nm}	0.82	-0.87	1.36	-1.36	-1.71	3.32
ζ_{nm}	-1.20	0.64	0.47	-0.15	7.28	-3.16

C

Cost Maps

C.1. Experiment (I)

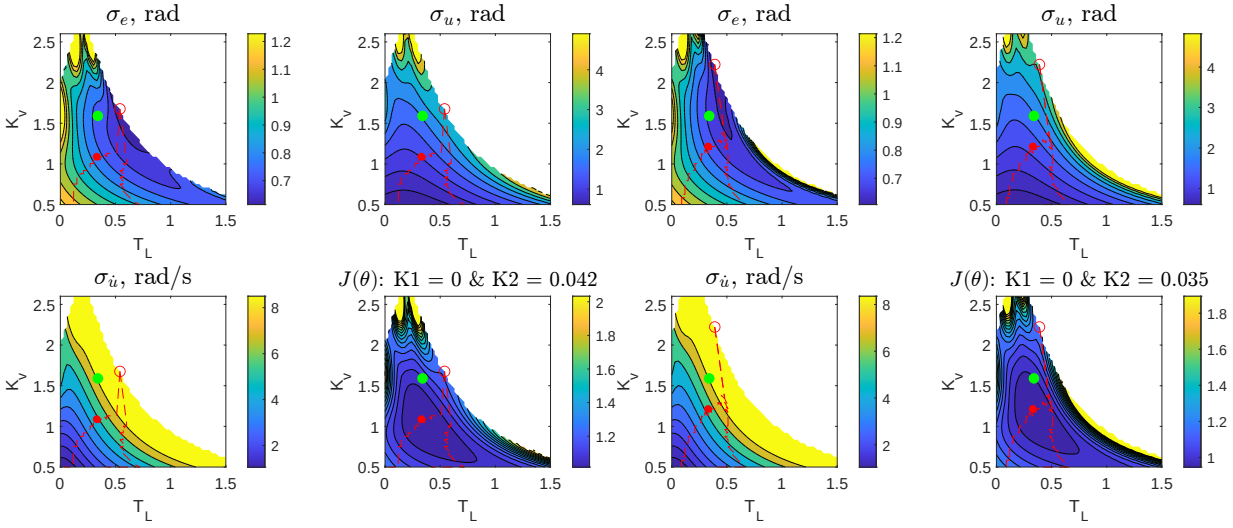

(a) Average case **(b)** Individual case

Figure C.1: Participant 1 cost maps - Exp. (I)

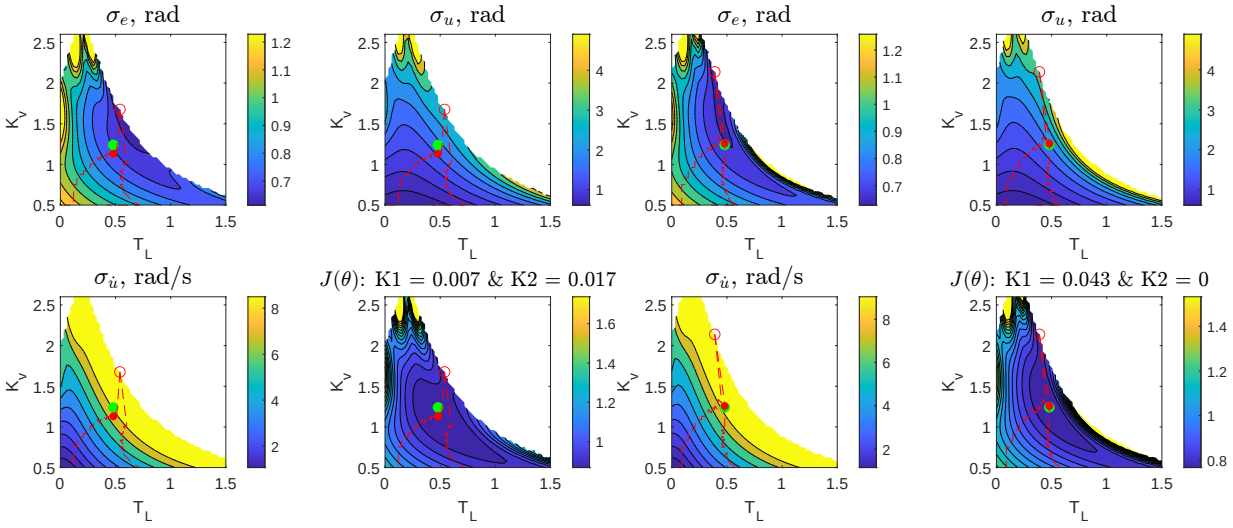

(a) Average case **(b)** Individual case

Figure C.2: Participant 2 cost maps - Exp. (I)

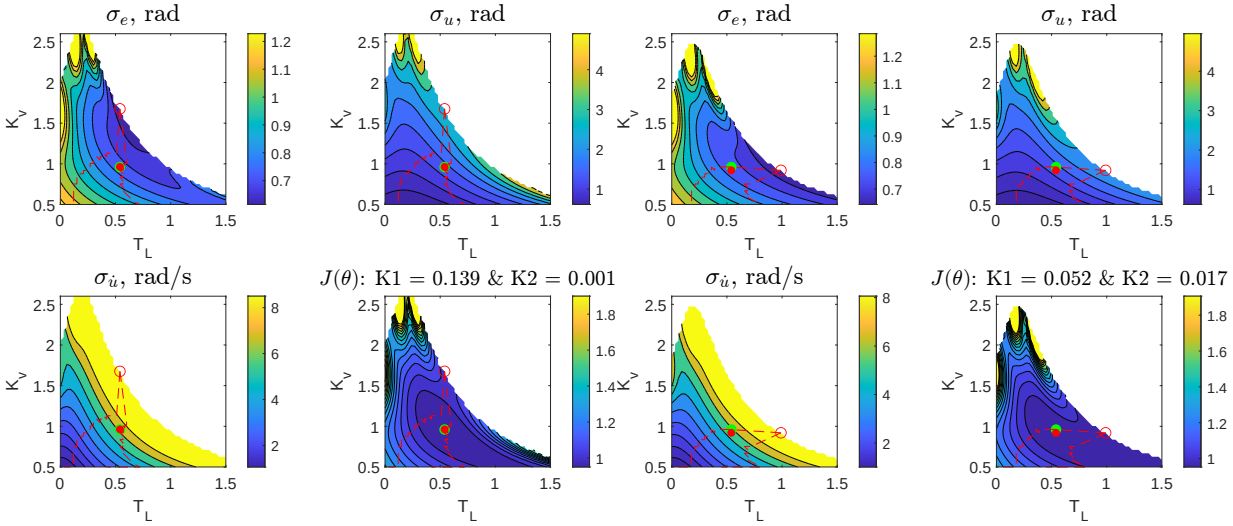

(a) Average case **(b)** Individual case

Figure C.3: Participant 3 cost maps - Exp. (I)

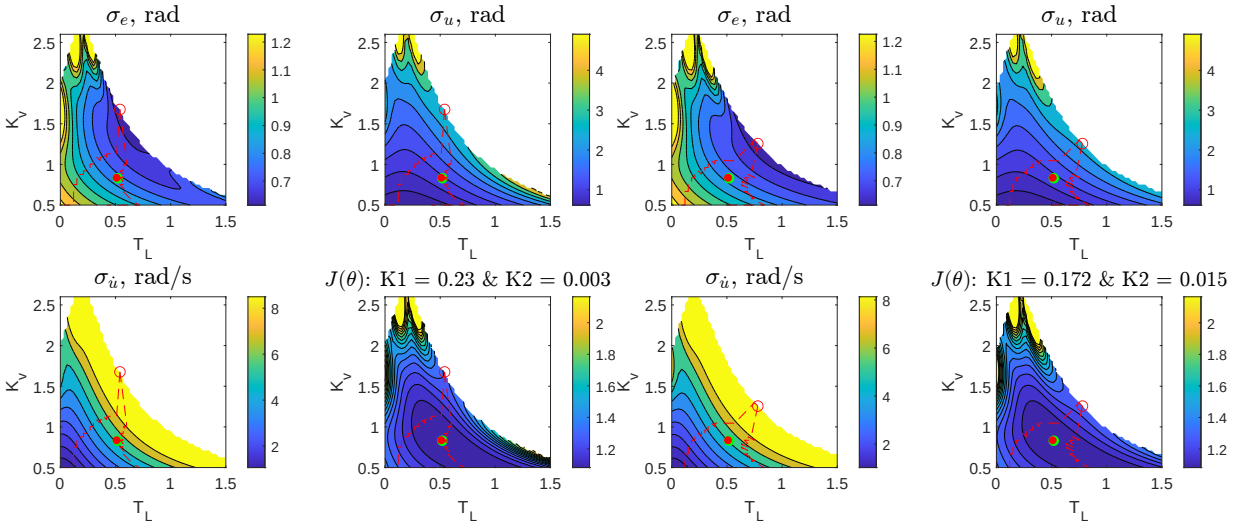

(a) Average case **(b)** Individual case

Figure C.4: Participant 4 cost maps - Exp. (I)

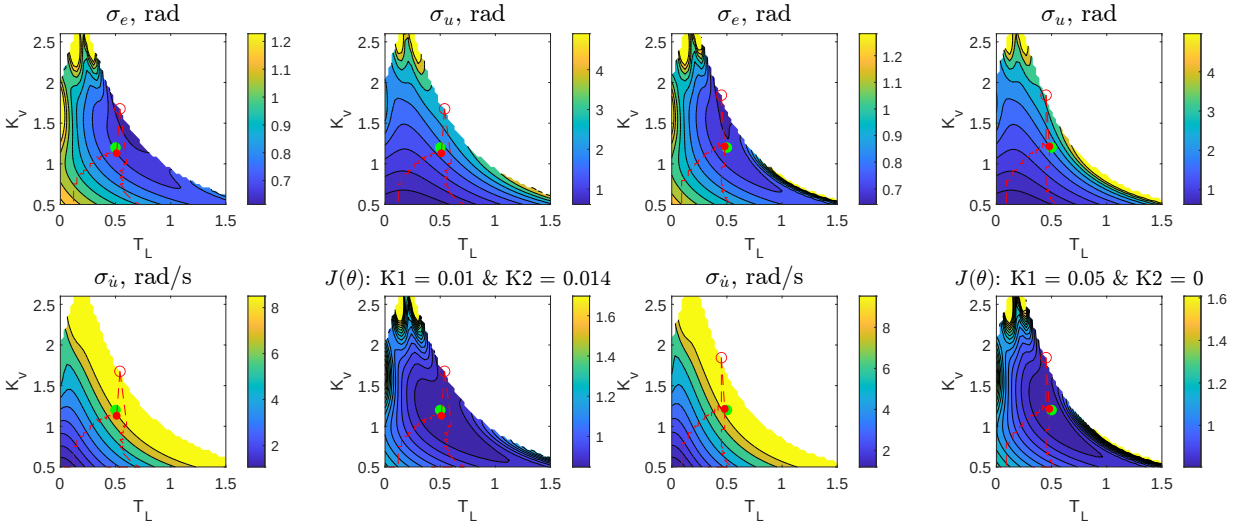

(a) Average case **(b)** Individual case

Figure C.5: Participant 5 cost maps - Exp. (I)

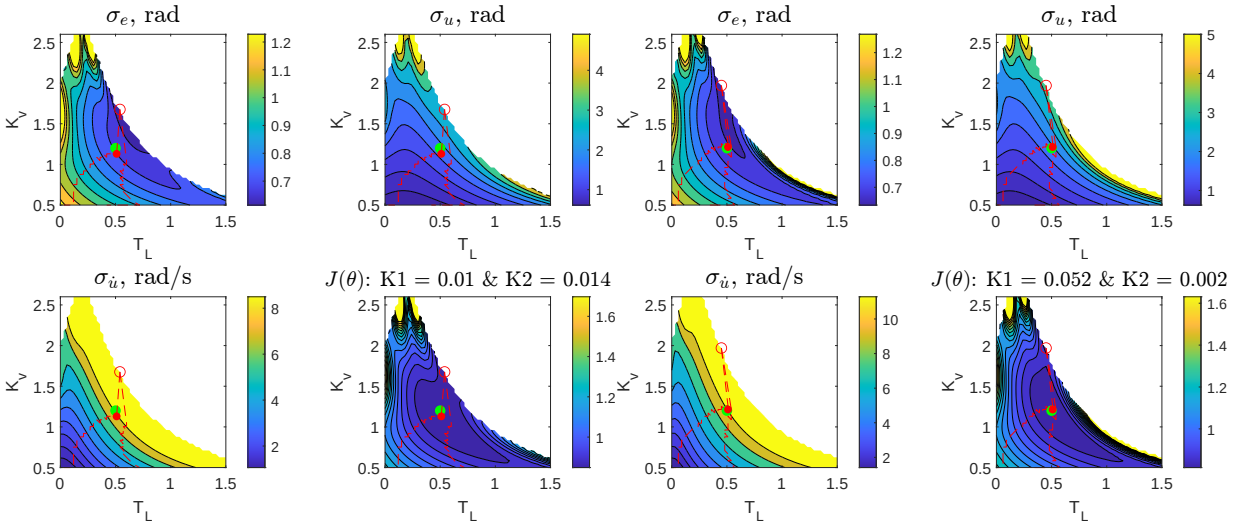

(a) Average case **(b)** Individual case

Figure C.6: Participant 6 cost maps - Exp. (I)

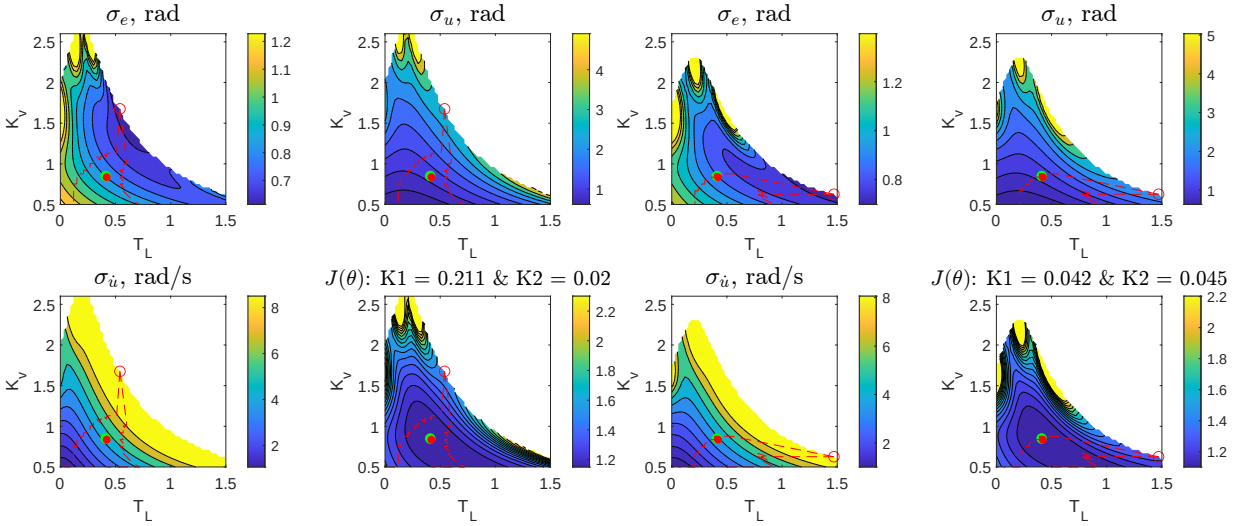

(a) Average case **(b)** Individual case

Figure C.7: Participant 7 cost maps - Exp. (I)

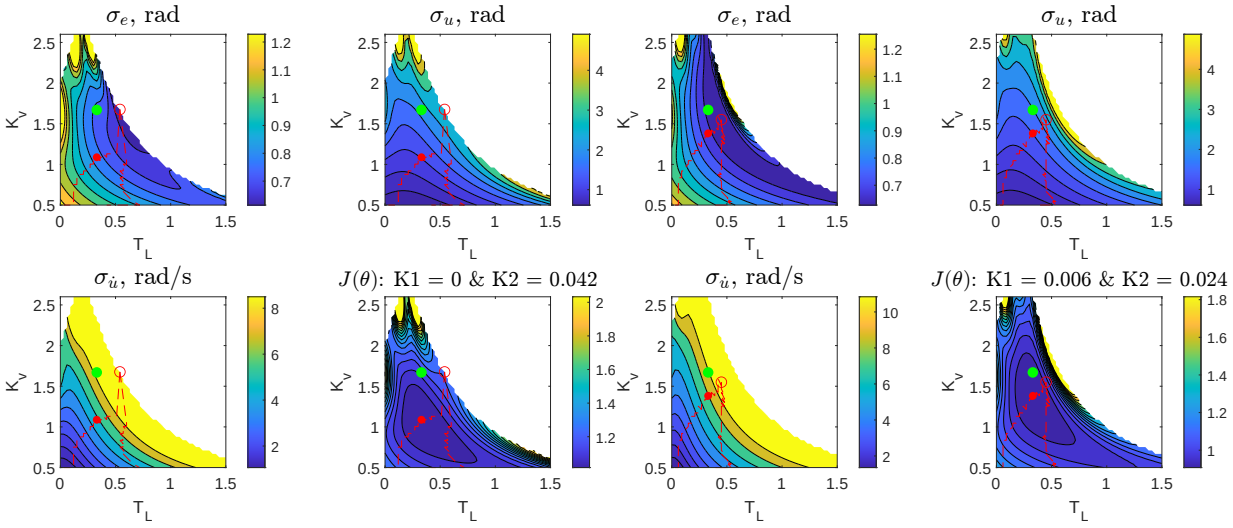

(a) Average case **(b)** Individual case

Figure C.8: Participant 8 cost maps - Exp. (I)

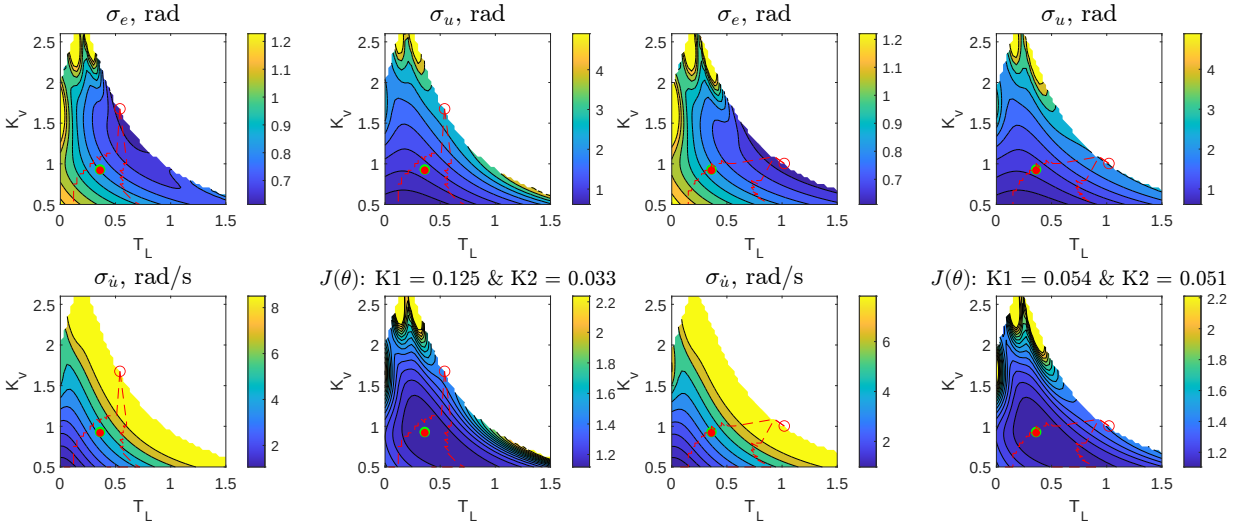

(a) Average case **(b)** Individual case

Figure C.9: Participant 9 cost maps - Exp. (I)

C.2. Experiment (II)

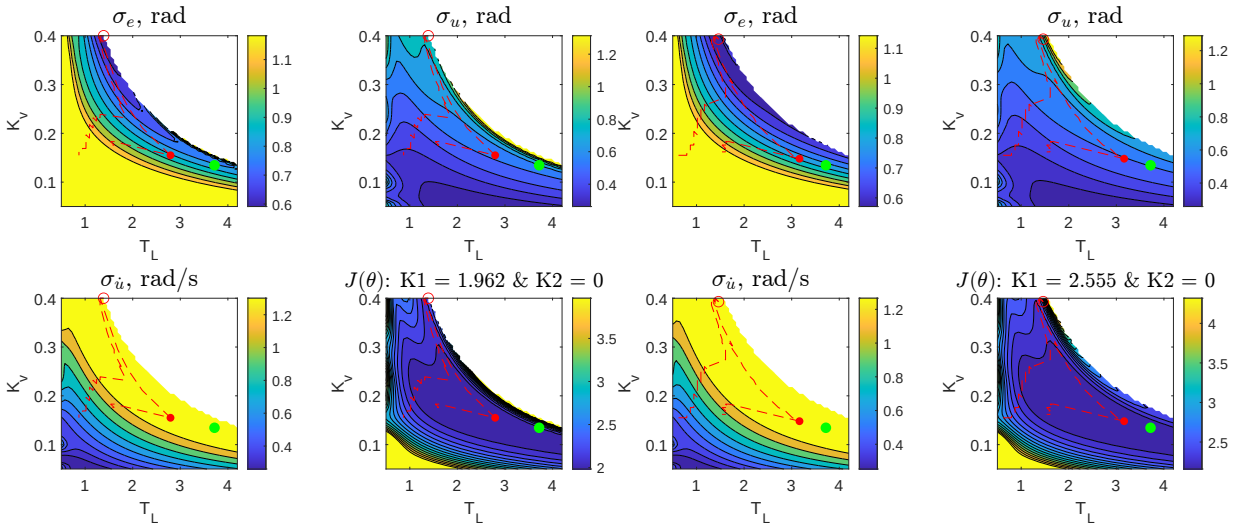

(a) Average case **(b)** Individual case

Figure C.10: Participant 1 cost maps - Exp. (II)

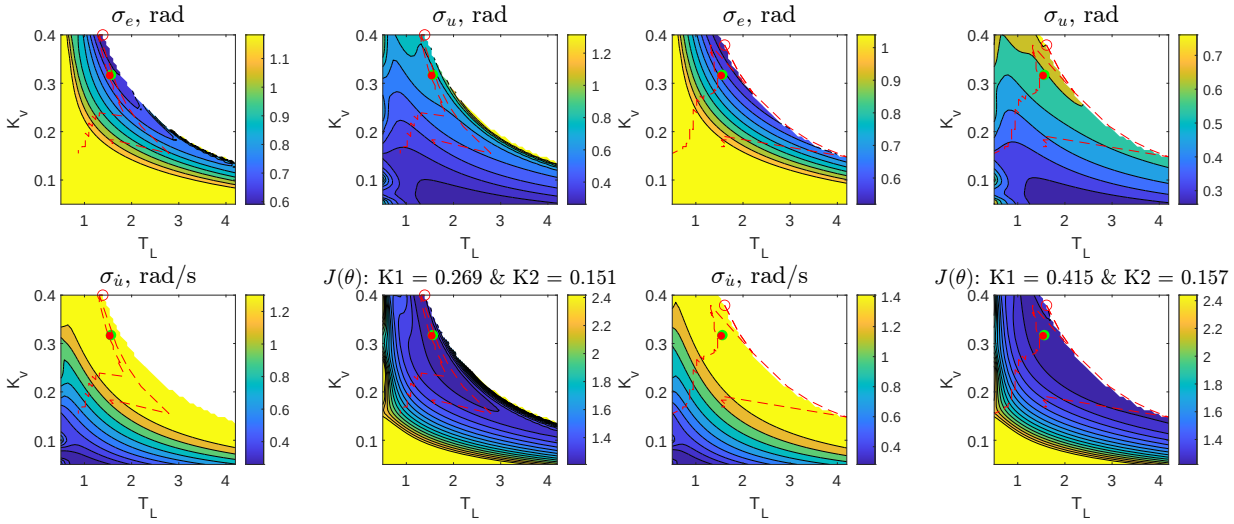

(a) Average case **(b)** Individual case

Figure C.11: Participant 2 cost maps - Exp. (II)

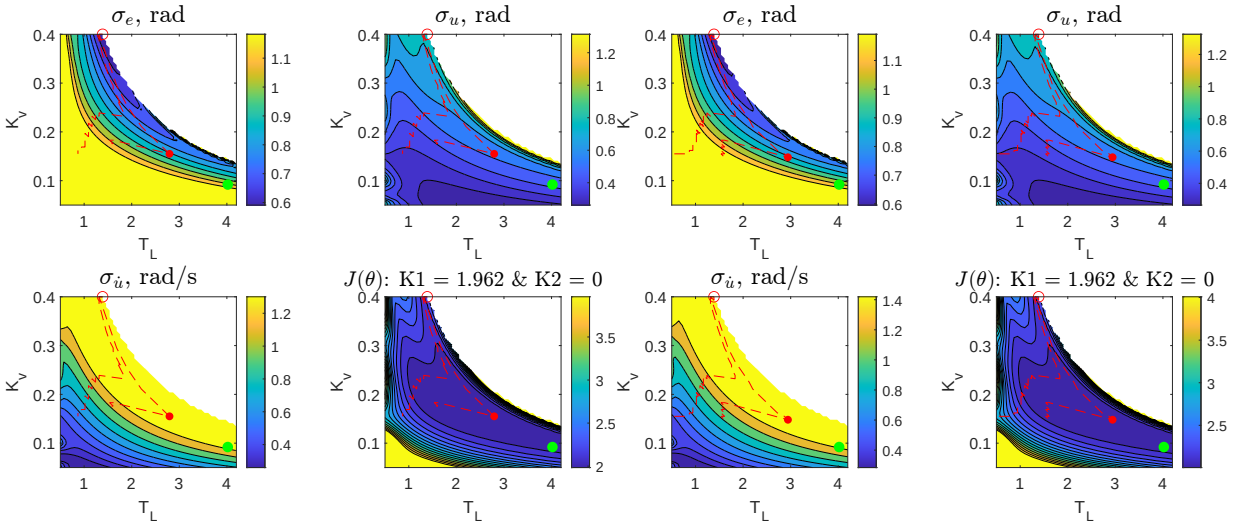

(a) Average case **(b)** Individual case

Figure C.12: Participant 3 cost maps - Exp. (II)

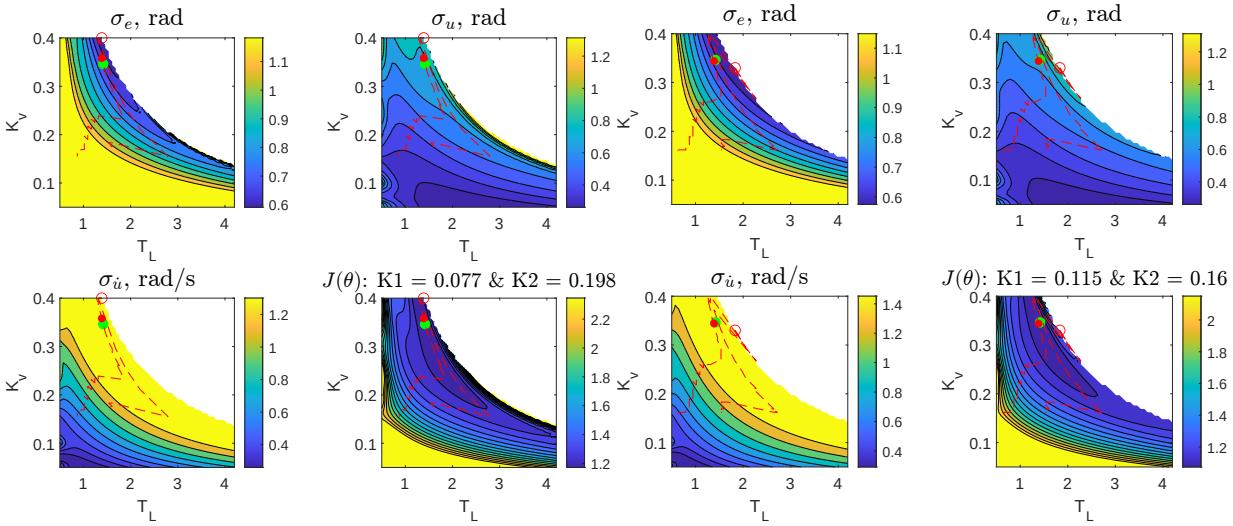

(a) Average case **(b)** Individual case

Figure C.13: Participant 4 cost maps - Exp. (II)

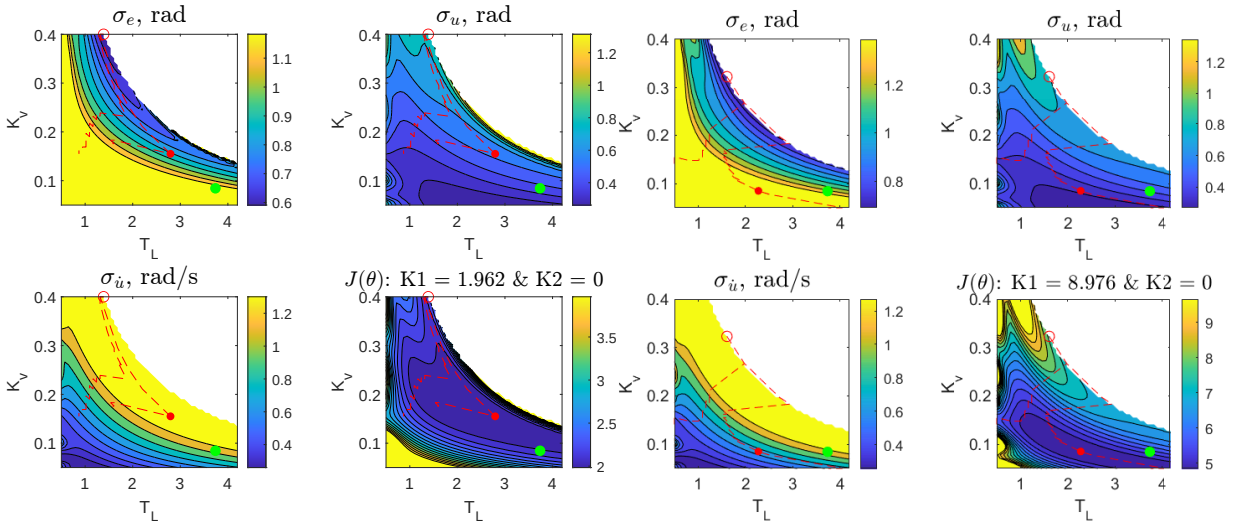

(a) Average case **(b)** Individual case

Figure C.14: Participant 5 cost maps - Exp. (II)

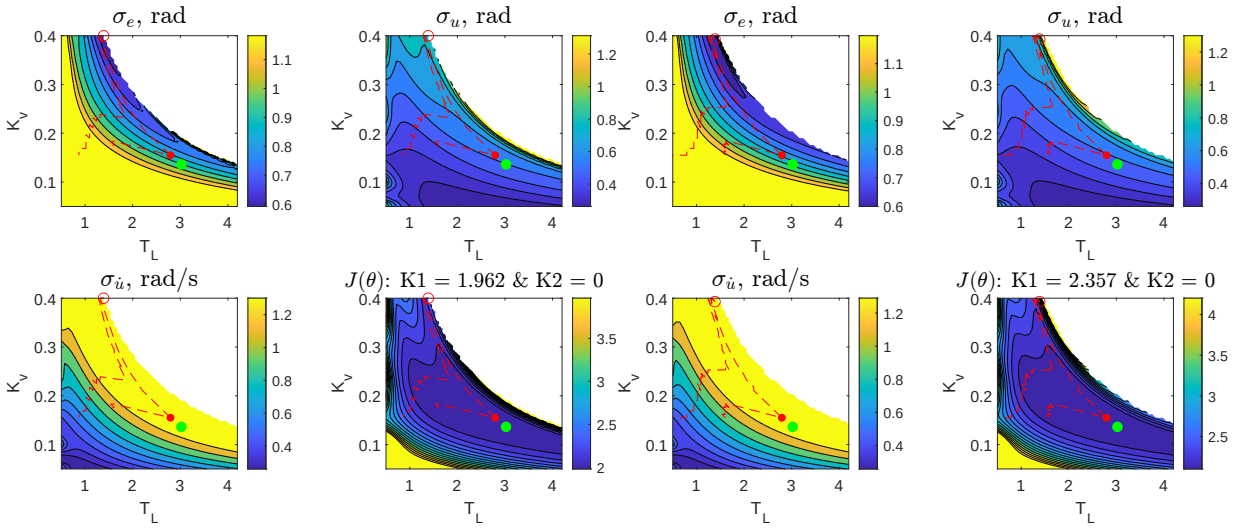

(a) Average case **(b)** Individual case

Figure C.15: Participant 6 cost maps - Exp. (II)

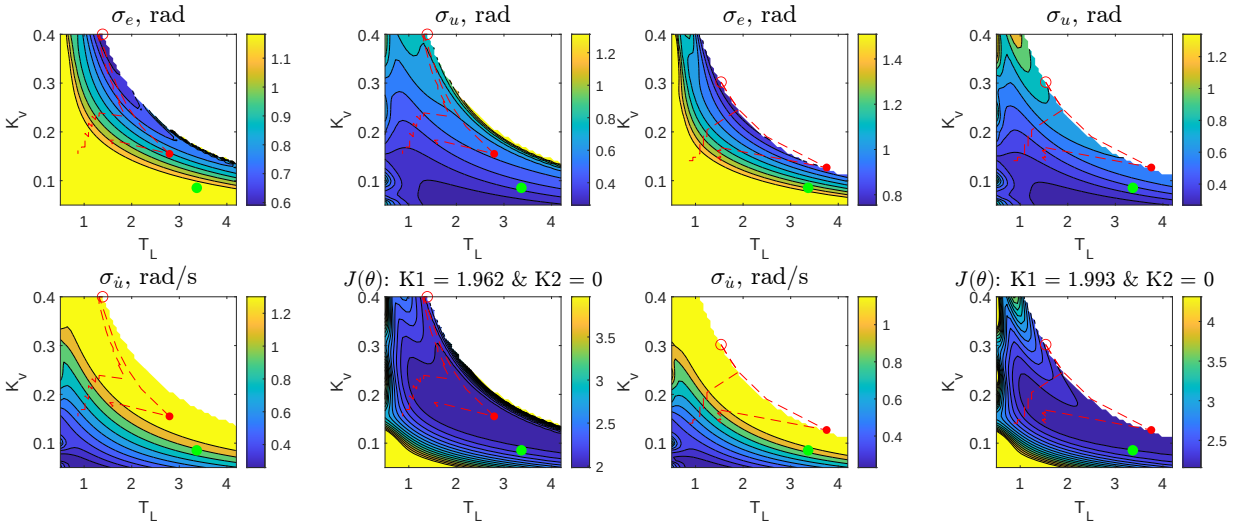

(a) Average case **(b)** Individual case

Figure C.16: Participant 7 cost maps - Exp. (II)

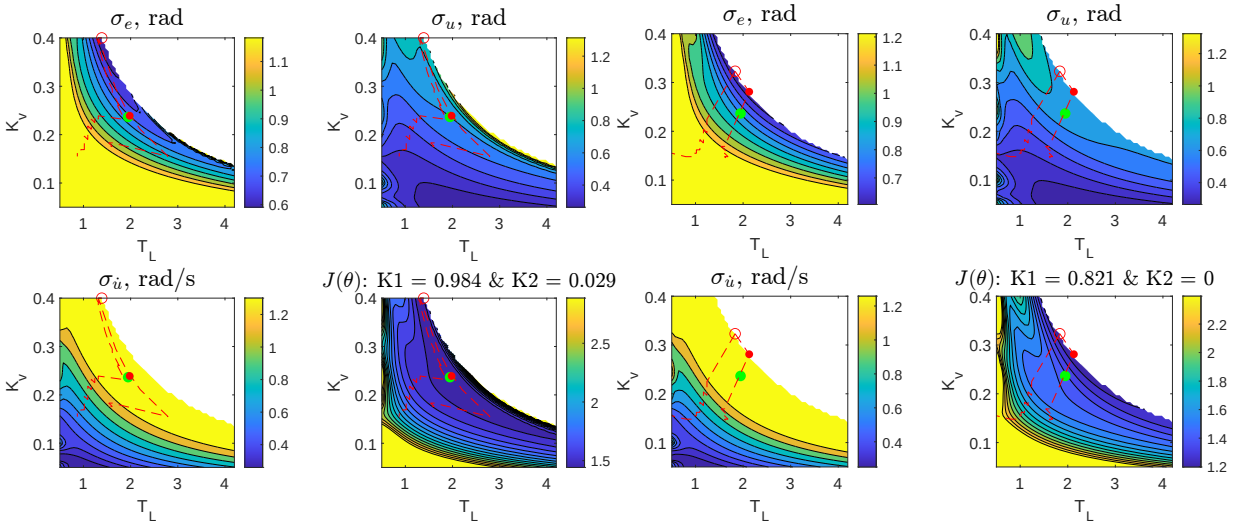

(a) Average case **(b)** Individual case

Figure C.17: Participant 8 cost maps - Exp. (II)

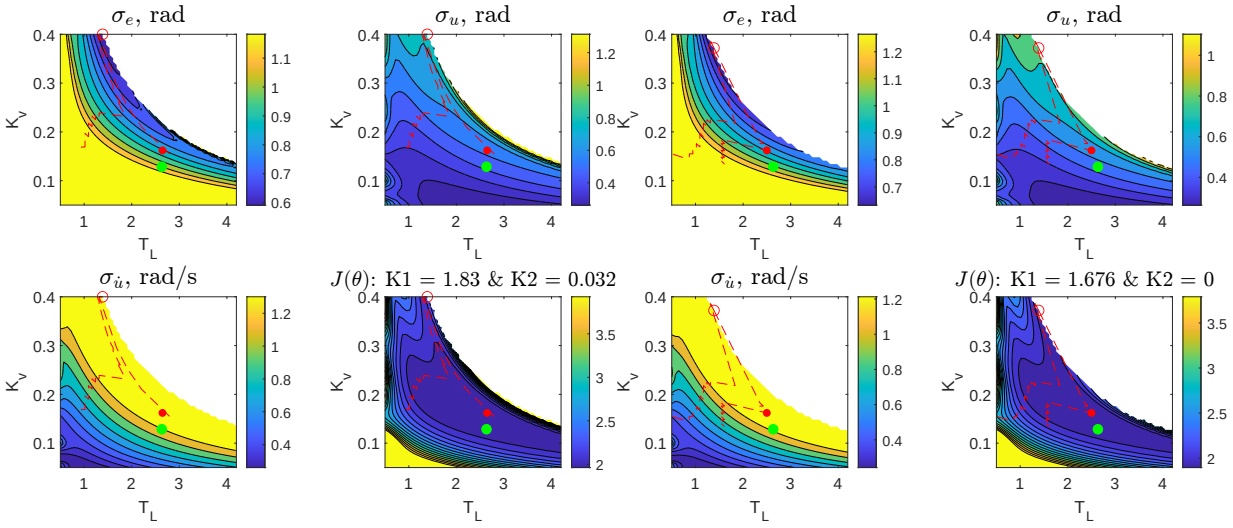

(a) Average case **(b)** Individual case

Figure C.18: Participant 9 cost maps - Exp. (II)

C.3. Experiment (III)

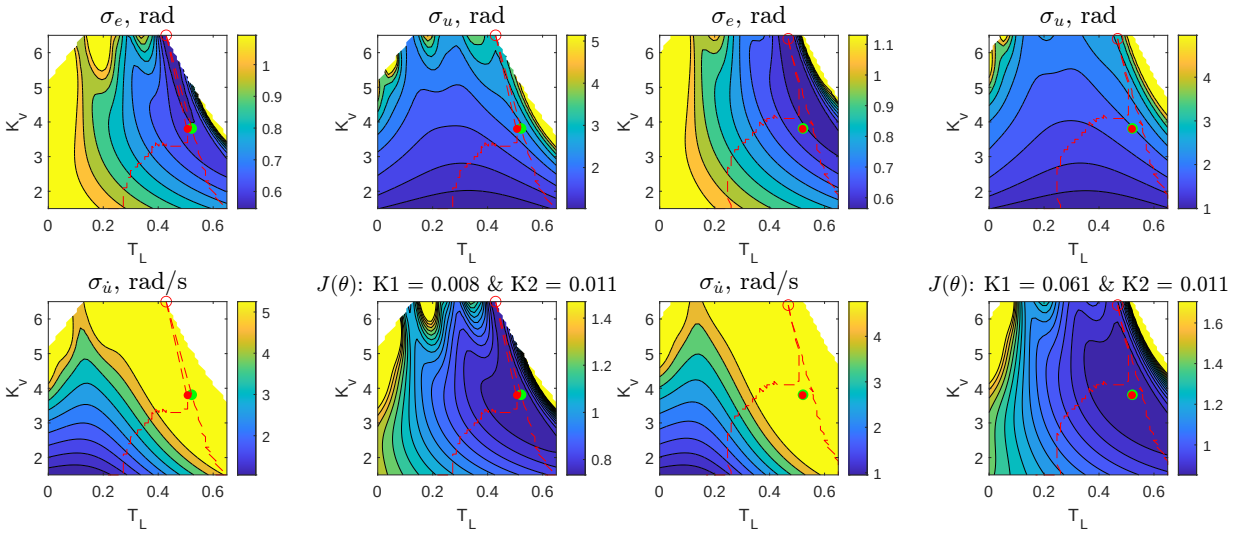

(a) Average case **(b)** Individual case

Figure C.19: Participant 1 cost maps - Exp. (III)

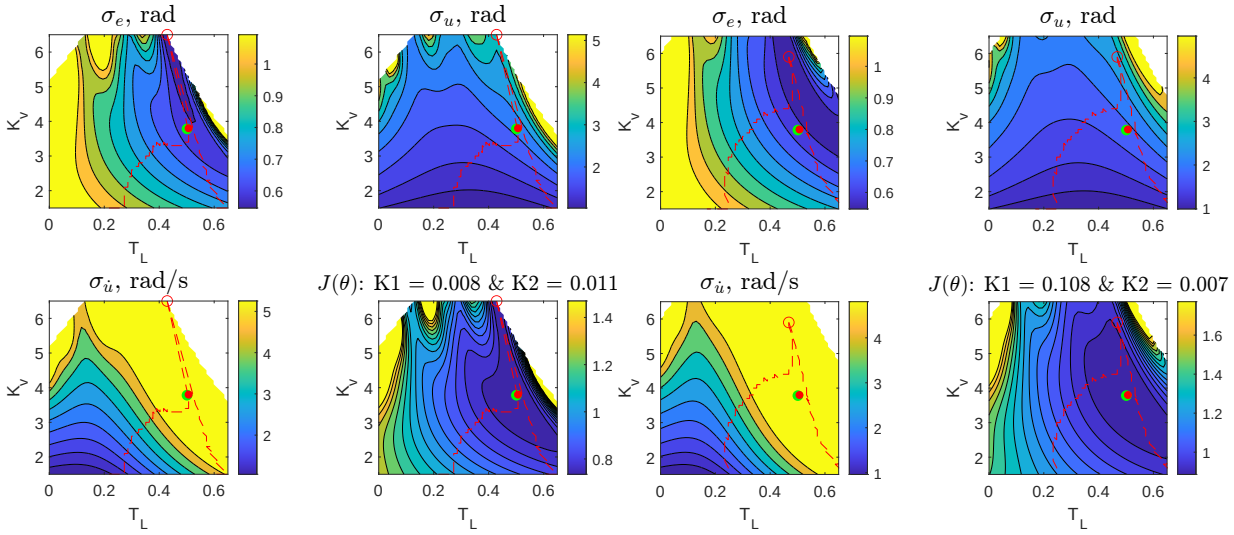

(a) Average case **(b)** Individual case

Figure C.20: Participant 2 cost maps - Exp. (III)

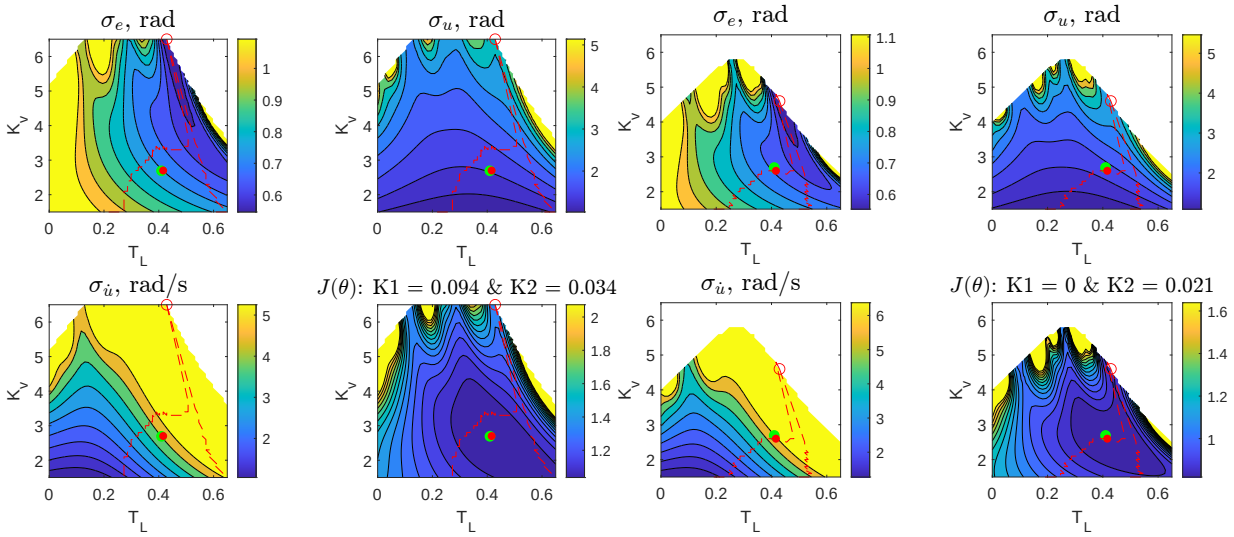

(a) Average case **(b)** Individual case

Figure C.21: Participant 3 cost maps - Exp. (III)

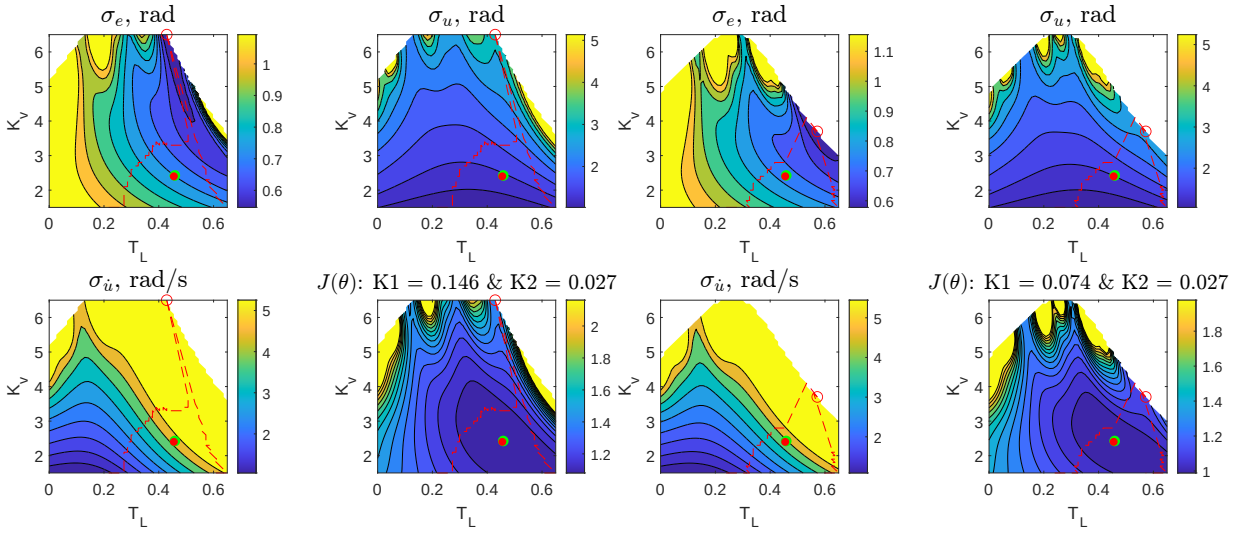

(a) Average case **(b)** Individual case

Figure C.22: Participant 4 cost maps - Exp. (III)

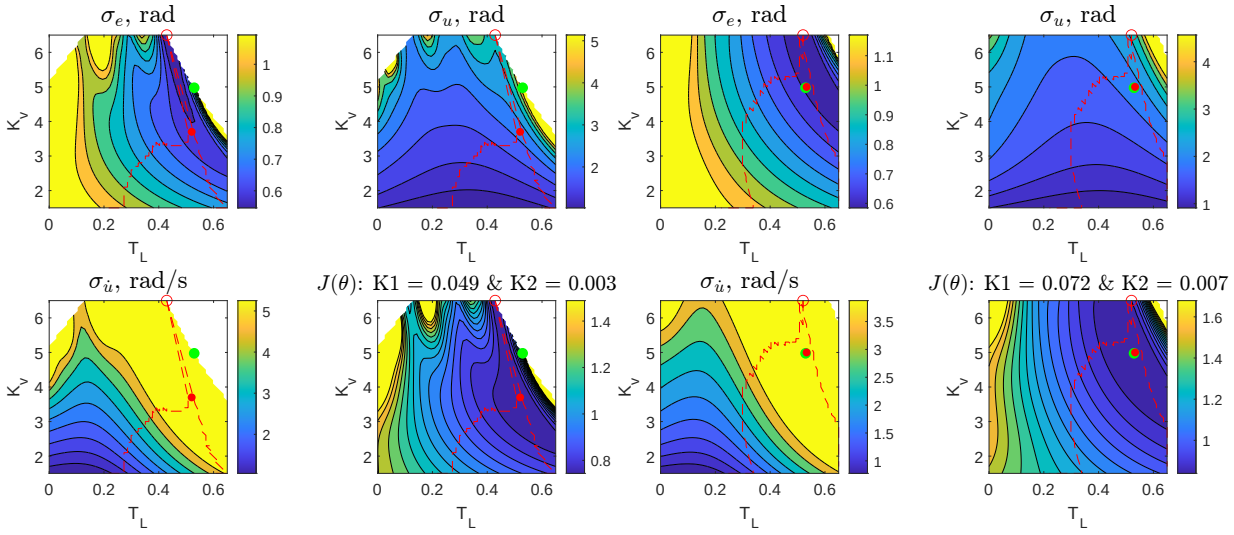

(a) Average case **(b)** Individual case

Figure C.23: Participant 5 cost maps - Exp. (III)

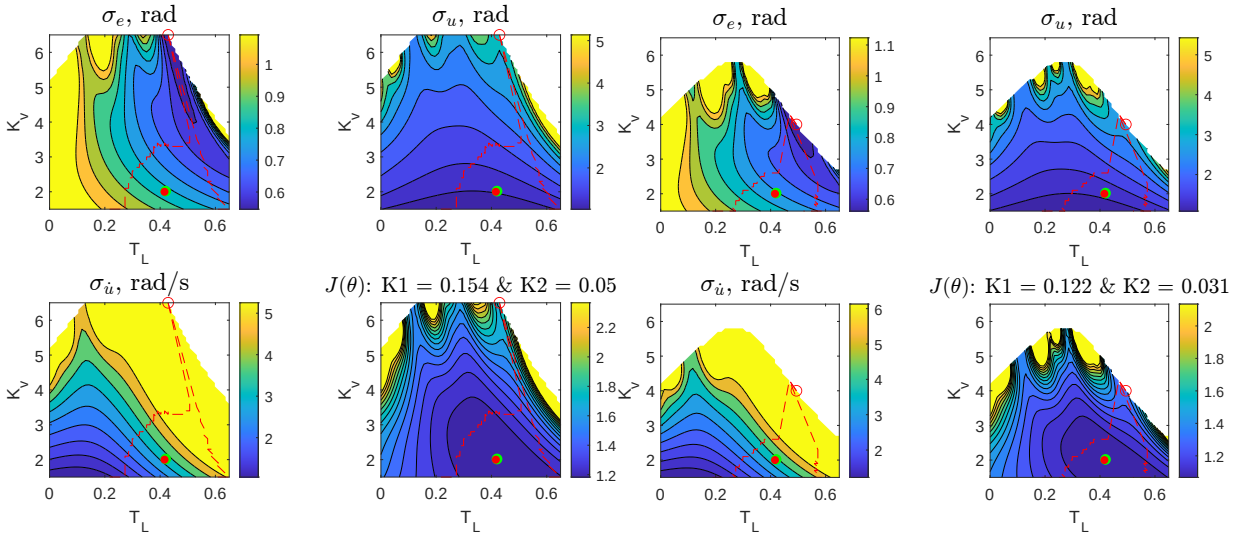

(a) Average case **(b)** Individual case

Figure C.24: Participant 6 cost maps - Exp. (III)

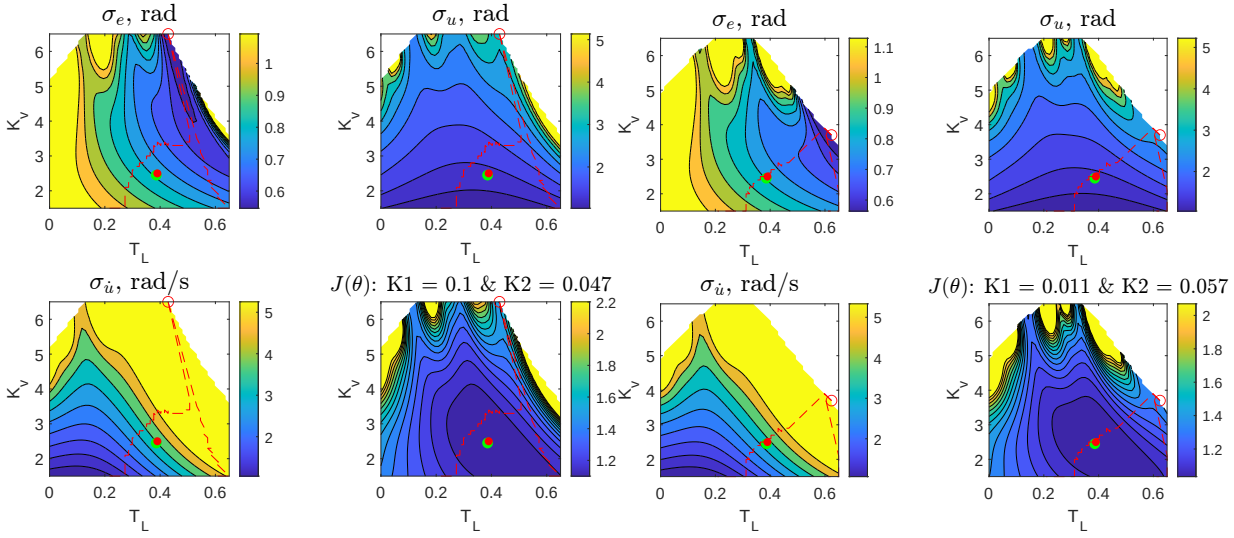

(a) Average case **(b)** Individual case

Figure C.25: Participant 7 cost maps - Exp. (III)

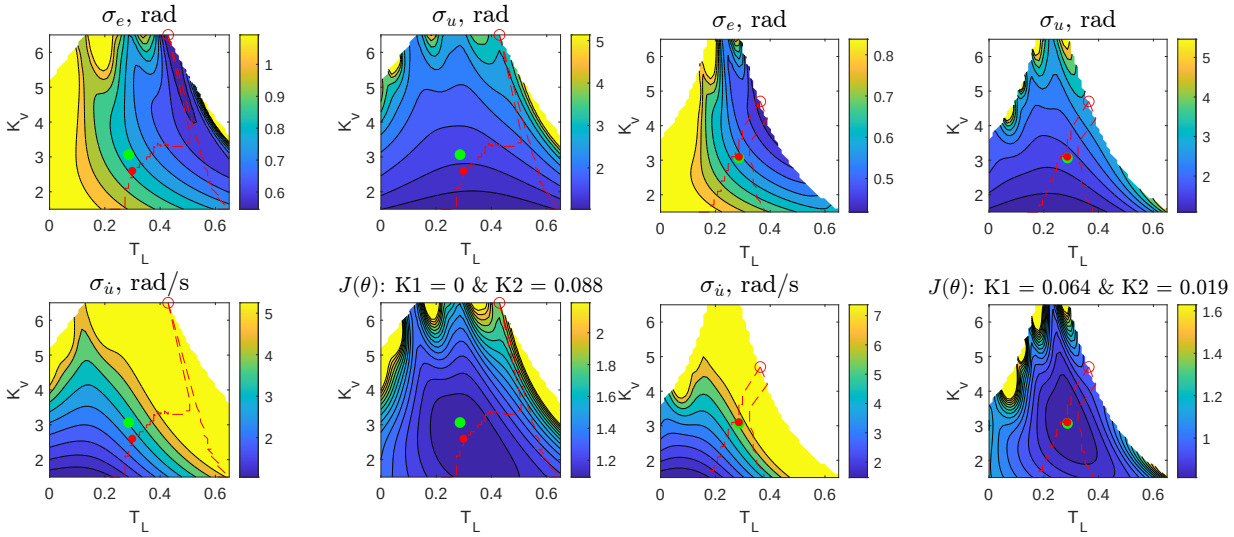

(a) Average case **(b)** Individual case

Figure C.26: Participant 8 cost maps - Exp. (III)

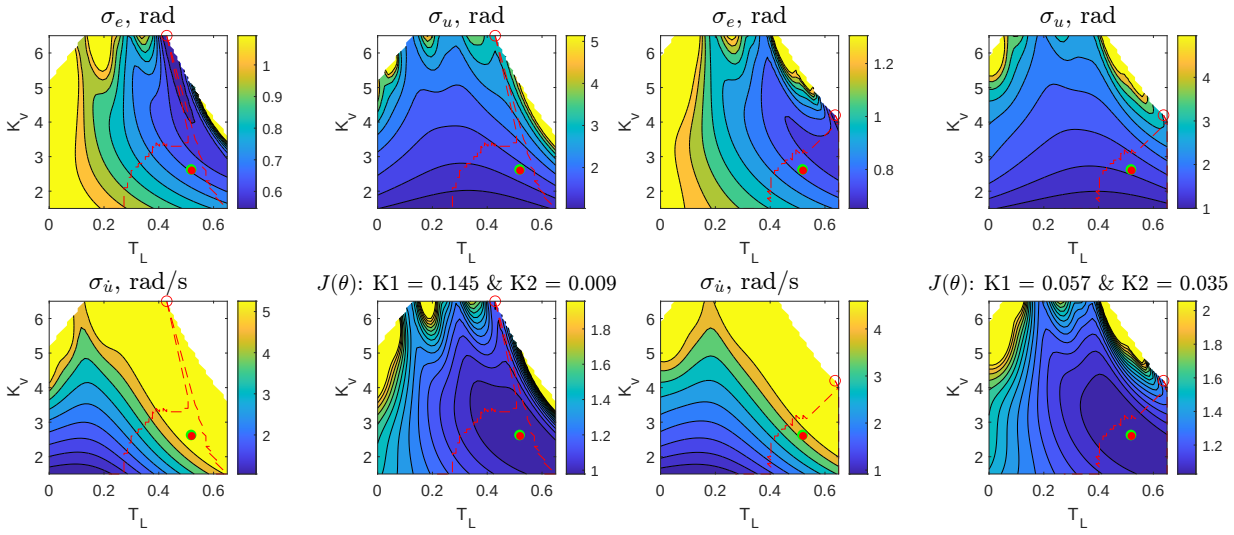

(a) Average case **(b)** Individual case

Figure C.27: Participant 9 cost maps - Exp. (III)

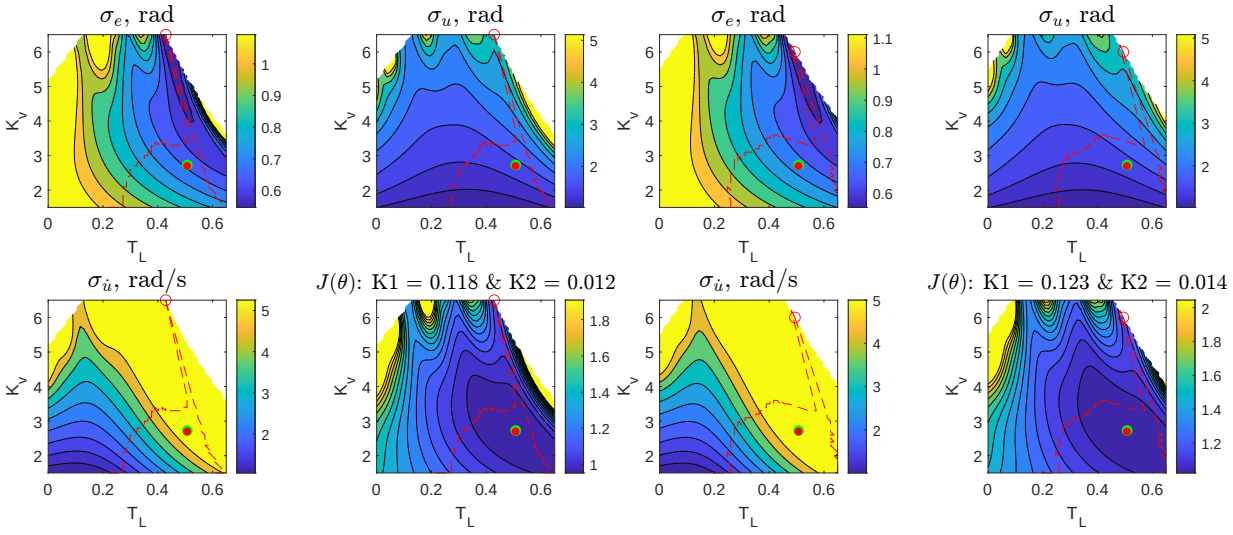

(a) Average case **(b)** Individual case

Figure C.28: Participant 10 cost maps - Exp. (III)

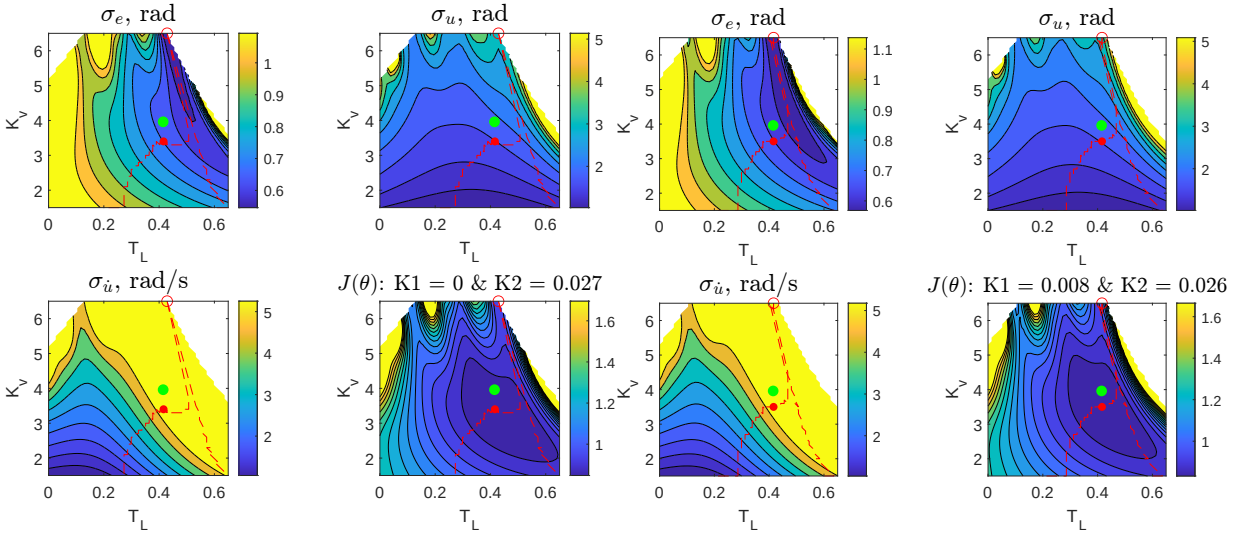

(a) Average case **(b)** Individual case

Figure C.29: Participant 11 cost maps - Exp. (III)

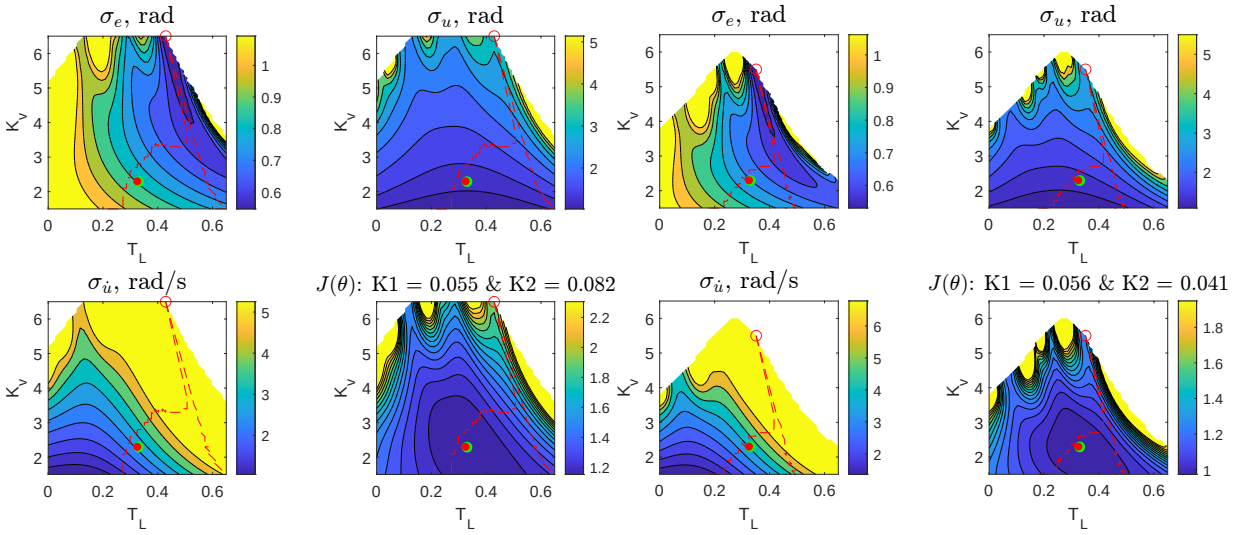

(a) Average case **(b)** Individual case

Figure C.30: Participant 12 cost maps - Exp. (III)

C.4. Identified Cost Function Weightings - Individual Case

Table C.1: Identified individual cost function weightings for all three data sets, italics indicate estimates

Participant #	Experiment (I)		Experiment (II)		Experiment (III)	
	K1 (1/rad)	K2 (s/rad)	K1(1/rad)	K2 (s/rad)	K1 (1/rad)	K2 (s/rad)
1	*0.000*	*0.035*	*2.555*	*0.000*	0.061	0.011
2	0.043	0.000	0.415	0.157	0.108	0.007
3	*0.052*	*0.017*	*1.962*	*0.000*	0.000	0.021
4	0.172	0.015	0.115	0.160	0.074	0.027
5	0.050	0.000	*8.976*	*0.000*	0.072	0.007
6	0.052	0.002	*2.357*	*0.000*	0.122	0.031
7	0.042	0.045	*1.993*	*0.000*	0.011	0.057
8	*0.006*	*0.024*	*0.821*	*0.000*	0.064	0.019
9	0.054	0.051	*1.676*	*0.000*	0.057	0.035
10	-	-	-	-	0.123	0.014
11	-	-	-	-	*0.008*	*0.026*
12	-	-	-	-	0.056	0.041

D

Prediction Plots - Individual Case

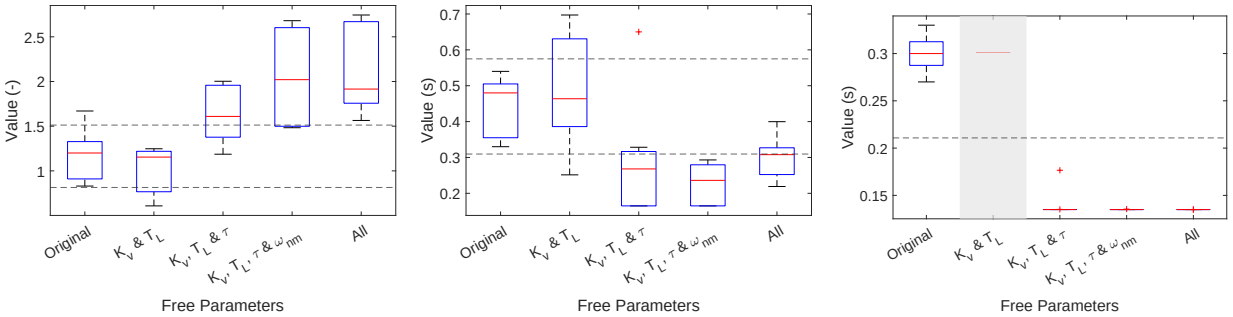

(a) Prediction plots for K_v **(b)** Prediction plots for T_L **(c)** Prediction plots for τ

(d) Prediction plots for ω_{nm} **(e)** Prediction plots for ζ_{nm}

Figure D.1: Prediction plots for Exp. (I)

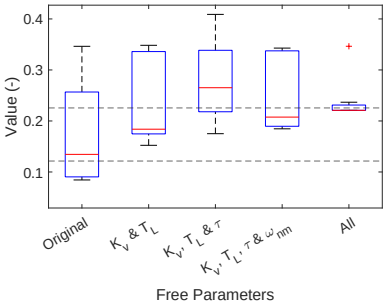

(a) Prediction plots for K_v

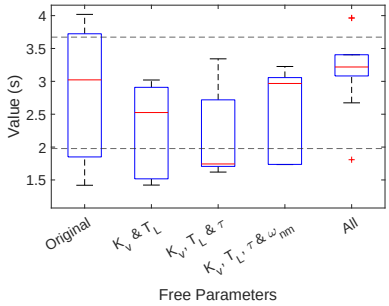

(b) Prediction plots for T_L

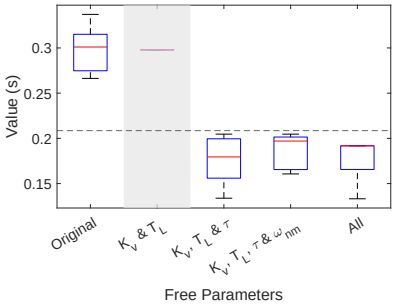

(c) Prediction plots for τ

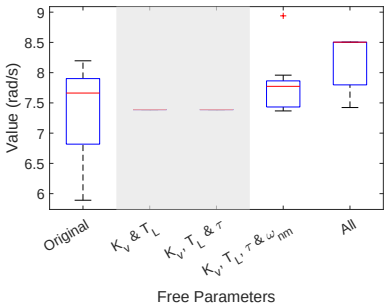

(d) Prediction plots for ω_{nm}

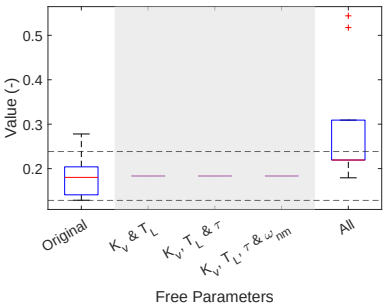

(e) Prediction plots for ζ_{nm}

Figure D.2: Prediction plots for Exp. (II)

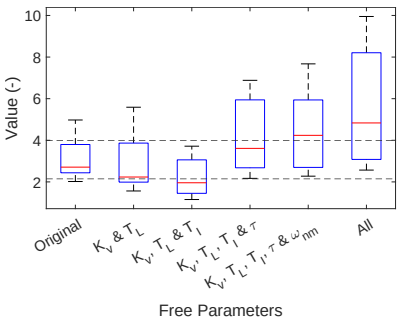

(a) Prediction plots for K_v

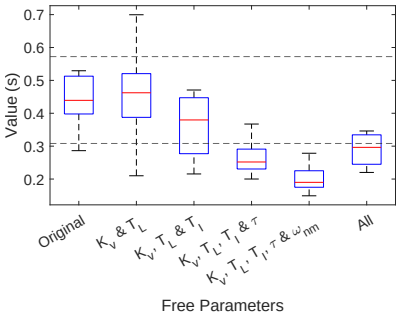

(b) Prediction plots for T_L

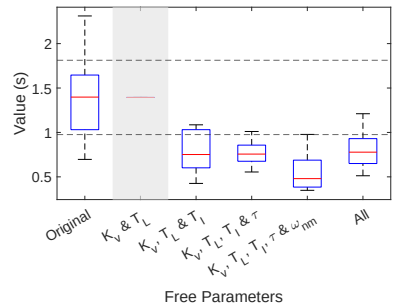

(c) Prediction plots for T_I

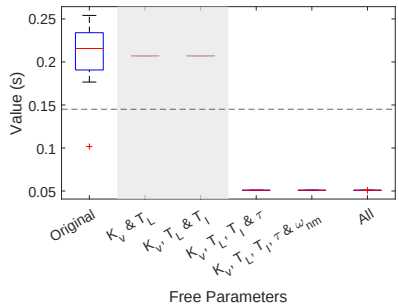

(d) Prediction plots for τ

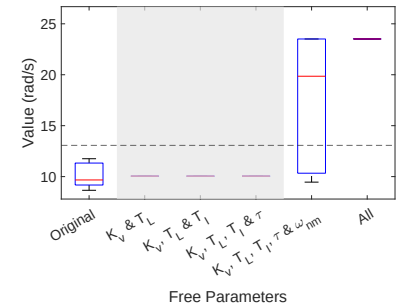

(e) Prediction plots for ω_{nm}

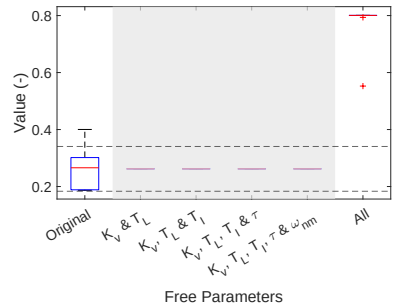

(f) Prediction plots for ζ_{nm}

Figure D.3: Prediction plots for Exp. (III)

E

Simulated Participant Results

E.1. Simulated Participant Cybernetic Parameter Histograms

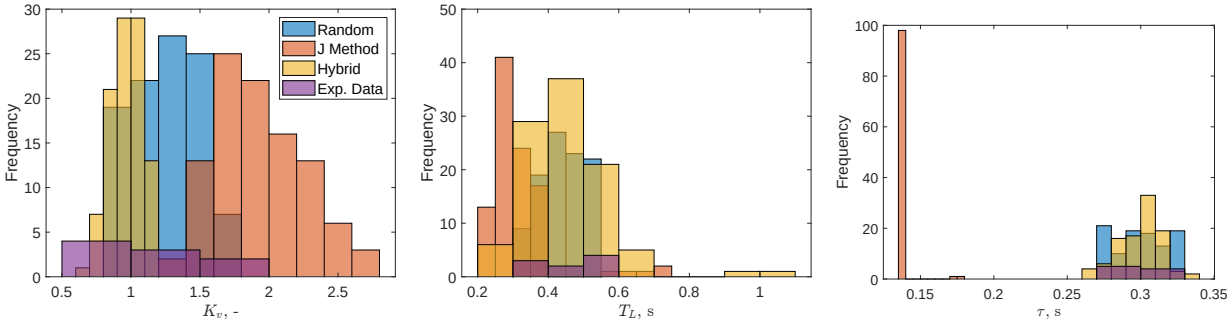

(a) Generated data - K_v **(b)** Generated data - T_L **(c)** Generated data - τ

(d) Generated data - ω_{nm} **(e)** Generated data - ζ_{nm}

Figure E.1: Simulated Participant Cybernetic Parameter Histograms - Exp. (I)

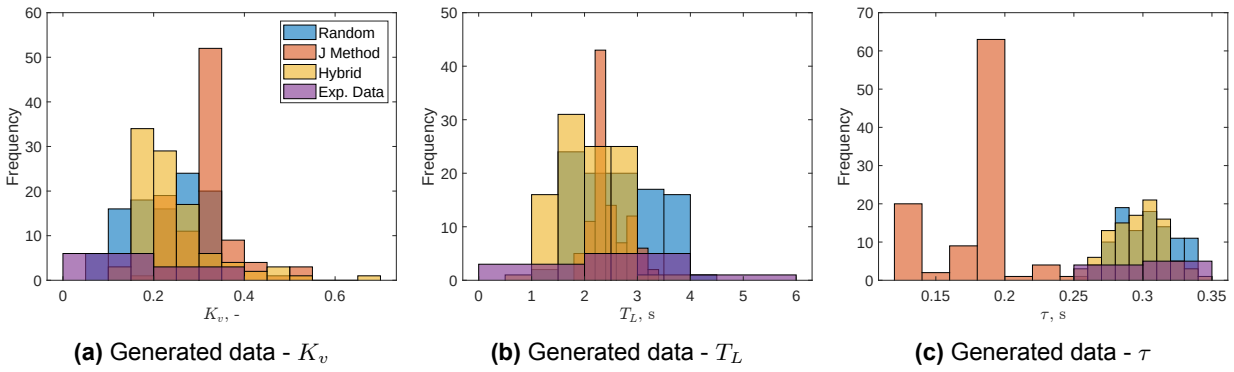

(a) Generated data - K_v **(b)** Generated data - T_L **(c)** Generated data - τ

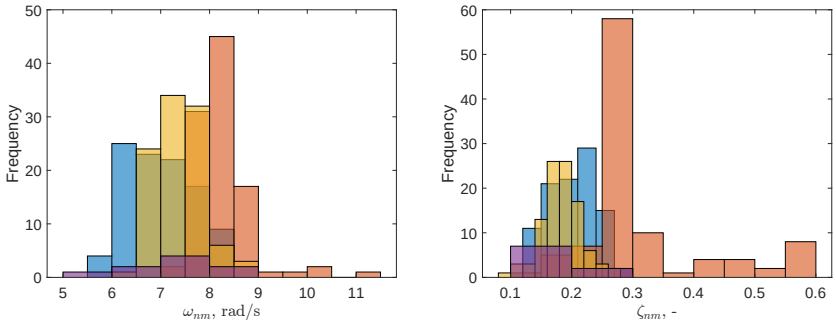

(d) Generated data - ω_{nm} **(e)** Generated data - ζ_{nm}

Figure E.2: Simulated Participant Cybernetic Parameter Histograms - Exp. (II)

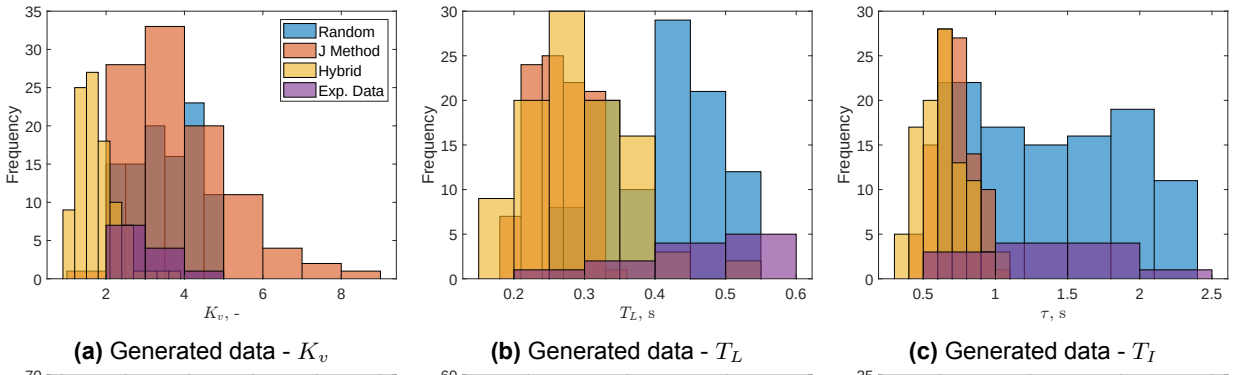

(a) Generated data - K_v **(b)** Generated data - T_L **(c)** Generated data - T_I

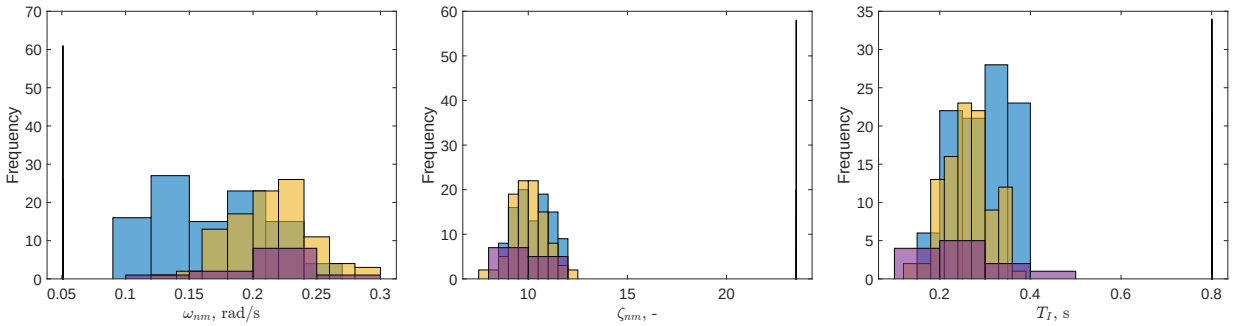

(d) Generated data - τ **(e)** Generated data - ω_{nm} **(f)** Generated data - ζ_{nm}

Figure E.3: Simulated Participant Cybernetic Parameter Histograms - Exp. (III)

E.2. Simulated Participant Phase Margin & Crossover Frequencies

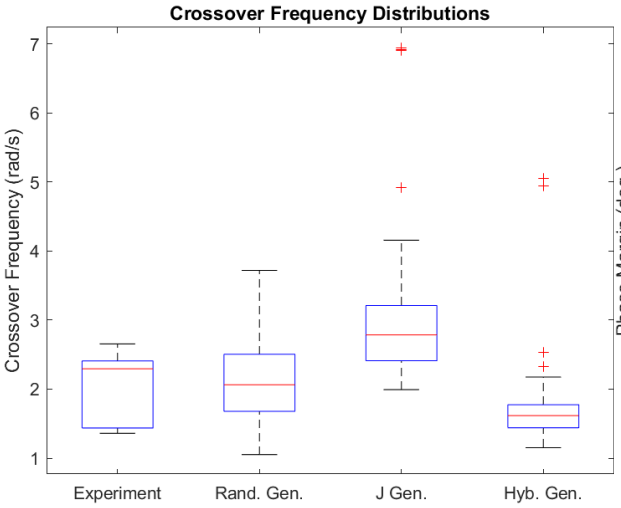

Figure E.4: Crossover frequency box plots of simulated participants - all methods, Exp. (I)

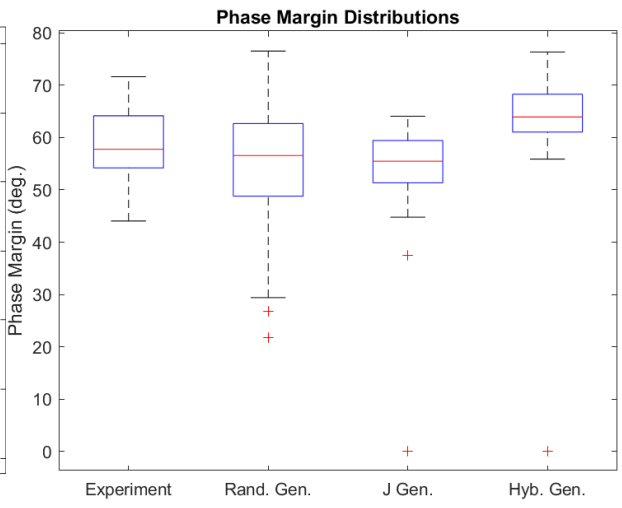

Figure E.5: Phase margin box plots of simulated participants - all methods, Exp. (I)

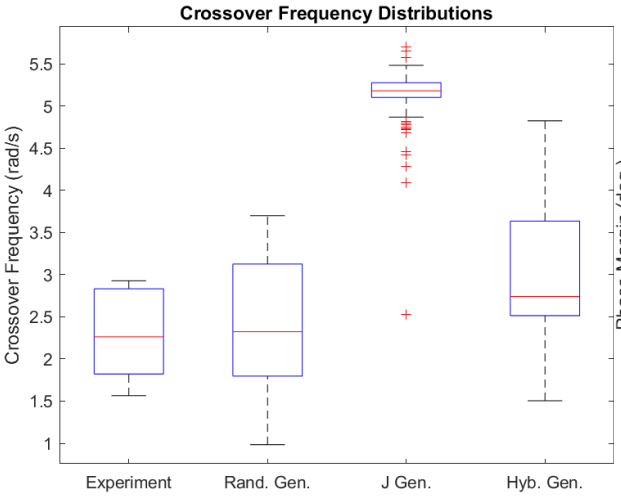

Figure E.6: Crossover frequency box plots of simulated participants - all methods, Exp. (II)

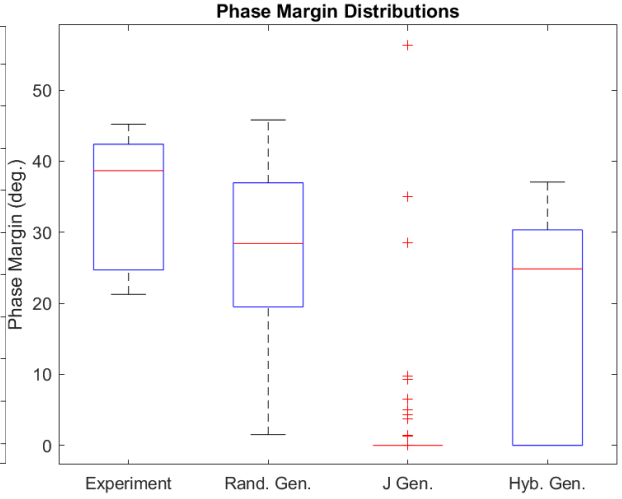

Figure E.7: Phase margin box plots of simulated participants - all methods, Exp. (II)

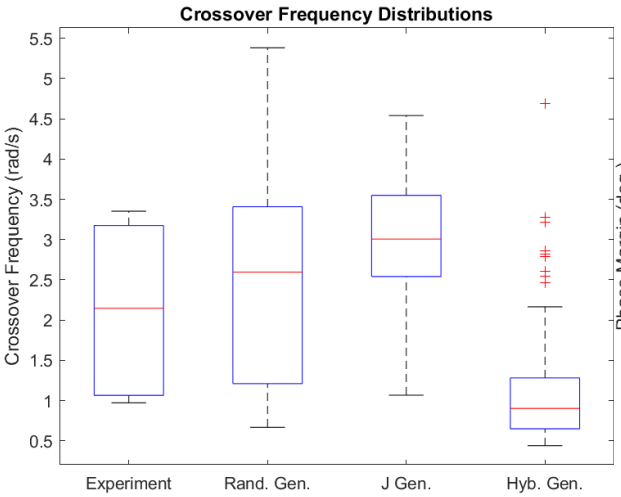

Figure E.8: Crossover frequency box plots of simulated participants - all methods, Exp. (III)

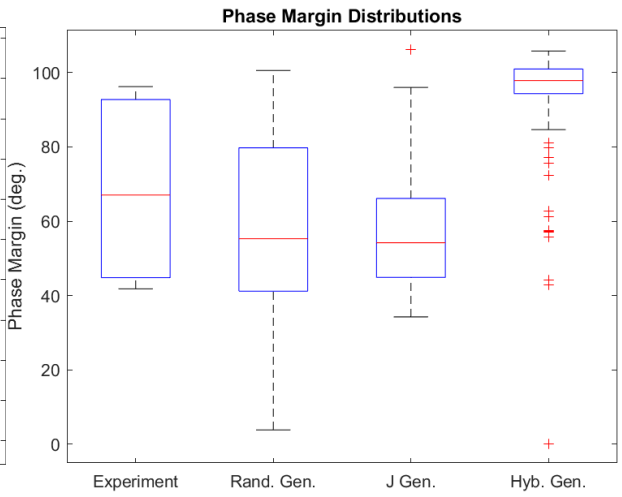

Figure E.9: Phase margin box plots of simulated participants - all methods, Exp. (III)